AD-A065 472 INSTITUTE FOR DEFENSE ANALYSES ARLINGTON VA F/G 4/1
STATUS OF REPRESENTATIVE TWO-DIMENSIONAL MODELS OF THE STRATOSP--ETC(U)
OCT 78 H HIDALGO DOT-FA-77WA-3965
UNCLASSIFIED P-1341 FAA-AEE-78-23 NL

1 OF 3
AD A065472

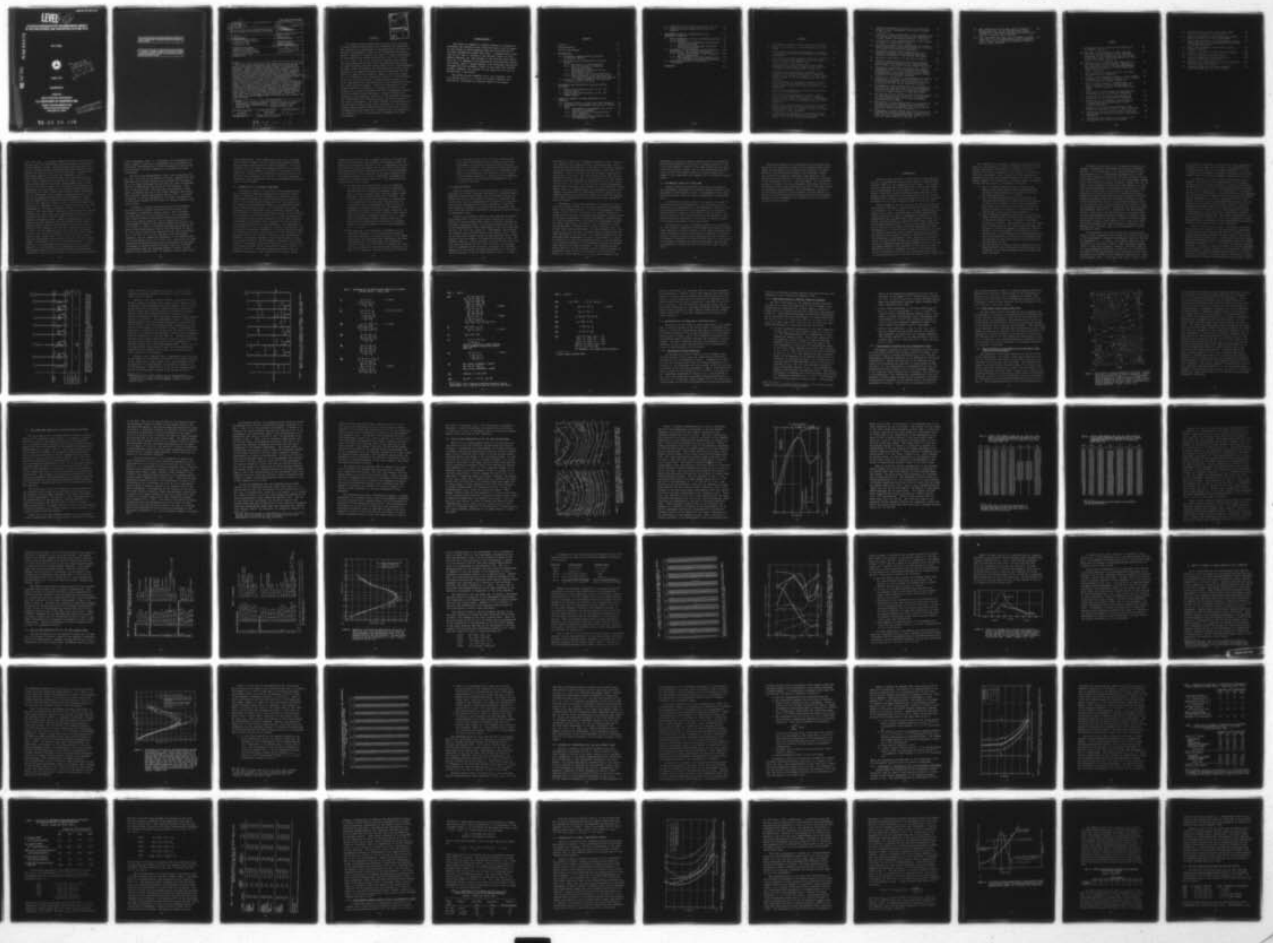

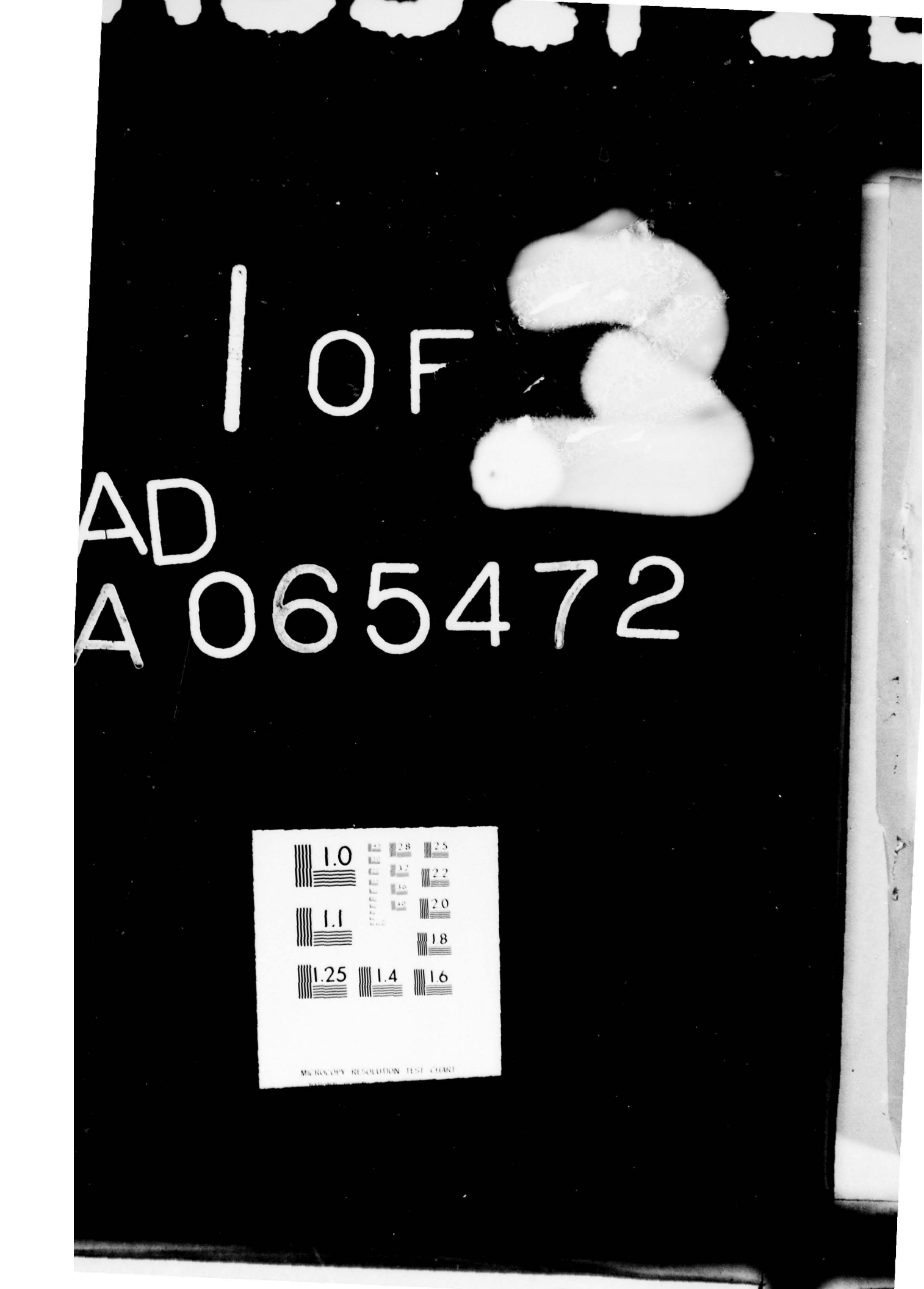
1 OF 3
AD
A065472
1.0
1.1
1.25
1.4
1.6
MICROCOPY RESOLUTION TEST CHART

Report No. FAA-AEE-78-23

LEVEL II

STATUS OF REPRESENTATIVE TWO-DIMENSIONAL MODELS OF THE STRATOSPHERE AND TROPOSPHERE AS OF MID-1978

Henry Hidalgo

October 1978

INTERIM REPORT

Prepared for

HIGH ALTITUDE POLLUTION PROGRAM

U.S. DEPARTMENT OF TRANSPORTATION

FEDERAL AVIATION ADMINISTRATION
Office of Environment and Energy
Washington, D.C. 20591

The work reported in this document was conducted under Contract No. DOT-FA-77WA3965 for the Department of Transportation. The publication of this IDA Report does not indicate endorsement by the Department of Transportation, nor should the contents be construed as reflecting the official position of that agency

Technical Report Documentation Page

1. Report No.	2. Government Accession No.	3. Recipient's Catalog No.
FAA-AEE-78-23		

4. Title and Subtitle
Status of Representative Two-Dimensional Models of the Stratosphere and Troposphere as of Mid-1978

5. Report Date
October 1978

6. Performing Organization Code

7. Author(s)
Henry Hidalgo

8. Performing Organization Report No.
P-1341

9. Performing Organization Name and Address
Institute for Defense Analyses
400 Army-Navy Drive
Arlington, Va. 22202

10. Work Unit No. (TRAIS)

11. Contract or Grant No.
DoT-FA-77WA-3965

12. Sponsoring Agency Name and Address
Department of Transportation
Federal Aviation Administration
Office of Environment and Energy
Washington, D.C. 20591

13. Type of Report and Period Covered
Interim April 15, 1977 to October 15, 1978

14. Sponsoring Agency Code

15. Supplementary Notes
Interim rept. 15 Apr 77-15 Oct 78,

16. Abstract

This paper reviews ongoing efforts aimed at the solution of basic problems dealing with ozone chemistry and atmospheric mass transports in representative two-dimensional (altitude and latitude) photochemical models of the troposphere and stratosphere. Emphasis is placed on the impact of recent measurements of the reaction rate coefficients for $HO_2 + NO \rightarrow OH + NO_2$ and $HO_2 + O_3 \rightarrow OH + 2\,O_2$ on: (a) the balance between ozone production and destruction on both ozone concentrations and columns at middle northern latitudes during summer for an oxygen-hydrogen-nitrogen (O-H-N) atmosphere; (b) the calculation of NO_x concentrations in the upper troposphere which are important for the effects of high-altitude subsonic flight on the ozone column; and (c) estimates of the tropospheric NO_x and OH concentrations as well as the removal rates of water-soluble species in the lower troposphere from considerations of the tropospheric ozone and carbon monoxide budgets. The severe limitations of arbitrary extensions of available 2-D parameterizations of the dynamics to an upper troposphere and lower stratosphere assumed to be perturbed by large emissions of engine effluents are brought out from numerical solutions of the primitive equations for instantaneous and continuous sources of inert material in the lower stratosphere. The paper includes (a) preliminary 2-D results based on the revised ozone chemistry for the trend of subsonic and supersonic flight effects on ozone, and (b) some recommendations for future work concerning the 2-D treatment of the dynamics for the perturbed upper troposphere and lower stratosphere.

17. Key Words	18. Distribution Statement
Atmospheric mass transports, Atmospheric ozone chemistry, 2-D atmospheric photochemical modeling, Aviation effects on atmospheric ozone	Document is available for unrestricted distribution through the National Technical Information Service, Springfield, Virginia 22151

19. Security Classif. (of this report)	20. Security Classif. (of this page)	21. No. of Pages	22. Price
UNCLASSIFIED	UNCLASSIFIED	145	

Form DOT F 1700.7 (8-72) Reproduction of completed page authorized

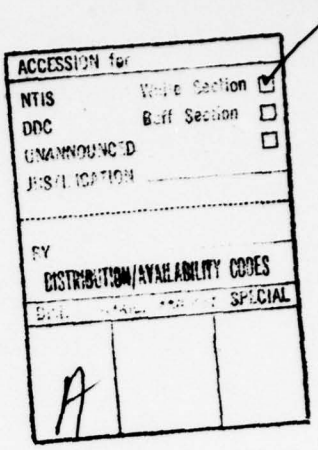

ABSTRACT

This paper reviews ongoing efforts aimed at the solution of basic problems dealing with ozone chemistry and atmospheric mass transports in representative two-dimensional (altitude and latitude) photochemical models of the troposphere and stratosphere. Emphasis is placed on the impact of recent measurements of the reaction rate coefficients for $HO_2 + NO \rightarrow OH + NO_2$ and $HO_2 + O_3 \rightarrow OH + 2\ O_2$ on (a) the balance between ozone production and destruction on both ozone concentrations and columns at middle northern latitudes during summer for an oxygen-hydrogen-nitrogen (O-H-N) atmosphere, (b) the calculation of NO_x concentrations in the upper troposphere which are important for the effects of high-altitude subsonic flight on the ozone column, and (c) estimates of the tropospheric NO_x and OH concentrations as well as the removal rates of water-soluble species in the lower troposphere from considerations of the tropospheric ozone and carbon monoxide budgets. The severe limitations of arbitrary extensions of available 2-D parameterizations of the dynamics to an upper troposphere and lower stratosphere assumed to be perturbed by large emissions of engine effluents are brought out from numerical solutions of the primitive equations for instantaneous and continuous sources of inert material in the lower stratosphere. The paper includes (a) preliminary 2-D results based on the revised ozone chemistry for the trend of subsonic and supersonic flight effects on ozone, and (b) some recommendations for future work concerning the 2-D treatment of the dynamics for the perturbed upper troposphere and lower stratosphere.

ACKNOWLEDGMENTS

The author is indebted to several modelers of atmospheric phenomena, who exhibited their scientific spirit both in regard to open access to their numerical data and self-criticism of the basic assumptions behind their data. In alphabetical order, they are Dr. Paul J. Crutzen of the National Center for Atmospheric Research, Dr. Jack Fishman of the Colorado State University, Dr. J.D. Mahlman of the Geophysical Fluid Dynamics Laboratory (NOAA), and Dr. George Widhopf of the Aerospace Corporation. Although they have reviewed a draft of this paper and provided valuable comments, the contents of this paper are the sole responsibility of the author.

The author is also indebted to Dr. G.D. Robinson, Prof. J.R. Holton, and Dr. R.C. Oliver for valuable comments and constructive criticism of a previous draft of this paper.

CONTENTS

	Abstract	iii
	Acknowledgments	v
	Overview and Summary	S-1
1.	INTRODUCTION	1
	1.1 Atmospheric Characteristics Relevant to Aviation Effects	5
	1.2 Mechanisms for the Modeling of Aviation Effects	13
	1.2.1 Absorption of Solar Radiation	13
	1.2.2 Rate Coefficients of Chemical Kinetics Processes	14
	1.2.3 Heterogeneous Processes for the Tropospheric Sinks	15
	1.2.4 Water Vapor (H_2O) Sources and Sinks	16
	1.2.5 Mass Transports in the Reference and Perturbed Troposphere and Stratospheres	16
	1.3 Summary of Pending Changes in the Modeling of Aviation Effects on Ozone	19
2.	TWO-DIMENSIONAL MODELING OF AVIATION EFFECTS ON OZONE	21
	2.1 Results and Characteristics of the 1976 Crutzen Model	25
	2.2 Results and Characteristics of the 1976 Widhopf Model	35
3.	IMPACT OF CHANGES IN OZONE CHEMISTRY ON 2-D MODELING	47
	3.1 Underdestruction of Ozone with 1977 Chemistry	49
	3.2 Estimates of Tropospheric NO_x and H_2O_2 Rainout Sinks	55
	3.2.1 Assessment of Tropospheric NO_x in the Northern Troposphere	58
	3.2.2 Ozone Change Due to Subsonics with 1977 Chemistry	62
	3.2.3 Heterogeneous Removal Rates of H_2O_2 in Tropospheric Sinks	67

3.3 Comparison of 2-D Model Tropospheric Results 69
3.4 Critical Chemical Reactions for Aviation Effects 75

4. ASSESSMENT OF THE 2-D FORMULATION OF THE ATMOSPHERIC DYNAMICS 83

4.1 Basic Assumptions in the 2-D Parameterizations of the Dynamics 83
4.1.1 Decoupling of Temperature and Dynamics from the Chemistry 84
4.1.2 Hypothesis of Large-Scale Diffusion in the Stratosphere 90
4.2 Evaluation of the Extension of the Diffusion Hypothesis to the Perturbed Atmosphere 106
4.2.1 Dynamic Meteorology of Eddy Transports in the Stratosphere 106
4.2.2 Mass Transports of Inert Material in the Reference and Perturbed Atmospheres 112
4.3 Statistical-Dynamical Formulation of 2-D Dynamics 134

REFERENCES 139

FIGURES

1. Approximate estimates of gas budgets of the world 7
2. Chemical mechanisms in the stratosphere and troposphere 9
3. Ozone column in reference atmosphere as a function of latitude and month in the Northern and Southern Hemispheres 17
4. Isolines of the daily average of UV solar radiation flux at a typical wavelength of 300.4 nm during winter (January) and summer (July) 26
5. Simulated ozone concentration and ozone column growth with decreasing altitude for the reference atmosphere at 45°N during summer (August 30) 28
6. Simulated vertical profiles of daylight, zonal average of the volume mixing ratio of indicated species in the reference atmosphere at 45°N during summer (August 30) by the Crutzen model with 1976 chemistry 33
7. Relative effects of individual subsonic or supersonic flight on the atmospheric ozone column during summer (August 30) after six years of fleet operations 34
8. Comparison of simulated and observed ozone mixing ratio at 35°N during June 38
9. Simulated vertical profiles of 24-hour, zonal average of the volume mixing ratio of indicated species in the reference atmosphere at 40°N during summer (August 15) by the Widhopf model with 1976 chemistry 42
10. Effects of a combined fleet of subsonic and supersonic aircraft on the atmospheric ozone column during summer (June 15) and fall (October 15) after five years of fleet operations 44
11. Illustration of the impact of the Howard-Evenson reaction rate coefficient on the simulated ozone mixing ratio for the reference atmosphere 51

12. Assumed tropospheric NO_x profiles for sensitivity analysis of the tropospheric ozone and CO budgets to NO_x and HO 59

13. Comparison of NO_x calculations in the troposphere by 2-D models utilizing 1976 (Crutzen and Widhopf) and revised (Widhopf and Fishman-Crutzen) chemistries 70

14. Illustration of H_2O parameterization in the Crutzen 2-D model at a grid point ($[T_{GP}]$) 73

15. Simulation of water vapor distribution in the reference atmosphere by the Crutzen model as a function of latitude in the Northern Hemisphere 76

16. Simulation of water vapor distribution in the reference atmosphere by the Widhopf model as a function of latitude in the Northern Hemisphere 77

17. Meridional Circulation as a function of season 91

18. Schematic representation of the slope (α) of the mixing length path necessary for countergradient eddy fluxes in the Prandtl mixing length hypothesis 94

19. Simulation of meridional circulation by a three-dimensional model of the troposphere-stratosphere-mesosphere ($0 < z < 70$ km) utilizing the condition of geostrophic equilibrium and the spectral representation of the dependent variables 111

20. Simulation of β-lines by a three-dimensional passive tracer model utilizing finite differences of the primitive equations for an instantaneous injection of material at 36°N and 65 mbar during January 116

21. Stratospheric tracer mixing ratio as a function of latitude, altitude and season for winter (December) of the fourth year after an assumed instantaneous release of tracer material at 35°N and 65 mbar 118

22. Interactions at the injection level (65 mbar) among the eddy and meridional motions in the dispersion of tracer material (Eq. 19) in the stratosphere during winter and summer 119

23. Enhancement of tracer mixing ratio as a function of latitude and altitude during winter (December) of the fifth year for a simulated SST-like continuous release of tracer material as per Eq. 20 123

24. Enhancement of tracer mixing ratio as a function of latitude and altitude during summer (August) of the sixth year for a simulated SST-like continuous release of tracer material as per Eq. 20 124

25. Eddy transports and the local rate of change of mixing ratio (Eq. 19) at 65 mbar during winter (December) of the fourth year after an instantaneous release of passive tracer material 126

26. Eddy transports and local rate of change of mixing ratio (Eq. 19) at 65 mbar during winter (December) after 5 years of an SST-like continuous release of passive tracer material 128

TABLES

1.	Mechanisms (M) for production and destruction of chemical species	10
2a.	Daylight, zonal averages of ozone, N_2O, NO_x, N_2O_5, NO_3 and HNO_3 species in the reference atmosphere as was simulated by the 2-D Crutzen photochemical model with 1976 chemistry at 45°N during late summer (August 30)	30
2b.	Daylight, zonal averages of H_2O, H_2O_2, OH, CO and CH_4 species in the reference atmosphere as was simulated by the 2-D Crutzen photochemical model with 1976 chemistry at 45°N during late summer (August 30)	31
3.	1976 reaction rate coefficients for an oxygen-hydrogen-nitrogen atmosphere	36
4.	24-hour, zonal average of species in the reference atmosphere as simulated by Widhopf, et al. (1977) at 40°N during late summer (August 15)	41
5.	Ratio of values based on Howard-Evenson rate (daily averages) to those corresponding in Table 4 (24-hour average) at 40°N during late summer	53
6.	Sensitivity of ozone budget to prescribed NO_x concentrations for the Northern Hemisphere	61
7.	Sensitivity of CO budget to prescribed NO_x concentrations for the Northern Hemisphere	61
8.	Sensitivity of tropospheric ozone production to prescribed NO_x concentrations for the Northern Hemisphere	64
9.	Competition of reactions involving the HO_2 radical for important subsonic flight conditions	66
10.	Sensitivity of OH to removal rates of H_2O_2 for the assumed NO_x profiles A and B in the Northern Hemisphere	68
11.	Average residence time of water vapor in the troposphere as a function of latitude	74

12. Sensitivity of the sign of the ozone change to rate coefficients of R21 and R13 — 80

13. Sample eddy parameters for Crutzen model during summer and winter in Northern Hemisphere — 99

14. Sample eddy parameters for Widhopf models during summer (August) in Northern Hemisphere and winter in Southern Hemisphere — 100

15. Sample eddy parameters derived from poleward transport of ozone — 103

16. Primitive equations for meridional circulation — 108

17. Primitive equations for eddy motions — 109

18. Slope of mixing length path as given by primitive equations, $[\alpha]$ (10^{-4}) — 129

19. Vertical eddy coefficients as given by primitive equations, K_{zz} $(10^4$ cm^2/sec) — 131

20. Horizontal eddy coefficients as given by primitive equations, K_{yy} $(10^{10}$ cm^2/sec) — 132

OVERVIEW AND SUMMARY

This paper is limited to a review of the status, as of mid-1978, of ongoing efforts aimed at the solution of basic problems which are involved in the development of two-dimensional (altitude and latitude) photochemical models of the stratosphere and troposphere. The interest in these two-dimensional (2-D) photochemical models stems from the following factors:

- A need to forecast the probable effect of future worldwide, high-altitude traffic of subsonic and supersonic aircraft on atmospheric ozone as a function of altitude, latitude, and season. High-altitude flight can have an impact on ozone through the interactions of NO_x (NO and NO_2) and H_2O engine effluents with a rather large family of trace chemical species that affect either directly or indirectly the ozone distributions in the stratosphere and troposphere.
- A need for proper interpretation of field observations of trace chemical species affecting ozone as a function of altitude, latitude, and season. These results are important for the gaining of physical insights for both photochemical modeling of the atmosphere and planning subsequent field observations.

The scope of this paper, therefore, excludes considerations of either the more limited 1-D models (altitude only) or the currently less practical 3-D models (including longitude) for the assessment of the latitudinal and seasonal effects on ozone from high-altitude flight. Furthermore, this paper describes

the ongoing development of 2-D modeling by considering in some depth two representative models of special interest to the High Altitude Pollution Program (HAPP), i.e., the Crutzen (Hidalgo and Crutzen, 1977) and the Widhopf (Widhopf et al., 1977, 1978) models.

The basic problems in the development of atmospheric photochemical models have involved the numerical simulation of complex couplings among atmospheric radiation, chemistry, and dynamics in the stratosphere and troposphere. *The complexity of these phenomena, coupled with the absence of adequate, relevant, laboratory, and field data, as well as the cost limitations of available computers have imposed severe constraints on the development of photochemical models.* A review of the development of representative 2-D photochemical models has become important due to recent drastic changes in the understanding of the ozone chemistry as a result of a direct measurement of the reaction rate for $HO_2 + NO \rightarrow OH + NO_2$ by Howard and Evenson (1977).

A summary of 2-D developments as of mid-1978 is given below for (a) a reference atmosphere defined as one without anthropogenic effects on ozone from either aircraft effluents or surface emissions of chlorofluoromethanes. This latter condition has implied omission of the more recent chlorine chemistry in 2-D models, (b) the formulation of the dynamics for an atmosphere assumed to be perturbed by large emissions of aircraft effluents, and (c) the probable trends of aviation effects on ozone due to the revised understanding of the atmospheric chemistry. This summary of 2-D developments is then followed by some recommended areas for future work.

S.1 REFERENCE ATMOSPHERE

Significant efforts have been concerned with the problem of calculating excessive ozone in the reference stratosphere from use of the Howard-Evenson (1977) rate coefficient for HO_2

+ NO → OH + NO_2. A 2-D model (Widhopf and Glatt, 1978), utilizing this 1977 rate coefficient along with other 1977 revisions of the chemistry, cannot calculate enough ozone destruction to obtain a balance between ozone production and destruction that matches the observed ozone in the stratosphere. Results from this model, based on a revised 1977 chemistry, yield (a) ozone concentrations that are larger than those based on previous (1976) chemistry by as much as 28 percent at 35 km altitude at middle northern latitudes during summer (Fig. 11 and Table 5), (b) ozone columns for the combined stratosphere and troposphere that were from 20 to 30 percent larger than either observations or those obtained with previous (1976) chemistry, and (c) tropospheric ozone columns, representing about 10 percent of the combined tropospheric and stratospheric columns, that are significantly higher than the corresponding values based on 1976 chemistry (Tables 4 and 5), but still lower than observations. Subsequent 1-D model results incorporating a 1978 measurement of the rate coefficient for $HO_2 + O_3 \rightarrow OH + 2\ O_2$ (Howard, 1978), indicated a decrease (by about 9 percent) of the reference 1-D ozone column as a consequence of using the 1978 instead of the 1977 rate coefficient for $HO_2 + O_3 \rightarrow OH + 2\ O_2$ (Zahniser and Howard, 1978). Similar considerations in the Widhopf 2-D model indicate that the reference ozone column at middle northern latitudes during summer also decreases when using the 1978 instead of the 1977 rate coefficient for $HO_2 + O_3 \rightarrow OH + 2\ O_2$ in combination with the 1977 rate coefficient for $HO_2 + NO \rightarrow OH + NO_2$; however, this later 2-D result represents an ozone column that is still about 10 percent higher than the corresponding observations at middle latitudes during summer. Furthermore, this 2-D ozone column decrease is caused mainly by a corresponding ozone decrease in the lower stratosphere; i.e., the calculated ozone imbalance in the middle stratosphere appears to be sensitive mainly to the 1977 rate coefficient of $HO_2 + NO \rightarrow OH + NO_2$ in an oxygen-hydrogen-nitrogen

(O-H-N) atmosphere (Fig. 11). Therefore, this preliminary 2-D result suggests a need for a reassessment of the remaining reaction rate coefficients for an O-H-N atmosphere as well as the consideration of chlorine chemistry in the middle and upper stratosphere.

The use of the Howard-Evenson (1977) rate coefficient for $HO_2 + NO \rightarrow OH + NO_2$ in the Widhopf 2-D model, together with 1977 chemistry and a revised rainout sink decreases the *calculated* NO_x in the upper troposphere by more than an order of magnitude from the corresponding value based on 1976 chemistry. This result indicates, then, calculated NO_x concentrations in the upper troposphere that are in far better agreement than before with available limited observations (Noxon, 1978). A correct calculation of the NO_x background in the upper troposphere is of particular interest for the effect of subsonic flight on the ozone column.

Estimates of the NO_x concentrations in the troposphere have been made by Fishman and Crutzen (1978) using a 2-D tropospheric, nondynamic, chemical model. These estimates are based mainly on (a) the sensitivity of the tropospheric ozone balance between photochemical production and destruction to NO_x amount (Table 6), (b) the sensitivity of the tropospheric CO budget to NO_x amount through the effect of NO_x on OH (Table 7), and (c) a revised chemistry and radiation as given by the Howard-Evenson (1977) rate coefficient for $HO_2 + NO \rightarrow OH + NO_2$, a third body component for the rate coefficient of $CO + OH + M \rightarrow H + CO_2 + M$, the NASA (1977) recommended chemistry, and the temperature dependence of the quantum yield in the photolysis of $O_2 + h\nu \rightarrow O(^1D) + O_2$. The results of these sensitivity calculations yield NO_x concentrations in the upper troposphere at middle northern latitudes that are in rather good agreement with the foregoing Widhopf 2-D model results based on 1977 chemistry (Fig. 13; Widhopf, 1978) as well as the

Noxon observations. This sensitivity study of the CO budget also provides estimates for the unknown heterogenous removal rate of water-soluble species in the troposphere. It is thus estimated that the inverse heterogenous removal rate constant of H_2O_2 in the troposphere is, at most, of the order of 14 hr (Table 10). Finally, it is important to note that the use of the 1977 rate coefficient for $HO_2 + NO \rightarrow OH + NO_2$ gives more reasonable values than before for the photochemical sources and sinks in the CO budget.

S.2 DYNAMICS OF THE PERTURBED ATMOSPHERE

The present extension of arbitrary 2-D parameterizations of the essentially unknown dynamics in the reference stratosphere to describe the *mass* transports of effluents in the stratosphere perturbed by aircraft effects has no scientific basis. The present parameterizations of the 2-D dynamics for the reference stratosphere are based on two arbitrary assumptions (Reed and German, 1965): (a) uncoupling of the mass transports by the meridional (2-D) circulation from the eddy mass transports by macroscale turbulence, which is not justified by the equations of motion (Tables 16, 17); and (b) adaptation of the Prandtl mixing length hypothesis for the eddy transport of momentum in microscale flow to describe the mass transport by macroscale turbulence in the atmosphere. The adaptation of this hypothesis to the stratosphere is based on assumptions concerning the *unobservable* magnitude of a mixing length path angle (α) defined by the ratio of the vertical to the horizontal eddy transports (Fig. 18). The use of the basic 3-D conservation equations for the mass transport from an instantaneous release of a passive tracer in the stratosphere indicates that the magnitudes of the mixing length path angles are not as given in the 2-D parameterizations of the stratospheric dynamics (Tables 13 through 15 and 18). The mixing length path angles from the conservation equations, when coupled with the mixing length

hypothesis, would then lead to negative values of the eddy diffusion coefficients for the reference stratosphere, which are physically unacceptable (Tables 19, 20). Furthermore, the relative behavior of the α-parameter is not the same in the reference and perturbed upper troposphere as well as stratospheres, as indicated by the 3-D solutions for the mass transport from a continuous release (i.e., SST or supersonic transport-like sources) of a passive tracer (Table 18). The significance of these results is as follows:

- Any empirical parameterization of the 2-D dynamics for the *reference* stratosphere based on appropriate observations would indeed be acceptable, even if they were to utilize concepts other than the mixing length approach. Two relevant points are as follows: (a) such observations have been difficult to achieve due to the smallness of the vertical transports in the stratosphere (Oört and Rasmusson, 1971), and (b) the available 2-D parameterizations for the reference atmosphere, based on the mixing length concept are not internally consistent at every latitude in the stratosphere and upper troposphere (Section 4.1.2). Hence, just as photochemical models identify their use of reaction rate coefficients, they must also document their use of eddy parameters in the lower atmosphere ($0 < z < 50$ km).

- The extension of any empirical 2-D dynamics for the reference atmosphere to the significantly enhanced mass eddy transports of engine effluents in the flight corridors of the perturbed upper troposphere and lower stratosphere is not justified by the conservation equations (Figs. 25 vs 26, Tables 18 through 20), which are the only means to describe the eddy transports of mass in the atmosphere perturbed by aircraft effluents.

It is important to note that the ozone perturbations due to the distribution of NO_x effluents in the upper troposphere, as calculated from the 1976 Crutzen 2-D model of the dynamics and chemistry (Hidalgo and Crutzen, 1977), are expected to increase due to subsequent revisions in the chemistry alone (Section 3.2.2). Hence, it also becomes important to revise the 1976 extensions of the dynamics of the reference atmosphere to the perturbed conditions.

S.3 AVIATION EFFECTS

Reliable assessments of aviation effects as a function of projected air traffic, latitude, and season for subsonic and/or supersonic high-altitude flight are not available because 2-D models have not yet incorporated validated (a) chemistry for an O-H-N and chlorine atmosphere and (b) dynamics for the perturbed upper troposphere and lower stratosphere. Therefore, the available preliminary 2-D results may be suggestive more of a trend than absolute assessments of probable aviation effects on atmospheric ozone.

Previous 2-D estimates based on 1976 chemistry by Hidalgo and Crutzen (1977) of the ozone column *increase* due to NO_x emissions from an assumed 1990 traffic of subsonic aircraft in the upper troposphere (Fig. 7) will become larger from the use of the Howard-Evenson (1977) measurement of the rate coefficient for $HO_2 + NO \rightarrow OH + NO_2$ (Table 9). Furthermore, the previous 2-D estimate based on 1976 chemistry by Widhopf, et al. (1977) of the peak ozone column *increase* by NO_x emissions from a 1990 combined fleet of subsonic and supersonic transports (Fig. 10) becomes larger by a factor of about 2.5 from the use of (a) the 1977 rate coefficient for $HO_2 + NO \rightarrow OH + NO_2$, (b) the NASA (1977) recommended rates for other reactions, (c) a modified dynamics for the middle and upper stratosphere, (d) the simultaneous emissions of NO_x and H_2O effluents, and (e) a larger

SST fleet by a factor of 3 (Widhopf and Glatt, 1978). However, this result for the combined fleet is indicative more of the direction than the magnitude of the effect of aircraft effluents on the ozone column from the 1977 revisions of the 1976 ozone chemistry. This is so because of the following constraints on this result: (a) use of the 1977 instead of the 1978 rate coefficient for $HO_2 + O_3 \rightarrow OH + 2\ O_2$, (b) use of the 1977 (none) instead of the 1978 temperature dependence for the rate coefficient of $HO_2 + NO \rightarrow OH + NO_2$, and (c) the calculated imbalance between ozone production and destruction in the reference stratosphere (Fig. 11). Nevertheless, the significance of these preliminary considerations for individual subsonic (Table 9) and combined subsonic and supersonic fleets is to make the modeling of the upper troposphere for aviation effects more important than ever before.

Furthermore, the absolute magnitude of current 2-D forecasts of aviation effects on the ozone column are inconclusive due to the following factors: (a) lack of experimental verification of the 1978 rate coefficients in several chemical reactions for the effects of subsonic and supersonic cruise flight in the upper troposphere and lower stratosphere, respectively; (b) lack of adequate data to determine the tropospheric budgets of species such as NO_x, OH, and CO. It is important to note that measurements of species with a short lifetime (e.g., OH) require simultaneous measurements of related species (e.g., H_2O, O_3, NO_x, H_2O_2, CO, and CH_4) to permit proper interpretation of their variability; and (c) lack of a validated dynamics for the perturbed upper troposphere and lower stratosphere as a result of extensions of arbitrary parameterizations of the dynamics of the reference atmosphere to an atmosphere perturbed by assumed large emissions of engine effluents. The foregoing factors become important for the forecast of small aviation effects on atmospheric ozone, which are the result of the difference between two large numbers; i.e., of the ozone columns of the

perturbed and reference (without aircraft effects) atmospheres. The absolute magnitude of forecasts of larger aviation (or any other anthropogenic) effects on the ozone column are also open to question, because current 2-D (or 1-D) photochemical models cannot account for feedback effects on ozone changes from changes in the temperature and dynamics of the perturbed stratosphere.

S.4 RECOMMENDED AREAS FOR FUTURE WORK

Although significant attention continues to be given to the experimental measurement of critical reaction rates for the assessment of anthropogenic effects on atmospheric ozone, there are other problem areas that merit consideration, as described below.

A sensitivity analysis, based on 1-D models, is needed to establish the relative importance on the ozone effects from aviation of the uncertainties in the knowledge of reaction rates and reaction mechanisms in the tropospheric ozone chemistry. This sensitivity analysis is becoming of interest because 2-D results, based on 1977 revisions of the ozone chemistry, indicate an increased importance of the effect of subsonic flight in the upper troposphere on the ozone column.

The extension of the 2-D parameterizations of the dynamics for the reference atmosphere to the dynamics perturbed by assumed large emissions of engine effluents in the upper troposphere and lower stratosphere should be evaluated by comparing 2-D distributions of passive tracers with corresponding zonal averages of 3-D numerical solutions for aircraft-like sources of such tracers in the upper troposphere and lower stratosphere, some of which are beginning to become available from the GFDL model (Mahlman, 1978).

Statistical-dynamical 2-D formulations of the dynamics are needed for the transports of mass in the perturbed upper troposphere and stratosphere for assumed large emissions of engine effluents from high-altitude subsonic and supersonic flight. Such statistical-dynamical approaches, when applied to the troposphere, have been able to simulate the three-cell structure of the troposphere (Fig. 19). The development of a statistical-dynamical 2-D model for the stratosphere would avoid the use of the Prandtl mixing length hypothesis, but will stress the current meteorological understanding of the stratosphere. Because of the relative difficulty of this endeavor, an early advent of a valid 2-D statistical-dynamical formulation of the stratospheric dynamics will also depend on the priority set for such endeavor by dynamic meteorologists.

1. INTRODUCTION

During the last few years, a great deal of effort has been devoted to understanding the potential impact of high-altitude aircraft flights on the atmospheric ozone column. The interest in ozone stems from its strong absorption of UV-B solar radiation at wavelengths (λ) in the range $290 < \lambda < 320$ nm. A decrease of the ozone column by aircraft engine effluents, for example, would increase the UV-B radiation flux at the ground; an effect that could have complex ramifications on the biosphere (Grobecker et al., 1974; National Academy of Sciences, 1975).

Flight regimes of current interest include future subsonic and supersonic transports (SSTs) operating at cruise altitudes (z) between $6 < z < 14$ km and $15 < z < 19$ km, respectively (e.g., Oliver et al., 1977). The mechanisms by which high-altitude flight would have an impact on atmospheric ozone are (1) the deposition of NO_x and water vapor (H_2O) engine effluents in the flight corridors, where NO_x stands for both nitric oxide (NO) and nitrogen dioxide (NO_2); (2) the eventual global dispersion by air motions of such engine effluents throughout the lower atmosphere ($0 < z < 50$ km), and (3) the photochemical and chemical kinetics reactions of the aircraft NO_x and H_2O effluents with species that control directly or indirectly the formation and destruction of atmospheric ozone. While any detrimental effect of high-altitude flights on atmospheric ozone could, of course, be reduced through worldwide regulations on the NO_x and H_2O engine emissions, the assessment of the effect of engine effluents on ozone is essential in order to (a) prevent any costly, unnecessary regulation; and (b) persuade governments, on an international basis, of the need for any necessary regulations.

The complexity of atmospheric phenomena involving UV solar radiation, photochemistry as well as chemical kinetics, and air motions represents a very difficult obstacle to the goal of achieving an accurate assessment of the effects of aircraft effluents on atmospheric ozone. While the overall scientific *methodology* for the ozone problem (relative to that for climate change) appears to be in hand (e.g., Hidalgo, 1978), the sources of basic difficulties are, in general, as follows:

- Lack of adequate laboratory data to help develop complete and valid models of the photochemistry and gas-phase chemical kinetics in important regions of the lower atmosphere ($0 < z < 50$ km).
- Lack of adequate laboratory data to establish the heterogeneous chemistry of water-soluble trace species or sinks for such species in the lower troposphere. These sinks are important because they can have significant effects, for example, on the long-term concentrations of NO_x in the lower atmosphere.
- Lack of adequate atmospheric statistics to define the global distributions of relevant trace chemical species in the lower atmosphere as a function of latitude, altitude, and season. These statistical data are important to help model (a) the chemistry by providing constraints on ratios and budgets of atmospheric chemical species, (b) the transports of such species by air motions, and (c) the variability of their distributions, due to the variability of both the UV-B radiation and air motions, for any given month or season during successive annual cycles.
- The limitations in current computer capabilities (i.e., speed and cost) when attempting to perform global calculations of the lower atmosphere with an without aircraft effluents.

A forceful appreciation of the foregoing constraints can perhaps be obtained by considering the following additional factors: (a) the smallness of the probable threshold value for permissible (i.e., unregulated) decreases in the ozone column due to NO_x and H_2O aircraft effluents (perhaps 0.5 percent, Grobecker et al., 1974), (b) the calculated small changes in the ozone column by aircraft effluents, changes that are the result of the difference between two large numbers; i.e., the ozone column perturbed by the aircraft effluents and a reference ozone column that is unperturbed by such effluents. It should be noted that this factor is of particular interest whenever the temperature field and mass transports in the perturbed atmosphere are actually different from those in the reference atmosphere, and (c) the long-term transient nature of the reference ozone column without aircraft effects, since the reference ozone column is a variable that depends on other time-dependent natural (i.e., variability) and anthropogenic effects. The latter stem from emissions at the ground level of chlorofluoromethanes (National Academy of Sciences, 1976); nitrous oxide resulting from use of industrial fixed nitrogen fertilizers (Crutzen, 1976; McElroy et al., 1976; Liu, 1977); and carbon monoxide (CO), which interacts, ultimately, with methane (CH_4), and water vapor in the stratosphere (Crutzen and Fishman, 1977).

It is therefore to be expected that the foregoing four types of basic constraints have brought about severe limitation on the development of adequate photochemical models of the lower atmosphere ($0 < z < 50$ km). For example, under the time constraints of the recent Climatic Impact Assessment Program (CIAP), it was only possible to develop a 3-D model based on (a) low geographical resolution ($\sim$ 1500 km), (b) an auxiliary 2-D model for the distribution of NO_x effluents, and (c) very restricted (now obsolete) 1974 chemistry (Cunnold et al., 1975, 1977; Hidalgo, 1976). In the same time scale of CIAP, it was

also possible to develop a 3-D model with a high geographical resolution (~ 250 km) for the study of the dispersion of a chemically inert tracer in the lower atmosphere ($z < 31$ km), a tracer that was assumed to dissipate ultimately only in the rainout sinks of the lower atmosphere (Mahlman, 1973, 1975).

To circumvent the severe restrictions brought about by computer limitations on the considerations of the complex chemistry, it also became necessary to consider, during CIAP, the development of 2-D and 1-D photochemical models (Grobecker et al., 1974; Hidalgo, 1976). The development of 2-D models was based on considerations of the time scales for the chemistry and air motions, which suggested that the longitudinal effects may be disregarded, as a first approximation, for aviation effects on ozone in time scales significantly longer than the diurnal cycle introduced by the earth's rotation. The 2-D photochemical models, then, had to describe the radiation, chemistry, and air motions in the lower atmosphere in terms of longitudinal or zonal averages of appropriate variables at each latitude and altitude. The further development of the more practical 2-D models in a time scale subsequent to CIAP, has continued to put emphasis on the couplings among radiation, chemistry, and dynamics in the lower atmosphere.

A main objective of this paper is therefore to describe the status, as of mid-1978, of the development of representative two-dimensional photochemical models of interest to the current High Altitude Pollution Program (HAPP) of the Federal Aviation Administration (FAA). As indicated previously, atmospheric photochemical models are indispensable tools to simulate the lower atmosphere ($0 < z < 50$ km) with and without aircraft effluents. An output of these 2-D models is then the assessment of the potential effects, subject to the four basic constraints noted before of subsonic and supersonic flights on the ozone column as a function of latitude, season, and both the location and intensity of present and near-future world airline traffic.

A review of the development of 2-D photochemical model has become important at this time because of recent drastic changes in the description of the relevant ozone chemistry. Important review considerations are also the several arbitrary parameterizations for the essentially unknown dynamics in the reference stratosphere and the arbitrary extensions of such parameterizations to the stratosphere and upper troposphere perturbed by assumed large emissions of engine effluents.

The scope of this paper excludes direct consideration not only of the 3-D but also of the 1-D (altitude only) photochemical models, since the latter are useful only to provide estimates of aviation effects on the global and annual averages of the ozone column for a globally and seasonally uniform air traffic at given flight altitudes.*

1.1 ATMOSPHERIC CHARACTERISTICS RELEVANT TO AVIATION EFFECTS

A clearer understanding of the basic problems in HAPP requires a brief review of the relevant atmospheric characteristics of the lower atmosphere between the ground and 50 km altitude. Basic characteristics of interest are the variation of temperature with altitude as well as the trace chemical gaseous species that can interact directly or indirectly with atmospheric ozone.

As described in the rather extensive body of literature (e.g., CIAP Monograph 1), the lower atmosphere between 0 and 50 km consists of the troposphere and stratosphere. The troposphere is the lowest atmospheric layer that extends from the

*1-D photochemical models have, however, been a powerful tool for examining the sensitivity of aviation effects to the uncertain knowledge of the chemistry.

from use of the Howard-Evenson (1977) rate coefficient for HO_2

ground to the tropopause. The location of the tropopause is at about 16 km at low latitudes, 0, (i.e., 30°N < 0 < 30°S) which decreases to about half as much at the colder high latitudes. The troposphere is characterized by a negative vertical temperature gradient, which tends to vanish at the tropopause. The layer immediately above the tropopause is the stratosphere, which extends upwards from the tropopause to the stratopause at about 50 km altitude. The stratosphere is characterized by a negligible vertical temperature gradient in the lower stratosphere ($z_t < z \lesssim 20$ km, where z_t denotes the tropopause altitude) and a positive vertical temperature gradient at the middle and upper stratosphere. The positive vertical gradient tends to vanish at the stratopause. It is important to indicate that the vertical temperature gradients in the stratosphere are produced by the absorption of UV solar radiation by ozone. Therefore, the altitude regime for subsonic cruise (6 < z < 14 km) extends to the upper troposphere and even lower stratosphere at middle latitudes, whereas that for SSTs (15 < z < 19 km) is located in the lower stratosphere.

Figure 1, after Crutzen (1978), summarizes schematically the atmospheric chemical species of main interest to HAPP. This figure shows the origin as well as the estimated world's budgets for the relevant gases in the ozone (O_3) chemistry; i.e., nitrous oxide (N_2O), oxides of nitrogen (NO_x), water vapor (H_2O), methane (CH_4), carbon monoxide (CO), hydrogen (H_2), methyl chloride (CH_3Cl), and fluorocarbons ($CFCl_3$, CF_2Cl_2). The arrows in the figure indicate whether a given chemical is being removed from or released to the atmosphere. The numbers at the ground level are their respective fluxes in molecules per cm^2sec. The numbers in the troposphere are estimated volume-mixing ratios (i.e., concentrations relative to air) whereas the percent values given at the tropopause indicate the fraction that reaches the stratosphere. The percent values at the bottom of the figure indicate the relative anthropogenic

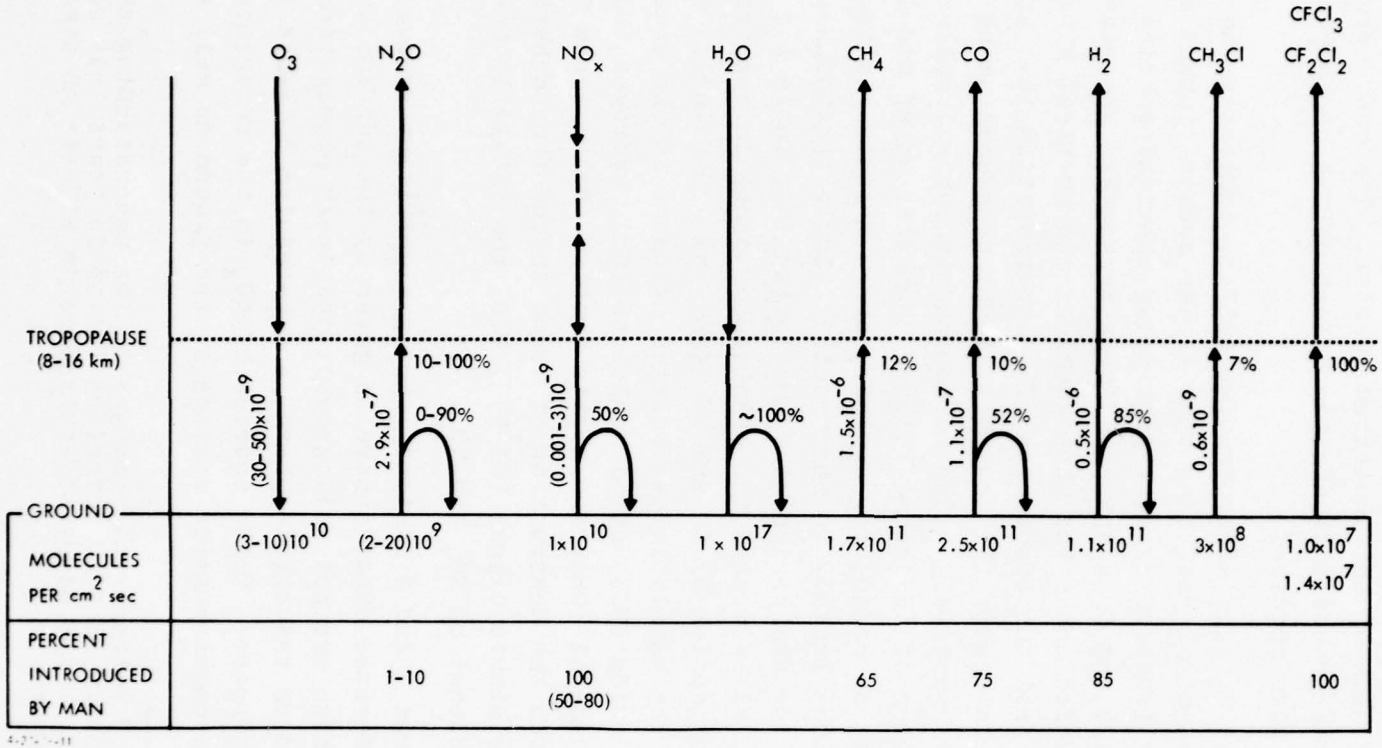

FIGURE 1. Approximate estimates of gas budgets of the world. Other gases not shown here are HCl and SO_2 from infrequent volcanic eruptions; the estimates for the HCl and SO_2 sources vary from 0.7×10^8 to 4.5×10^8 molecules per cm^2-sec, with 4% of these amounts penetrating the stratosphere. (Source: Crutzen, 1978)

coefficient of $HO_2 + NO \rightarrow OH + NO_2$ in an oxygen-hydrogen-nitrogen

based on 1977 chemistry (Fig. 13, Wuebbles, 1981).

S-4

source for each of the indicated species. The bent arrows touching the ground indicate the effect of the tropospheric sinks for such species.

Figure 2, also after Crutzen (1978), indicates the mechanisms or chemical reactions that either create (inward arrows) or destroy (outward arrows) particular chemical species in the stratosphere and troposphere. These mechanisms are given in Table 1, which shows the photochemical and chemical kinetics processes from the absorption of solar radiation ($h\nu$) at several wavelengths (λ) and collisional processes among chemical species, respectively. The mechanisms in Table 1 reflect the understanding of the ozone-related chemistry as of mid-1978.* In the case of ozone, for example, arrow 1 indicates the creation of ozone (mainly in the tropical middle stratosphere) by photolysis or absorption of UV radiation (M1, Table 1); whereas arrow 4(a, b) indicates the creation of ozone in the troposphere from the oxidation of CO and CH_4 (M4a, b). Similarly, arrow 2 indicates the catalytic destruction of ozone in the stratosphere by nitric oxide (NO), atomic chlorine (Cl), hydrogen (H), hydroxyl radical (OH), and atomic bromine (Br). Arrow 3 (a, b, c) indicates the destruction of ozone in the troposphere by metastable atomic oxygen [$O(^1D)$], H_2O, the catalytic $OH\text{-}HO_2$ cycle, and that of NO_x and NO_3.

Figures 1 and 2 indicate that a significant source for NO_x in the reference stratosphere is given by the surface emissions of N_2O (which are not well known), its inert propagation from the ground to the stratosphere, and mechanism 6 (Table 1) in the stratosphere. Other sources of NO_x in the reference atmosphere are anthropogenic sources at the ground as well as

*Because of rather rapid changes in the understanding of the chemistry, a time reference (given in years) has become necessary in the study of anthropogenic effects on atmospheric ozone.

conservation equations, when coupled with the mixing length

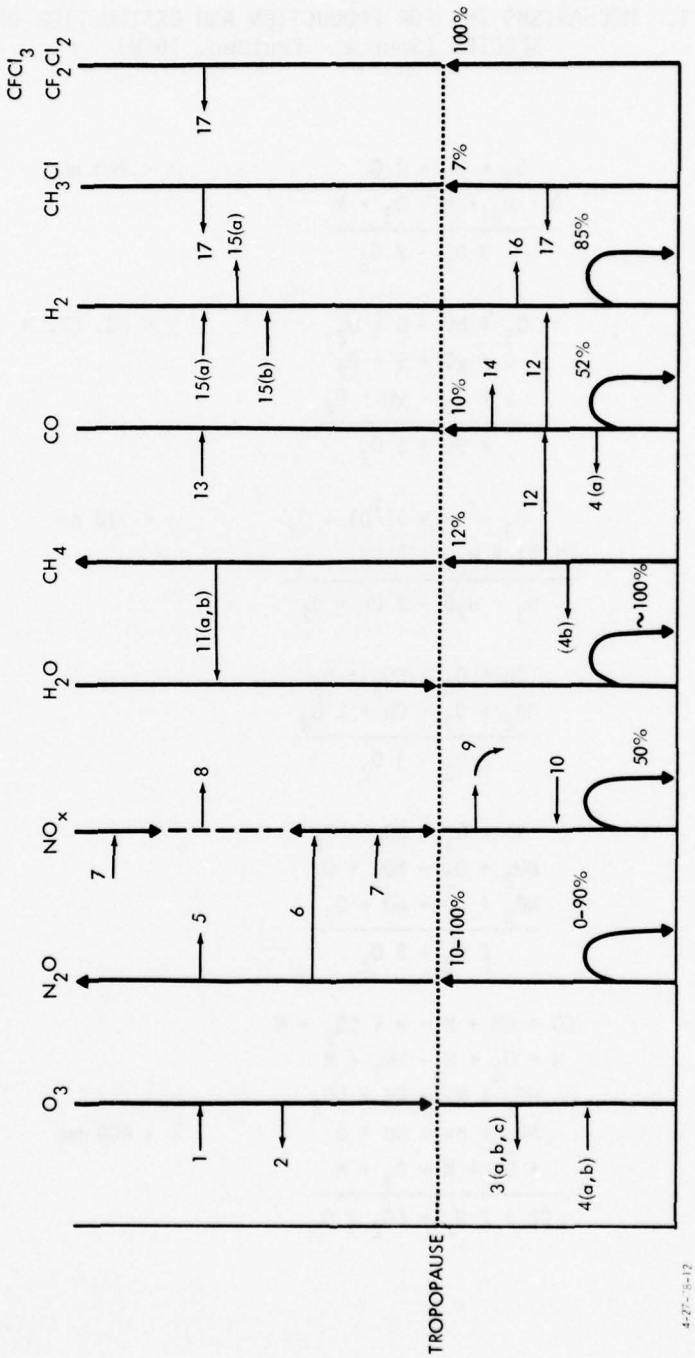

FIGURE 2. Chemical mechanisms in the stratosphere and troposphere. The bent arrows indicate removal of trace species by tropospheric sinks. (Source: Crutzen, 1978)

TABLE 1. MECHANISMS (M) FOR PRODUCTION AND DESTRUCTION OF CHEMICAL SPECIES (Source: Crutzen, 1978)

M1	$O_2 + h\nu \rightarrow 2\ O$	$\lambda < 240$ nm
	$O + O_2 + M \rightarrow O_3 + M$	
	$3\ O_2 \rightarrow 2\ O_3$	
M2	$O_3 + h\nu \rightarrow O + O_2$	X = NO, Cl, H, OH, Br
	$O + XO \rightarrow X + O_2$	
	$X + O_3 \rightarrow XO + O_2$	
	$2\ O_3 \rightarrow 3\ O_2$	
M3a	$O_3 + h\nu \rightarrow O(^1D) + O_2$	$\lambda < 310$ nm
	$O(^1D) + H_2O \rightarrow 2\ OH$	
	$O_3 + H_2O \rightarrow 2\ OH + O_2$	
M3b	$OH + O_3 \rightarrow HO_2 + O_2$	
	$HO_2 + O_3 \rightarrow OH + 2\ O_2$	
	$2\ O_3 \rightarrow 3\ O_2$	
M3c	$NO + O_3 \rightarrow NO_2 + O_2$	
	$NO_2 + O_3 \rightarrow NO_3 + O_2$	
	$NO_3 + h\nu \rightarrow NO + O_2$	
	$2\ O_3 \rightarrow 3\ O_2$	
M4a	$CO + OH + M \rightarrow H + CO_2 + M$	
	$H + O_2 + M \rightarrow HO_2 + M$	
	$HO_2 + NO \rightarrow OH + NO_2$	
	$NO_2 + h\nu \rightarrow NO + O$	$\lambda < 400$ nm
	$O + O_2 + M \rightarrow O_3 + M$	
	$CO + 2\ O_2 \rightarrow CO_2 + O_3$	

taneous emissions of NO_x and H_2O effluents, and (e) a larger

TABLE 1. (cont'd)

M4b*

$$CH_4 + OH \rightarrow CH_3 + H_2O$$
$$CH_3 + O_2 + M \rightarrow CH_3O_2 + M$$
$$CH_3O_2 + NO \rightarrow CH_3O + NO_2$$
$$CH_3O + O_2 \rightarrow CH_2O + HO_2$$
$$CH_2O + h\nu \rightarrow H + HCO \qquad \lambda \leq 350 \text{ nm}$$
$$H + O_2 + M \rightarrow HO_2 + M$$
$$HCO + O_2 \rightarrow HO_2 + CO$$
$$HO_2 + NO \rightarrow OH + NO_2$$
$$NO_2 + h\nu \rightarrow NO + O \qquad \lambda < 400 \text{ nm}$$
$$O + O_2 + M \rightarrow O_3 + M$$

$$CH_4 + 8\ O_2 \rightarrow 4\ O_3 + CO + H_2O + 2\ OH$$

M5

$$N_2O + O(^1D) \rightarrow N_2 + O_2$$
$$N_2O + h\nu \rightarrow N_2 + O \qquad \lambda < 337 \text{ nm}$$

M6

$$N_2O + O(^1D) \rightarrow 2NO$$

M7

$$X + e, h\nu \rightarrow X^* + 2e, e$$
$$X = N_2, O_2, O$$

(Particles, precipitation, protons, electrons, aurorae, extreme UV, X-rays) solar, galactic, cosmic rays.

M8

$$NO + h\nu \rightarrow N + O \qquad \lambda < 191 \text{ nm}$$
$$N + NO \rightarrow N_2 + O$$

$$2NO \rightarrow N_2 + 2\ O$$

M9

$$NO_2 + \text{aerosol, hydrometeors} \rightarrow \text{products}$$
$$NO_2 + OH(+ M) \rightarrow HNO_3(+ M)$$
$$HNO_3 + \text{aerosol, hydrometeors} \rightarrow \text{products}$$

M10

Lightning, $F \approx 1\ (10)$, cm^2/s

M11a

$$CH_4 + OH \rightarrow \ldots\ldots \rightarrow CO, H_2 \rightarrow CO_2, H_2O$$

*The net result in M4b is obtained by considering multiples of the last three reactions; i.e., 4 times the last two, and 3 times the remaining one.

between two large numbers; i.e., of the ozone columns of the

TABLE 1. (cont'd)

M11b	$CH_4 + O(^1D) \rightarrow .... \rightarrow CO, H_2 \rightarrow CO_2, H_2O$	
M12	$CH_2O + h\nu \rightarrow CO + H_2$	$\lambda \leq 350$ nm
M13	$CO_2 + h\nu \rightarrow CO + O$	
M14	$CO + OH(+ M) \rightarrow CO_2 + H(+ M)$	
M15a	$H_2 + O(^1D) \rightarrow H + OH$	
M15b	$H + HO_2 \rightarrow H_2 + O_2$	
M16	$H_2 + OH \rightarrow H + H_2O$	
M17*	$CH_3Cl + OH \rightarrow CH_2Cl + H_2O....\rightarrow ClX$	
	$CFCl_3 + h\nu \rightarrow CFCl_2 + Cl.... \rightarrow 3ClX$	
	$CF_2Cl_2 + h\nu \rightarrow CF_2Cl + Cl.... \rightarrow 2ClX$	
	$CH_3CCl_3 + OH \rightarrow CH_2CCl_3 + H_2O..\rightarrow 3ClX$	
	$ClX = Cl + ClO + HCl + ClNO_3$	
	(In troposphere: rain, washout, aerosol attachment.)	

*Crutzen, Isaksen and McAfee (1978)

natural sources (M7, 10), and sinks (M8, 9), in the troposphere and stratosphere. Figures 1 and 2 also indicate that the stratosphere is a relatively dry medium with natural H_2O sources provided by tropical upwelling (as a function of longitude) of tropospheric moisture as well as reactions of CH_4 with OH and $O(^1D)$ (i.e., M11a, b). The fluorocarbons ($CFCl_3$ and CF_2Cl_2) are of particular importance in a reference atmosphere without aviation effects alone, because of their chemical destruction of stratospheric ozone (M17, 2) and their interaction with the NO_x aircraft effluents.

1.2 MECHANISMS FOR THE MODELING OF AVIATION EFFECTS

Because of the four types of basic constraints in the assessment of aviation effects on the ozone column, as indicated previously, a difficult challenge has been that of achieving a rather accurate modeling of the global distributions of the chemical species shown in Figs. 1 and 2 for a reference troposphere and stratosphere without aircraft effluents and emissions of fluorocarbons. The main mechanisms that must be considered in such modeling, as well as some illustration of the uncertainties involved in each mechanism, are as follows:

1.2.1 Absorption of Solar Radiation

The absorption of solar radiation ($h\nu$) by oxygen, ozone, nitrogen dioxide, nitric acid, etc. takes place at different wavelengths (λ), as indicated in Table 1. Parameters of interest here are the photolysis rates (as defined subsequently in Section 3.2) for mechanisms (M) such as those in M1, M2, and M3a. An example of the uncertain knowledge of some of these photolysis rates is given by the reaction $O_3 + h\nu \rightarrow O(^1D) + O_2$ in M3a; recent laboratory measurements (Arnold et al., 1977; Moortgat et al., 1977) have shown that the quantum yield (defined also in Section 3.2) of metastable atomic oxygen, $O(^1D)$, for ozone photolysis between 300 and 320 nm decreases with decreasing temperature.

Previous calculations had used quantum yield data found at room temperature (e.g., Moortgat and Warneck, 1975).

1.2.2 Rate Coefficients of Chemical Kinetics Processes

The rate coefficients of the chemical kinetics processes (denoted by k's) establish the speed or rate of change of the concentrations (molecules/cm^3) of given chemical species in either the two or three (involving the M species) body reactions in Table 1. The uncertain knowledge of these rate coefficients can be illustrated by recent measurements of these coefficients for (a) $HO_2 + NO \rightarrow OH + NO_2$ (e.g., M4a, b), (b) $HO_2 + O_3 \rightarrow OH + 2\ O_2$ (e.g., M3b), and (c) $CO + OH + M \rightarrow H + CO_2 + M$ (e.g., M4a). Recent developments for these reactions are as follows:

- A direct laboratory measurement of the rate coefficient for $HO_2 + NO \rightarrow OH + NO_2$ yielded a value of $k = (8.1 \pm 1.5)\ 10^{-12} cm^3$/molecule-sec* at a temperature of 296°K (Howard and Evenson, 1977). This result turned out to be higher by a factor of about 40 than the previous accepted value (2.2×10^{-13}), which was used in the 1976 assessments of the effect of high-altitude flight on the ozone column (Hidalgo and Crutzen, 1977; Widhopf et al., 1977). This 1977 result for the rate coefficient of the $HO_2 + NO \rightarrow OH + NO_2$ reaction has had a profound impact on the modeling of the reference ozone column as a function of latitude and season. It is important to indicate that the Howard-Evenson result for the rate coefficient of $HO_2 + NO \rightarrow OH + NO_2$ has been verified at other laboratories (Burrows et al., 1978; Kaufman and Reimann, 1978; Margitan and Anderson, 1978). More recent developments concerning this rate coefficient have yielded its temperature dependence as $k = (3.3 \pm 0.7)10^{-12} exp[(254 \pm 50)/T]$ cm^3/molecule-sec (Howard, 1978). A preliminary

*i.e., $k = (8.1 \pm 1.5)10^{-12}$ cm^3 $molecule^{-1}$ sec^{-1}, which has been broken up as shown for editorial reasons.

result of the temperature dependence for this rate coefficient in the range $270 \leq T \leq 425°K$ has also yielded $k = (4.6 \pm 1.3)10^{-12} \exp [(200 \pm 90)/T]$ cm^3/molecule-sec, where the uncertainties represent double standard deviations (Ming-Taun Leu, 1978).

- A more recent measurement of the rate coefficient for $HO_2 + O_3 \rightarrow OH + 2\ O_2$ yielded $k = (1.4 \pm 0.4)10^{-14} \exp [-(580 \pm 100)/T]$ cm^3/molecule-sec (Howard, 1978). This result is faster than the NASA (1977) recommended rate coefficients ($7.3 \times 10^{-14} \exp -1275/T$) by factors of 3.3 to 4.5 at the (standard) temperature range of the lower (~220°K) and middle (~240°K) stratosphere.
- For the rate coefficient of the $CO + OH \rightarrow CO_2 + H$ reaction, evidence has been found recently of a three-body component (in addition to the two-body component) that becomes important at the high pressure of the troposphere (Sie et al., 1976; Cox et al., 1976; and Chan et al., 1977).

1.2.3 Heterogeneous Processes for the Tropospheric Sinks

Heterogeneous chemical processes determine the removal rate of water-soluble species such as NO_x, nitric acid (HNO_3), hydrogen peroxide (H_2O_2), nitrogen pentoxide (N_2O_5), etc. from the troposphere, and become important in the modeling of their global distributions. The NO_x distributions in the reference troposphere and stratosphere are important in establishing the magnitudes of (a) the perturbations of atmospheric NO_x by the corresponding aircraft effluents, and (b) the consequent changes in the reference ozone column by such effluents. The uncertainty in the magnitude of the observed NO_x concentrations in the troposphere is rather large, because of the variability of polluted and unpolluted conditions at the earth's surface for different geographical locations. Nitric acid is an important sink for

NO_x through mechanism 9 (Table 1), whereas hydrogen peroxide is important for the global distributions in the troposphere of species such as OH, CH_4, and CO (Fishman and Crutzen, 1978). Therefore, the modeling of the heterogeneous processes in the tropospheric sinks becomes important for the assessment of aircraft effects on the ozone column.

1.2.4 Water Vapor (H_2O) Sources and Sinks

The water vapor sources and sinks in the troposphere and stratosphere are important in determining the H_2O distributions in the reference stratosphere, which are in turn important to establish (a) the magnitude of the perturbations of H_2O by the corresponding engine effluents, and (b) the consequent changes in the reference ozone column by such effluents. The uncertainty in the magnitude of the observed H_2O concentrations in the stratosphere is significant, because of the uncertain knowledge of the tropospheric sources and sinks or the transport of H_2O across the tropopause due to (a) the temperature variations as a function of longitude in the upwelling branch of the Hadley cell at low latitudes, and (b) the subsidence or descending transports as a function of latitude.

1.2.5 Mass Transports in the Reference and Perturbed Tropospheres and Stratospheres

The importance of the mass transports by the air motions in the stratosphere, for example, comes about from the facts that (a) they export ozone from the production regions at low latitudes to the northern high latitudes. This mechanism becomes most evident during the polar night of the winter hemisphere, where the ozone column is about twice as large as that at the equatorial latitudes (Fig 3, Dütsch, 1971); and (b) they likewise establish the stratospheric water vapor distributions, which are a result of the H_2O transports across the tropopause or tropospheric sources and sinks in addition to M11(a, b) in Fig. 2. The prevailing practice in the 2-D parameterization of

restricted (now obsolete) 1974 chemistry (Cunnold et al., 1975, 1977; Hidalgo, 1976). In the same time scale of CIAP, it was

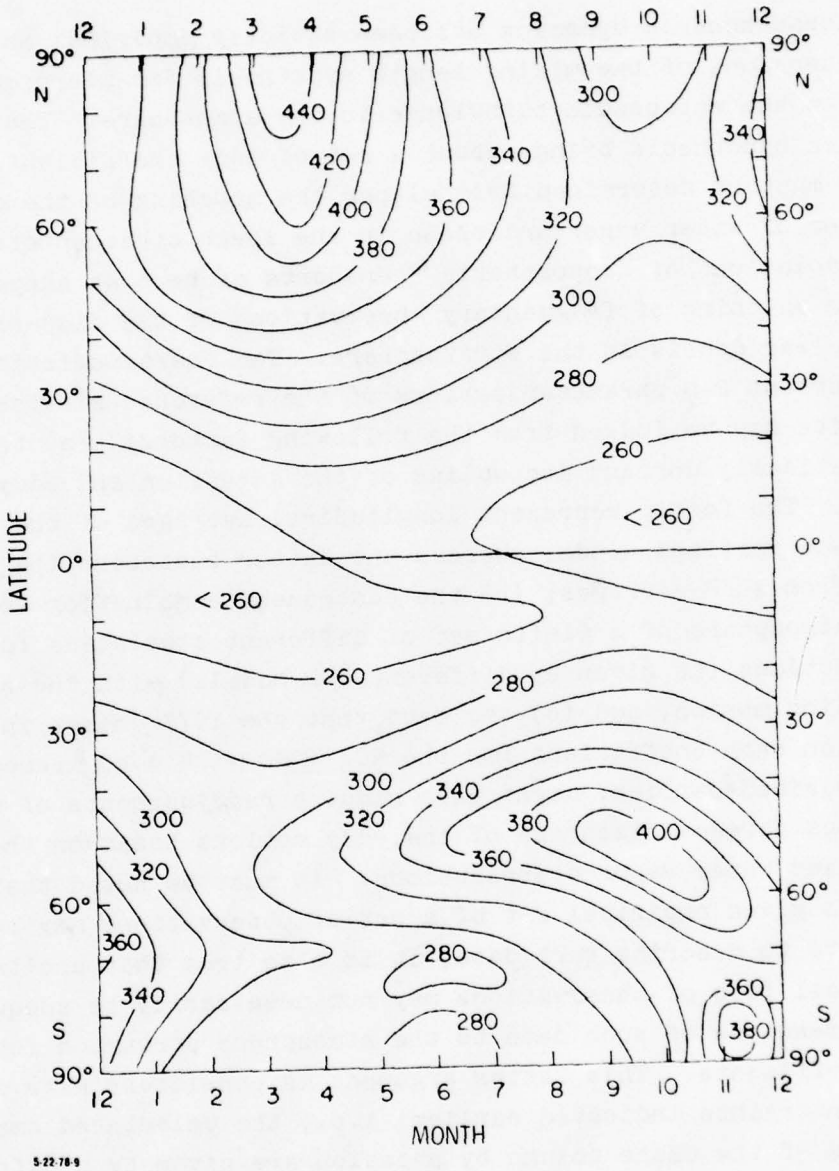

FIGURE 3. Ozone column in reference atmosphere as a function of latitude and month in the Northern and Southern Hemispheres. Numbers are in Dobson units or m-atm-cm; i.e., if the ozone column would be compressed to standard pressure and temperature, its height at 90°N during spring, for example, would be 0.440 cm. Note the asymmetry in the ozone columns in the Northern and Southern Hemispheres. (Source: Dütsch, 1971)

the stratospheric dynamics has been strictly empirical and based on extensions of the mixing length hypothesis for microscale flow to the macroscale turbulence in the atmosphere. The use of this hypothesis brings about a set of eddy coefficients, which must be determined from either the matching of the distributions of water vapor and ozone in the lower stratosphere or extrapolations of tropospheric transports of heat as supported by the matching of fragmentary observations of the dispersion of nuclear debris in the stratosphere. The characteristics of the current 2-D parameterizations of the reference stratospheric dynamics may be judged from the following factors: (a) the theoretically unsound decoupling of the advection and eddy motions. The former represent longitudinal averages of the northward and vertical winds, whereas the latter represent the departure from such averages; (b) the consequent combination for the same atmosphere of a finite set of different statistics for the eddy motions (as given by different 2-D models) with the same advection motion; and (c) the fact that the 1977 change in the reaction rate coefficient for the $HO_2 + NO \rightarrow OH + NO_2$ reaction as described earlier, might also require readjustments of the previous parameterizations of the eddy motions based on the ozone and water vapor distributions. It must be noted that while a given empirical fit of a set of observations may be adequate to describe such data, it is also true that arbitrary empirical fits of observations may not necessarily be adequate for *extensions* of such data to the atmosphere perturbed for aircraft effluents. This latter argument is consistent with one of the constraints indicated earlier; i.e., the calculated small changes of the ozone column by aviation are given by a difference between two large ozone columns for the reference and perturbed atmospheric conditions.

1.3 SUMMARY OF PENDING CHANGES IN THE MODELING OF AVIATION EFFECTS ON OZONE

The foregoing considerations imply a need for significant pending revisions in the 2-D modeling of aviation effects on ozone as a consequence of results from ongoing research in (a) the chemical mechanisms in Table 1 and (b) the numerical solutions of the 3-D equations of motion for instantaneous or continuous releases of passive tracers in the lower stratosphere, to be described later. The basic pending revisions as of mid-1978 of representative 2-D photochemical modeling of the troposphere and stratosphere are as follows:

- Incorporation of chlorine chemistry in the stratosphere, i.e., mechanisms M17, 2 (with χ = Cl) in Table 1; which becomes important in defining a reference atmosphere for aviation effects that takes into account the effects from emissions of fluorocarbons at the earth's surface (Fig. 2). The use of rate coefficients for the chlorine chemistry must consider the NASA (1977) recommended values together with results of ongoing research as they become available. However, any significant ozone decrease from fluorocarbons would also require consideration of feedback effects from the ozone decrease on the temperature and vertical transports of a 2-D reference stratosphere with fluorocarbons.

- Use of the Howard-Evenson (1978) rate coefficients for (a) the reaction $HO_2 + NO \rightarrow OH + NO_2$, including the temperature dependence which has been measured recently; and (b) the reaction $HO_2 + O_3 \rightarrow OH + 2\ O_2$.

- Use of the third body component for the rate coefficient of the reaction $CO + OH + M \rightarrow CO_2 + H + M$ as well as the temperature dependence for the quantum yield in the photolysis rate of $O_3 + h\nu \rightarrow O(^1D) + O_2$.

- Validation of the modeling of the water vapor distributions in the reference stratosphere, which is important for the assessment of the simultaneous effects of NO_x and H_2O engine effluents on the ozone column. While parameterizations of the H_2O distributions in the reference atmosphere are available, the understanding of the actual H_2O budget in the stratosphere is not yet conclusive.
- Other basic considerations involve the 2-D modeling of the dynamics in the upper troposphere and stratosphere, which ought to consider the development of more basic approaches that do not rely on utilizations of the mixing length hypothesis for microscale flow to describe the macroscale turbulence of the atmosphere. A physically correct formulation of the dynamics in the upper troposphere and stratosphere is of special interest for applications to the perturbed atmosphere.

Subsequent sections attempt to elaborate on the foregoing pending revisions of the 2-D modeling of the troposphere and stratosphere. These sections include (a) a brief review of the most recent 2-D model results for HAPP, which are based on 1976 chemistry, (b) the impact of recent revisions of the ozone chemistry on 2-D modeling, and (c) assessment of the 2-D formulation of the atmospheric dynamics for the atmosphere perturbed by aircraft effluents.

2. TWO-DIMENSIONAL MODELING OF AVIATION EFFECTS ON OZONE

The first task in the 2-D photochemical modeling of aviation effects on the reference ozone column is to attempt to simulate numerically, with a fair degree of precision, the meridional (i.e., latitude-altitude) distributions of the important chemical species for the ozone chemistry in the reference troposphere and stratosphere (e.g., Figs. 1 and 2). This task involves the use of the radiative, chemical, and dynamical mechanisms for the production and destruction as well as transport by air motions not only of ozone, but also of every chemical constituent that interacts either directly or indirectly with ozone. The production and destruction mechanisms consist of the gas-phase chemical reactions given in Table 1 and the heterogenous chemical processes in the tropospheric sinks (Fig. 1), while the transports by air motions must take into account those by the advection and eddy motions. The accuracy of the numerical simulations of the reference troposphere and stratosphere may be assessed from comparisons between the calculated and observed vertical profiles as a function of latitude and season for as many species as data are available.

The second task in the 2-D modeling of aviation effects on the reference ozone column is to prescribe the aircraft NO_x and H_2O emissions in the flight corridors of the upper troposphere and lower stratosphere. The results of these considerations are the determination of the aircraft NO_x and H_2O effluents as a function of altitude and latitude for each type of aircraft. These emissions can, of course, also be a function of time (years) as given by projections of future changes in the structure of the world's airline fleets and traffic.

There are two 2-D photochemical models of special interest to HAPP, because they have utilized aircraft emissions of interest

to the FAA. They are the Crutzen model at the National Center for Atmospheric Research (NCAR) and the Widhopf model at the Aerospace Corporation. The Crutzen model has been used to study the effect of individual subsonic or supersonic fleets, assumed to operate by themselves at cruise altitudes in the range of $10.8 \leq z \leq 18$ km, so as to isolate the effect of flight altitude and aircraft type on the total ozone column. The Widhopf model has been used to study the effect of a combined fleet of subsonic and supersonic aircraft operating simultaneously at altitudes in the range $6 \leq z \leq 19$ km. The need for at least two different 2-D photochemical models stems from their complexity, since such results help to identify model-dependent effects which are unrelated to the aircraft effluents.

A unique characteristic of the foregoing 2-D models was their incorporation of the ozone production mechanisms in the troposphere due to CO and CH_4 reactions with OH (i.e., M4a, b, Table 1). As a consequence of these mechanisms, results from the Crutzen model indicated that subsonic flight in the upper troposphere may produce a small increase of the reference ozone column at the northern middle latitudes of the assumed heaviest airline traffic (Hidalgo and Crutzen, 1977). These results were considered tentative in view of the uncertainty in some of the 1976 reaction rate coefficients as well as in the heterogenous removal rates of chemical species in the rainout sinks of the lower troposphere. The magnitude of the increase in the reference ozone column by subsonic flight was apparently large enough to provide a net small increase of the ozone column for a combination of a large subsonic and a small supersonic aircraft fleet (Widhopf et al., 1977). The results from these 2-D models contradicted previous assessments of the net effect of high-altitude aircraft which had been based on the use of 1-D global models that neglected the ozone production mechanisms in the troposphere (Grobecker et al., 1974; National Academy of Sciences, 1975).

As indicated earlier, the foregoing results from the Crutzen and Widhopf models did not incorporate chlorine chemistry (i.e., M17, 2, Table 1) in the reference stratosphere. A question of interest for aircraft effects was then the relative roles of the tropospheric ozone production (M4a, b) and stratospheric ozone destruction (M2, with χ = NO and Cl = Br = 0) mechanisms as indicated in Fig. 2. Thus, even for subsonic flight alone (e.g., at 10.8 km), these two mechanisms would come into play as the aircraft NO_x effluents propagated eventually from the upper troposphere to the middle stratosphere. The Crutzen model indicated that the relative roles of these two mechanisms depended on the flight altitude of aircraft fleets assumed to operate individually at a given cruise altitude. It was found that the CO and CH_4 mechanisms (M4a, b) in the troposphere would prevail over that of the NO_x catalytic cycle (M2) in the stratosphere for subsonic flight at 10.8 km, but that the opposite would be true in the operation of SSTs alone at 18 km altitude (Hidalgo and Crutzen, 1977). For combined instead of individual aircraft fleets, the CO and CH_4 mechanisms in the troposphere would still dominate over that of the NO_x catalytic cycle for assumed conditions of a rather overwhelming subsonic traffic relative to that of SSTs (Widhopf et al., 1977).

It must be emphasized that the foregoing Crutzen model results for the individual aircraft fleets were based on the 1976 estimate of the rate coefficient for the reaction $HO_2 + NO \rightarrow OH + NO_2$, an estimate that turned out to be smaller (i.e., slower) by a factor of about 40 than the value determined subsequently by direct measurements of HO_2 (Howard and Evenson, 1977). The use of the slower rate coefficient for the above reaction also yielded calculated NO_x concentrations in the reference troposphere that were significantly larger than some subsequent NO_2 observations (Noxon, 1978).* As indicated in a subsequent section, the

*The NO_2 observations may be interpreted as NO_x (i.e., NO + NO_2) because the ratio NO/NO_2 is zero for night conditions and approximately unity for daylight conditions.

effect from the much faster rate coefficient for $HO_2 + NO \rightarrow OH + NO_2$ on the perturbation of the ozone column by subsonic aircraft is to increase the effects of the CO and CH_4 mechanisms (M4a, b) as well as to decrease the effect of the stratospheric NO_x catalytic cycle. Furthermore, the Howard-Evenson (1977) rate coefficient yields, now, lower background NO_x concentrations in the reference troposphere which produce larger NO_x perturbations than before for the same level of NO_x emissions by subsonic aircraft. The probable net effect of the faster Howard-Evenson rate coefficient for subsonic flight alone appears then to be an augmentation of the previous increase in the ozone column at northern middle latitudes. For supersonic flight alone, the weakening of the stratospheric NO_x catalytic cycle would tend to diminish the previous decrease in the ozone column at the northern middle and high latitudes.

The results for the combined fleet of subsonic and supersonic aircraft in the Widhopf model were based on a reaction rate coefficient for the $HO_2 + NO \rightarrow OH + NO_2$ reaction that was nearly identical to that in the Crutzen model. Hence, the same qualitative arguments given above for individual fleets indicate that for a combined fleet of subsonic and supersonic aircraft, the faster Howard-Evenson reaction rate coefficient may also augment the previous net increase in the ozone column at the northern middle latitudes for the same combination of NO_x emissions.

The foregoing qualitative considerations suggest a probable combination of a stronger effect from the tropospheric mechanism of ozone production with a weaker effect from the stratospheric mechanism of ozone destruction than before. *The consequence of this result is to make the 2-D modeling of the reference and perturbed troposphere nearly as important as that of the stratosphere, in spite of the fact that the contribution of unperturbed tropospheric ozone to the total ozone column is only of*

the order of 10 percent or so. For this reason, it becomes of interest to review the available 2-D results for the effects of aviation on ozone, as determined from the Crutzen and Widhopf models, which are based on 1976 chemistry.

2.1 RESULTS AND CHARACTERISTICS OF THE 1976 CRUTZEN MODEL

Because of the rather massive amount of data generated by 2-D models for both the reference and perturbed (by aircraft effluents) tropospheres and stratospheres, it becomes necessary to examine such data by emphasizing situations of major interest. These latter conditions may be taken to be the northern middle latitudes during late summer on the following grounds: (a) most of the world's airline traffic is usually assumed to be concentrated at latitudes in the range $15°N \leq \theta \leq 55°N$, with peak NO_x and H_2O emissions occurring at about 45°N (Hidalgo and Crutzen, 1977; Widhopf et al., 1977), (b) the consequent changes in the reference ozone column from subsonic flight are largest in the latitude range $25°N \leq \theta \leq 45°N$, changes that tend to be of the same order of magnitude during any season. However, the changes in the ozone column from a combined fleet of subsonics and supersonics show that they tend to be larger during late summer than in early summer; (c) the intensity of the UV-B solar radiation is largest during summer, as illustrated by Figs. 4a and 4b (Venkateswaran et al., 1975) for winter and summer. These figures indicate that the UV-B radiation at a typical wavelength at the northern middle latitudes decreases by more than two orders of magnitude during winter as compared with summer. These results are also typical of those in Western and Northern Europe (Venkateswaran et al., 1975), and (d) outdoor human activity (with the consequent exposure to UV-B radiation) increases during the longest daylight conditions of the summer season at middle latitudes.

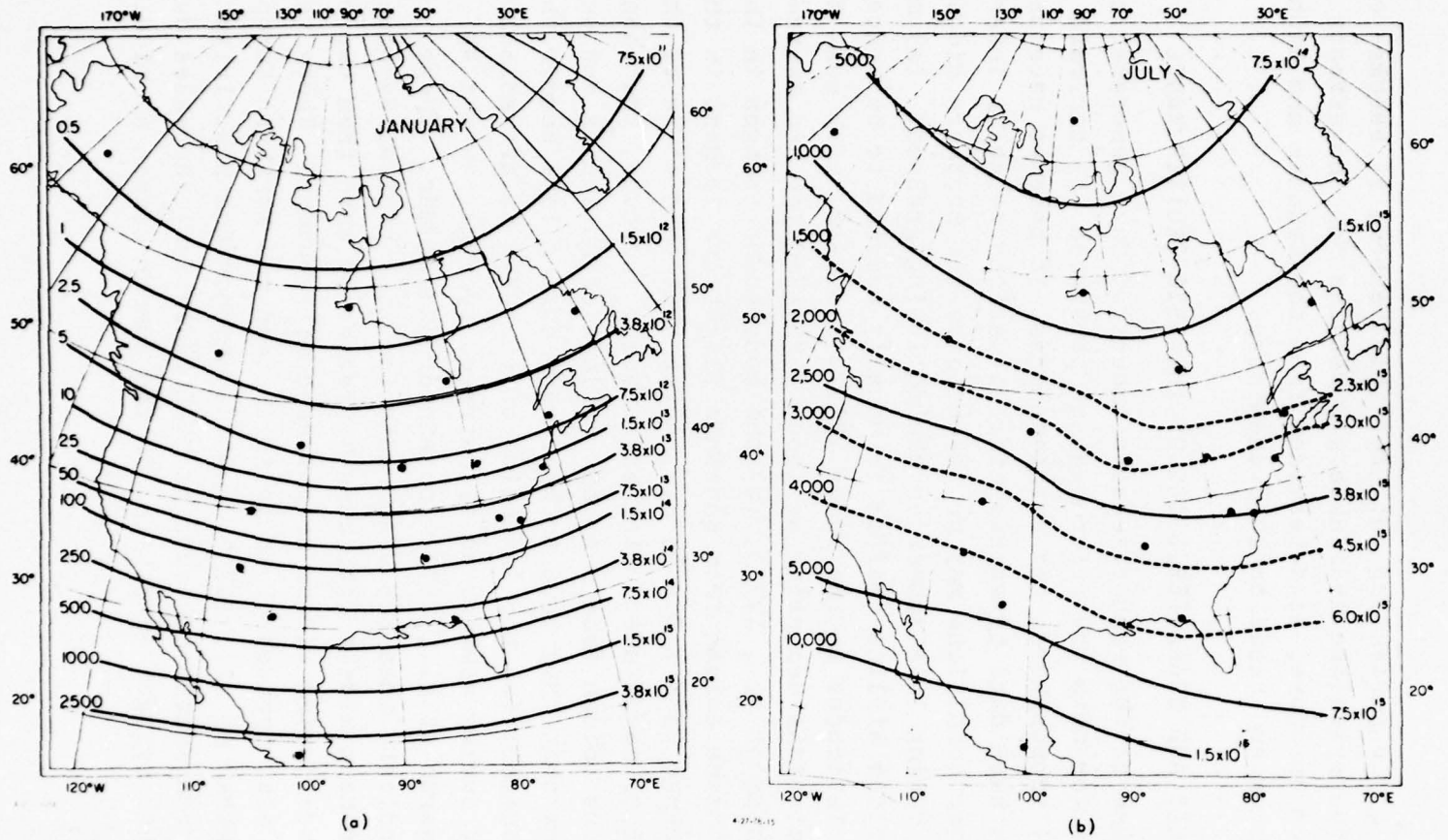

FIGURE 4. Isolines of the daily average of UV solar radiation flux at a typical wavelength of 300.4 nm during winter (January) and summer (July). Numbers on left-hand side are in microwatts/m^2-nm, whereas those on the right are in photons/m^2-sec-nm. (Source: Venkateswaran et al, 1975)

Figure 2 indicated schematically that ozone is generated mainly in the stratosphere by mechanism 1, and the downward direction of the arrow (in that figure) showed that zone descended towards the earth's surface. The ozone concentration as a function of altitude is then the net result of the chemical mechanisms of ozone production and destruction, as indicated in Fig. 2, and the ozone transports by the air motions. Figure 5 shows quantitative results for ozone in the reference atmosphere at 45°N latitude during late summer (August 30) as was simulated by the Crutzen model. This figure shows both the ozone concentration and the growth of the ozone column with decreasing altitude. The ozone concentration reaches a peak value near 23 km (34 mbar), when the ozone column has reached about 52 percent of its total value. The negative vertical gradient of the stratospheric ozone concentration above about 25 km is controlled by the interplay between mechanism M1 and M2 (Fig. 2) as well as the air motions. The ozone production mechanism (M1) becomes weaker with decreasing altitude due to the decay of atomic oxygen with decreasing altitude. For the conditions of Fig. 5, the calculated concentration of atomic oxygen drops from 5.7×10^9 per cm^3 at the stratopause to 4×10^6 per cm^3 at 20 km. Comparisons of the characteristic times for the chemistry and dynamics indicate that the former are short relative to that of the dynamics in the upper and middle stratosphere, while the opposite is true in the lower stratosphere (e.g., Johnston, 1975). Therefore, the chemistry is fast and in near equilibrium in the upper and middle stratosphere but slow in the lower stratosphere, where ozone has been considered in the past to be nearly chemically inert. These different relative roles of the chemistry and dynamics as a function of altitude in the stratosphere will be used in subsequent sections for considerations of either the parameterizations of the dynamics in the lower stratosphere or the consistency of the chemistry itself. Hence, the positive vertical gradient of the stratospheric ozone concentration below

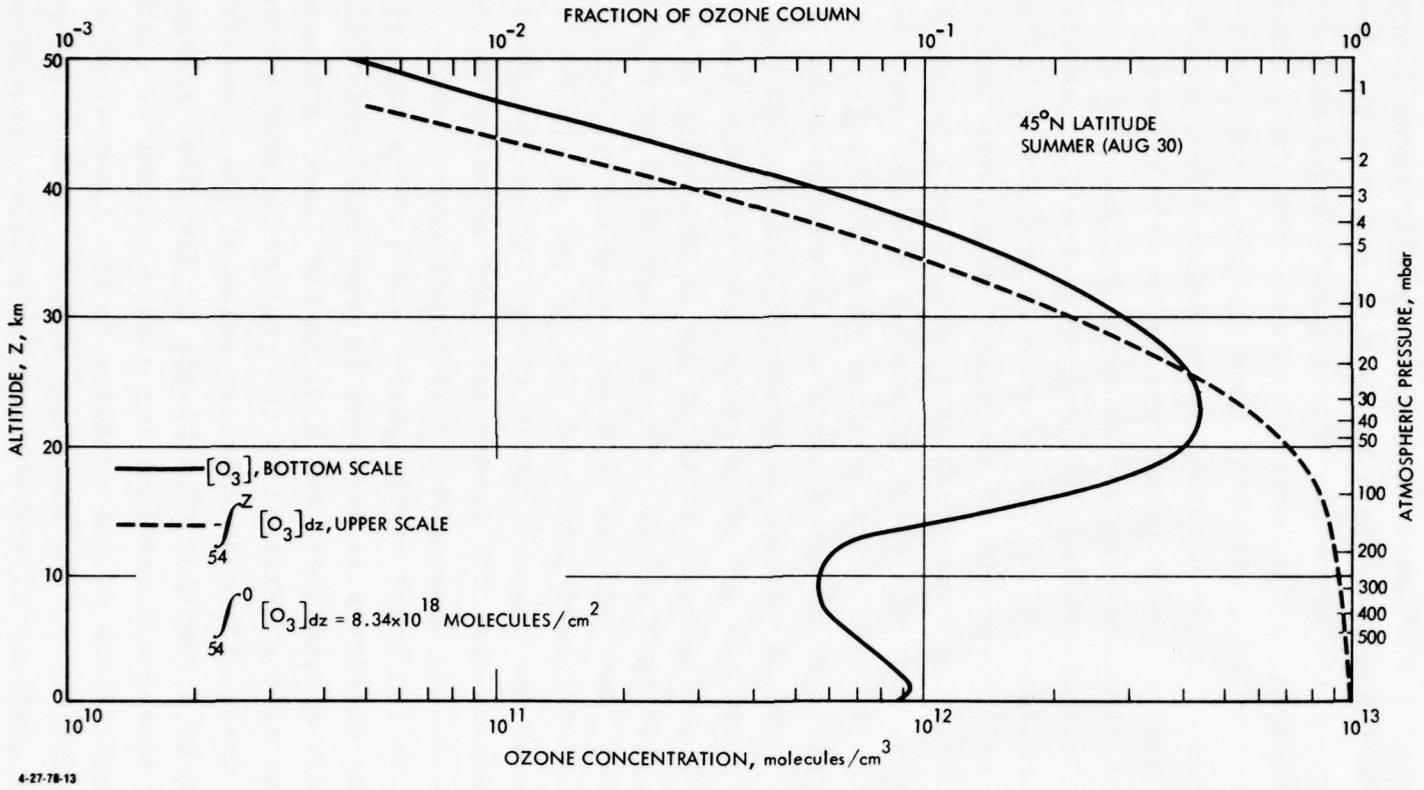

FIGURE 5. Simulated ozone concentration (bottom scale) and ozone column growth with decreasing altitude (top scale) for the reference atmosphere at 45°N during summer (August 30). (Source: Hidalgo and Crutzen, 1977)

about 23 km in Fig. 5 is the result of the dominant role of the ozone transports by the air motions. The results for the buildup of the ozone column with decreasing altitude (Fig. 5) shows that (a) about 3 percent of the ozone column is created above 40 km (2.7 mbar) and (b) the contribution of the tropospheric ozone (below 10 km) is about 9 percent of the total ozone column, which has a value of 328.6 m-atm-cm (or Dobson units) at 45°N latitude during late summer. The former result for the upper stratosphere becomes of interest in attempts to validate the understanding of the NO_x chemistry by taking advantage of the locally large perturbations of ozone during the infrequent solar proton events (i.e., M7, Table 1; Heath et al., 1977); whereas the latter result, for the contribution of tropospheric ozone to the ozone column, is of interest in considerations of the effect of high-altitude subsonic flight on the ozone column.

Table 2a shows the vertical distributions of the daylight, zonal averages of O_3 and NO_x related species as simulated by the Crutzen model with 1976 chemistry at 45°N latitude during late summer. The first ozone column represents its concentration in molecules per cm^3. The subsequent columns provide the volume mixing ratio (i.e., the concentration of a given chemical constituent normalized with that of air) of ozone, nitrous oxide, NO_x (defined here as $NO + NO_2 + 2N_2O_5 + NO_3$), nitrogen pentoxide ($N_2O_5$), NO_3, and nitric acid (HNO_3). The numbers in parentheses denote exponents for the given value. For example, the peak ozone concentrations at 23.41 km given as 4.38(12) denotes 4.38×10^{12} molecules/cm^3. Table 2b shows similar data for water vapor, HO_x, CO, and CH_4. The first H_2O column is the simulated relative humidity, whereas the subsequent columns represent the volume mixing ratio for water vapor, hydrogen peroxide (H_2O_2), OH, CO, and CH_4.

TABLE 2a. DAYLIGHT, ZONAL AVERAGES OF OZONE, N_2O, NO_x, N_2O_5, NO_3 and HNO_3 SPECIES IN THE REFERENCE ATMOSPHERE AS WAS SIMULATED BY THE 2-D CRUTZEN PHOTOCHEMICAL MODEL WITH 1976 CHEMISTRY AT 45°N DURING LATE SUMMER (AUGUST 30)*

Z(km)	$[O_3]$	O_3	N_2O	NO_x	N_2O_5	NO_3	HNO_3
54.39	4.23(10)	3.70(-6)	1.51(-8)	1.00(-8)	0	0	3.84(-12)
52.13	2.88(10)	1.94(-6)	1.51(-8)	1.51(-8)	0	0	3.84(-12)
49.85	4.69(10)	2.42(-6)	1.81(-8)	1.71(-8)	0	0	8.00(-12)
47.61	7.52(10)	2.96(-6)	2.32(-8)	1.77(-8)	0	0	1.73(-11)
45.38	1.34(11)	3.92(-6)	2.99(-8)	1.77(-8)	0	0	4.07(-11)
43.18	2.44(11)	5.29(-6)	3.84(-8)	1.71(-8)	0	0	9.35(-11)
41.02	4.39(11)	7.00(-6)	4.89(-8)	1.62(-8)	0	0	2.03(-10)
38.89	7.26(11)	8.50(-6)	6.12(-8)	1.49(-8)	0	0	3.76(-10)
36.81	1.13(12)	9.67(-6)	7.44(-8)	1.36(-8)	1.28(-10)	3.35(-12)	4.90(-10)
34.78	1.63(12)	1.02(-5)	8.74(-8)	1.24(-8)	3.35(-10)	4.61(-12)	7.08(-10)
32.79	2.17(12)	9.98(-6)	1.00(-7)	1.12(-8)	5.65(-10)	5.18(-12)	9.65(-10)
30.82	2.73(12)	9.23(-6)	1.13(-7)	9.89(-9)	7.95(-10)	4.99(-12)	1.32(-9)
28.92	3.29(12)	8.18(-6)	1.26(-7)	8.45(-9)	9.40(-10)	4.23(-12)	1.79(-9)
27.08	3.81(12)	6.96(-6)	1.42(-7)	6.79(-9)	9.27(-10)	3.17(-12)	2.34(-9)
25.24	4.19(12)	5.65(-6)	1.59(-7)	5.03(-9)	7.73(-10)	2.25(-12)	2.79(-9)
23.41	4.38(12)	4.37(-6)	1.77(-7)	3.42(-9)	5.54(-10)	1.45(-12)	2.93(-9)
21.61	4.33(12)	3.19(-6)	1.96(-7)	2.13(-9)	3.34(-10)	8.13(-13)	2.71(-9)
19.81	3.91(12)	2.15(-6)	2.13(-7)	1.20(-9)	1.73(-10)	4.25(-13)	2.14(-9)
18.03	3.15(12)	1.28(-6)	2.27(-7)	6.08(-10)	6.76(-11)	1.68(-13)	1.42(-9)
16.25	2.13(12)	6.41(-7)	2.37(-7)	2.86(-10)	1.99(-11)	5.02(-14)	7.49(-10)
14.47	1.20(12)	2.74(-7)	2.42(-7)	1.43(-10)	6.40(-12)	1.67(-14)	3.43(-10)
12.66	7.17(11)	1.25(-7)	2.46(-7)	8.43(-11)	0	0	2.04(-10)
10.82	5.18(11)	6.99(-8)	2.48(-7)	6.54(-11)	0	0	1.65(-10)
8.90	5.47(11)	5.66(-8)	2.49(-7)	6.36(-11)	0	0	1.59(-10)
6.88	6.02(11)	4.97(-8)	2.49(-7)	7.12(-11)	0	0	1.47(-10)
4.75	7.09(11)	4.63(-8)	2.50(-7)	1.49(-10)	0	0	3.15(-10)
2.52	8.60(11)	4.50(-8)	2.50(-7)	3.90(-10)	0	0	9.67(-10)
1.94	9.07(11)	4.47(-8)	2.50(-7)	5.28(-10)	0	0	1.13(-9)
1.36	9.34(11)	4.33(-8)	2.50(-7)	8.78(-10)	0	0	1.20(-9)
0.78	9.26(11)	4.02(-8)	2.50(-7)	1.53(-9)	0	0	1.09(-9)
0.21	8.67(11)	3.53(-8)	2.50(-7)	2.82(-9)	0	0	5.11(-10)

*The first ozone column is the concentration (molecules/cm^3); the subsequent columns denote the volume mixing ratio. Numbers in parentheses denote powers of 10; e.g., the concentration of ozone at 54.39 km is 4.23×10^{10} molecules/cm^3.

TABLE 2b. DAYLIGHT, ZONAL AVERAGES OF H_2O, H_2O_2, OH, CO AND CH_4 SPECIES IN THE REFERENCE ATMOSPHERE AS WAS SIMULATED BY THE 2-D CRUTZEN PHOTOCHEMICAL MODEL WITH 1976 CHEMISTRY AT 45°N DURING LATE SUMMER (AUGUST 30)*

Z(km)	[H_2O]	H_2O	H_2O_2	OH	CO	CH_4
54.39	7.2(-7)	4.44(-6)	0	8.15(-11)	1.00(-7)	2.31(-7)
52.13	5.0(-7)	4.44(-6)	5.37(-10)	5.52(-10)	7.36(-8)	2.31(-7)
49.85	4.4(-7)	4.46(-6)	6.05(-10)	4.99(-10)	6.30(-8)	2.53(-7)
47.61	4.3(-7)	4.46(-6)	7.02(-10)	4.47(-10)	5.81(-8)	2.88(-7)
45.38	7.0(-7)	4.45(-6)	8.73(-10)	4.05(-10)	5.48(-8)	3.34(-7)
43.18	1.1(-6)	4.39(-6)	1.03(-9)	3.37(-10)	5.19(-8)	3.90(-7)
41.02	2.0(-6)	4.32(-6)	1.20(-9)	2.52(-10)	4.85(-8)	4.55(-7)
38.89	5.0(-6)	4.23(-6)	1.45(-9)	1.65(-10)	4.46(-8)	5.26(-7)
36.81	1.1(-5)	4.16(-6)	1.86(-9)	9.84(-11)	4.06(-8)	5.96(-7)
34.78	2.7(-5)	4.12(-6)	2.50(-9)	5.51(-11)	3.63(-8)	6.58(-7)
32,79	6.0(-5)	4.10(-6)	3.06(-9)	2.97(-11)	3.24(-8)	7.15(-7)
30.82	1.3(-4)	4.12(-6)	3.34(-9)	1.61(-11)	2.89(-8)	7.70(-7)
28.92	3.0(-4)	4.16(-6)	3.19(-9)	9.03(-12)	2.60(-8)	8.27(-7)
27.08	7.5(-4)	4.24(-6)	2.70(-9)	5.23(-12)	2.38(-8)	8.92(-7)
25.24	1.6(-3)	4.45(-6)	2.09(-9)	3.14(-12)	2.22(-8)	9.68(-7)
23.41	3.4(-3)	4.96(-6)	1.55(-9)	1.97(-12)	2.17(-8)	1.05(-6)
21.61	8.7(-3)	6.09(-6)	1.14(-9)	1.30(-12)	2.28(-8)	1.13(-6)
19.81	1.9(-2)	8.11(-6)	8.69(-10)	9.04(-13)	2.64(-8)	1.22(-6)
18.03	4.7(-2)	1.07(-5)	6.34(-10)	6.11(-13)	3.35(-8)	1.29(-6)
16.25	1.1(-1)	1.28(-5)	4.37(-10)	3.67(-13)	4.34(-8)	1.34(-6)
14.47	1.4(-1)	1.88(-5)	3.77(-10)	2.14(-13)	5.52(-8)	1.38(-6)
12.66	2.4(-1)	3.54(-5)	4.24(-10)	1.35(-13)	7.24(-8)	1.40(-6)
10.82	3.5(-1)	9.48(-5)	6.59(-10)	1.15(-13)	9.07(-8)	1.43(-6)
8.90	5.4(-1)	2.05(-4)	7.34(-10)	8.60(-14)	9.98(-8)	1.44(-6)
6.88	5.1(-1)	7.32(-4)	1.44(-9)	1.17(-13)	1.09(-7)	1.44(-6)
4.75	5.8(-1)	2.23(-3)	6.27(-10)	7.60(-14)	1.24(-7)	1.45(-6)
2.52	4.8(-1)	6.06(-3)	2.45(-9)	1.48(-13)	1.46(-7)	1.47(-6)
1.94	4.9(-1)	7.11(-3)	2.32(-9)	1.45(-13)	1.56(-7)	1.47(-6)
1.36	5.2(-1)	8.59(-3)	1.41(-9)	1.31(-13)	1.69(-7)	1.48(-6)
0.78	6.0(-1)	1.04(-2)	5.12(-10)	1.07(-13)	1.85(-7)	1.49(-6)
0.21	7.3(-1)	1.34(-2)	5.12(-10)	1.0(-13)	2.02(-7)	1.50(-6)

*The first H_2O column denotes the relative humidity, and the subsequent ones the volume mixing ratio.

Figure 6 is a plot of the data for the volume mixing ratios in Tables 2a, b. The abscissa of the figure extends over 13 orders of magnitude as split at the bottom for the solid lines (for NO_x, HNO_3, OH, and H_2O_2) and at the top for the dashed lines (N_2O, CO, CH_4, O_3, H_2O). This figure shows that the ozone mixing ratio has a broad peak near 35 km (5.5 mbar), which is of interest in considerations of the heating of stratospheric air by the absorption of UV radiation by ozone. The N_2O mixing ratio is nearly constant in the troposphere and decreases with increasing altitude in the stratosphere as a consequence of the mechanisms M5 and M6 (Table 1). The NO_x mixing ratio in the troposphere decreases with increasing altitude from the high values of the NO_x emissions at the earth's surface to a broad minimum in the upper troposphere. The NO_x mixing ratio increases in the stratosphere as a consequence of mechanisms that start with M6 (Table 1). The OH profile is of interest because, through the reaction $OH + NO_2(+M) \rightarrow HNO_3(+M)$, it is (a) a temporary reservoir for NO_x that weakens the stratospheric NO_x cycles (M2, M3c), and (b) a permanent tropospheric sink due to the solubility of HNO_3 in water (M9). The tropospheric OH profile is also important because OH is a sink for CO and CH_4 (M4a, b). Furthermore, OH scavenges not only CO and CH_4, but also NO_2 and SO_2 (M9) as well as CH_x Cl_yF_z (M17). Finally, Fig. 6 shows that the simulated volume mixing ratio of H_2O drops rapidly in the troposphere and lower stratosphere from the surface value of 1.3×10^{-2} to about 4×10^{-6} in the middle stratosphere.

Figure 7 shows results of high-altitude flight on the reference ozone column as obtained from the Crutzen model with 1976 chemistry (Hidalgo and Crutzen, 1977). This figure shows the computed change in the reference ozone column as a function of latitude for assumed individual fleets of subsonic and SST aircraft after 6 years of fleet operations. The former is assumed to be a large fleet operating in the year 1990 at 10.8 km, and the latter a small fleet operating at 18 km. The total NO_x

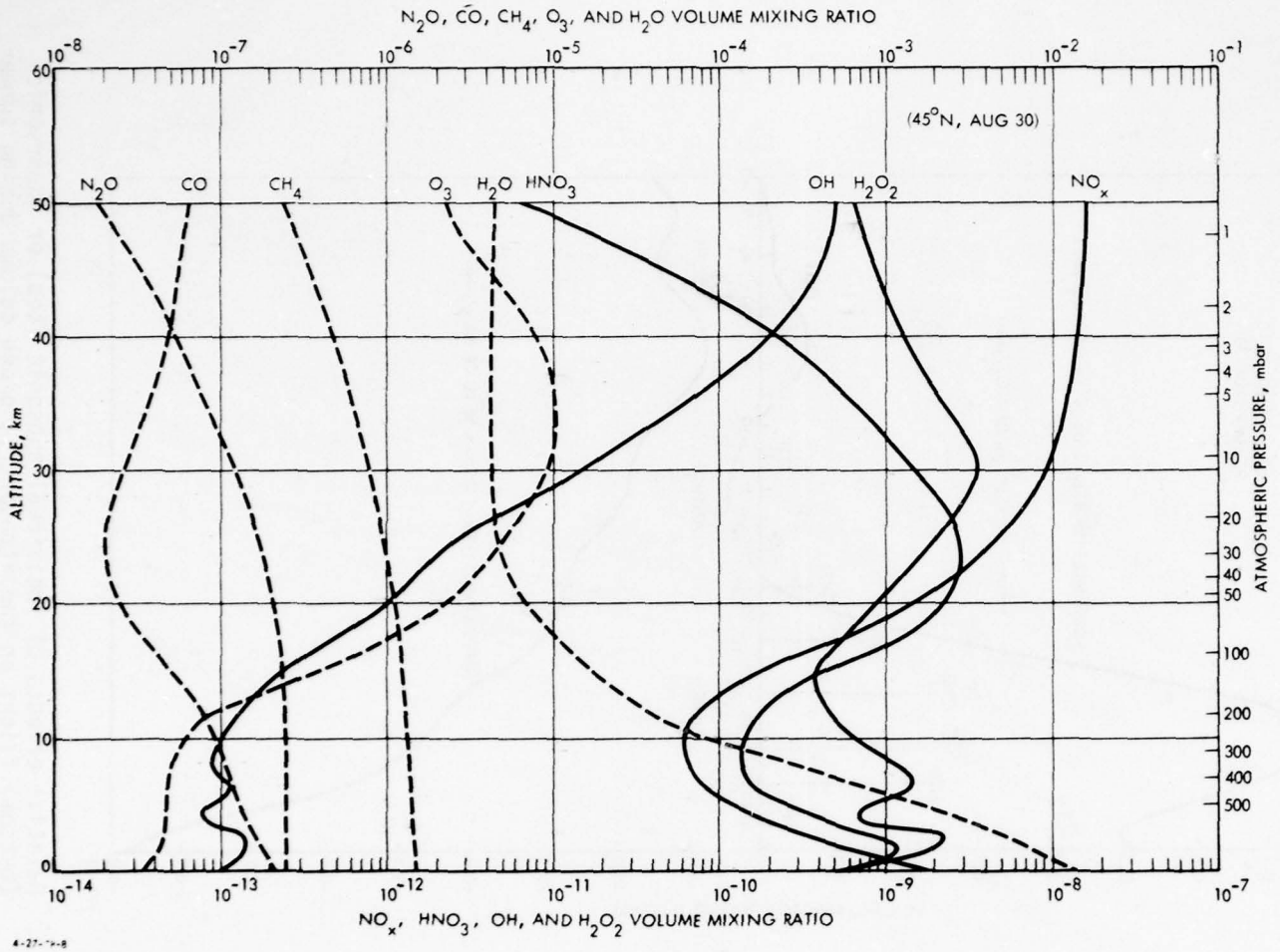

FIGURE 6. Simulated vertical profiles of daylight, zonal average of the volume mixing ratio of indicated species in the reference atmosphere at 45°N during summer (August 30) by the Crutzen model with 1976 chemistry. (Source: Hidalgo and Crutzen, 1977)

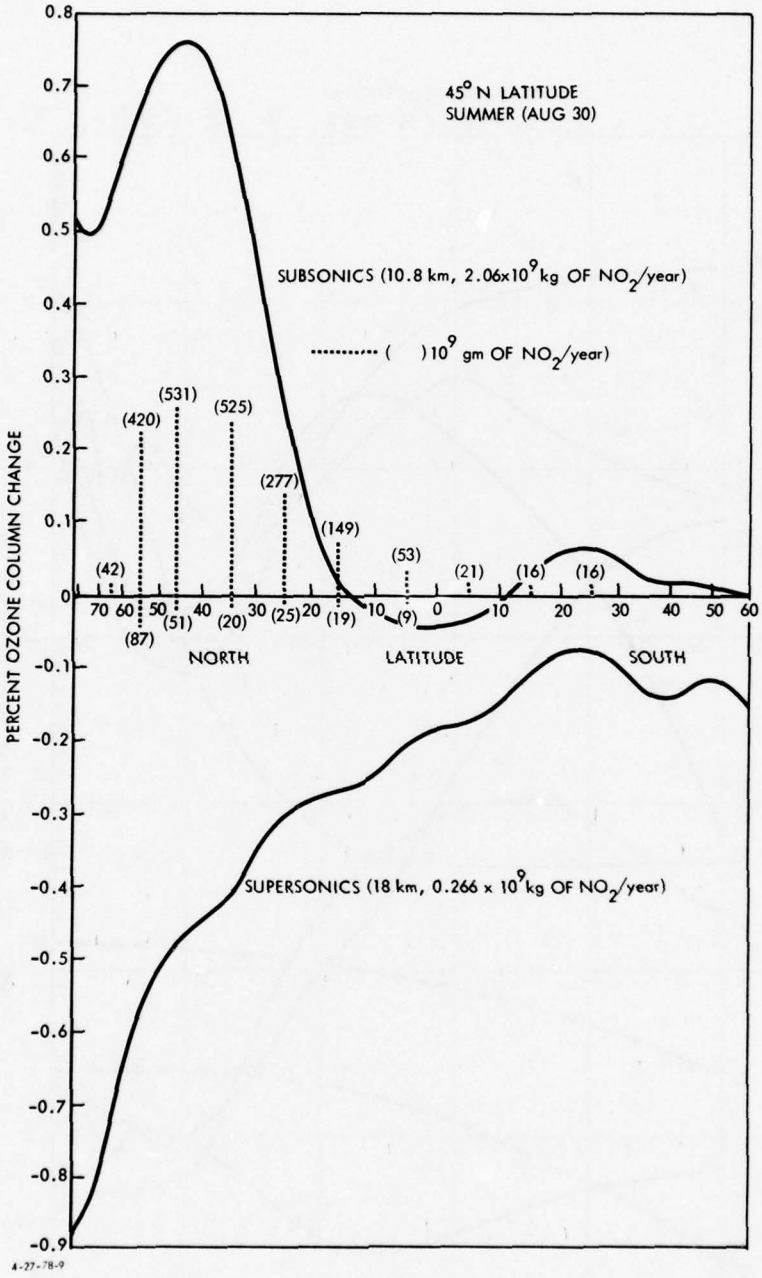

FIGURE 7. Relative effects of individual subsonic (top) or supersonic (bottom) flight on the atmospheric ozone column during summer (August 30) after six years of fleet operations. NO_x emissions were for hypothetical fleets assumed to operate in the 1990 time frame. (Source: Hidalgo and Crutzen, 1977)

emissions (as NO_2) were 2.06 x 10^9 kg per year for the subsonics and about 10 percent of this value for the SSTs. The dashed lines in the figure indicate the assumed latitudinal distributions of the NO_x emissions in units of 10^9 gm of NO_2 per year. It is thus seen that the bulk of the NO_x emissions were assumed to take place at the northern middle latitudes. This figure shows that subsonic aircraft produce near 45°N latitude a maximum ozone increase of 0.76 percent, as the result of the increase in the reference ozone column (Fig. 5) from 328.6 to the perturbed value of 331.1 Dobson units. *The corresponding NO_x perturbation at 10.8 km was about 300 percent* (Hidalgo and Crutzen, 1977).

The numerical data from the Crutzen model for the reference atmosphere was obtained after 15 years of integrations. The basic structure of the model was based on the conservation of chemical species, dynamics that were empirically constructed so as to match the H_2O and O_3 observations in the lower stratosphere, and rate constants for the chemical mechanisms in Table 1 as given in Table 3. The model was completed by specifying boundary conditions at the ground and near the tropopause (approximately 54 km) as well as the heterogenous removal rates for the tropospheric rainout sinks of NO_x, HNO_3, H_2O_2, and CH_3O_2H. Figure 8 shows a comparison of the simulated and observed O_3 mass mixing ratio, a result that is constrained (as that of H_2O) in the lower stratosphere by the empirical adjustments of the 2-D eddy coefficients. Further considerations of the 2-D dynamics will be given in a subsequent section.

2.2 RESULTS AND CHARACTERISTICS OF THE 1976 WIDHOPF MODEL

The basic formulation of the Widhopf 2-D model was the same as in the Crutzen 2-D model, except for the empirical representation of the eddy motions. Instead of using the H_2O and O_3 distributions, as in the Crutzen model, the Widhopf model was based

TABLE 3. 1976 REACTION RATE COEFFICIENTS FOR AN OXYGEN-HYDROGEN-NITROGEN ATMOSPHERE*
SOURCE: HIDALGO AND CRUTZEN, 1977

Oxygen Reactions		
R1	$O_2 + h\nu \rightarrow O + O$	$\lambda < 242$ nm
R2	$O + O_2 + M \rightarrow O_3 + M$	$k_2 = 1.1 \times 10^{-34} \exp(500/T)$
R3a	$O_3 + h\nu \rightarrow O_2 + O(^1D)$	$\lambda < 310$ nm
R3b	$O_3 + h\nu \rightarrow O_2 + O$	$\lambda < 1140$ nm
R4	$O_3 + O \rightarrow O_2 + O_2$	$k_4 = 1.9 \times 10^{-11} \exp(-2300/T)$
R5	$O(^1D) + M \rightarrow O + M$	$k_5 = 6.0 \times 10^{-11}$
Reactions Defining Relative Concentrations of Odd Hydrogen Related Species		
R6	$O + OH \rightarrow H + O_2$	$k_6 = 4.2 \times 10^{-11}$
R7	$O_3 + OH \rightarrow HO_2 + O_2$	$k_7 = 1.6 \times 10^{-12} \exp(-1000/T)$
R8	$CO + OH \rightarrow H + CO_2$	$k_8 = 2.1 \times 10^{-13} \exp(-75/T)$
R9	$H_2 + OH \rightarrow H + H_2O$	$k_9 = 2.3 \times 10^{-11} \exp(-2450/T)$
R10	$O_3 + H \rightarrow OH + O_2$	$k_{10} = 2.6 \times 10^{-11}$
R11	$O_2 + H + M \rightarrow HO_2 + M$	$k_{11} = 2.1 \times 10^{-32} \exp(290/T)$
R12	$O + HO_2 \rightarrow OH + O_2$	$k_{12} = 2.0 \times 10^{-11}$
R13	$O_3 + HO_2 \rightarrow OH + 2\,O_2$	$k_{13} = 1.0 \times 10^{-13} \exp(-1250/T)$
R14	$HO_2 + NO \rightarrow OH + NO_2$	$k_{14} = 2.2 \times 10^{-13}$
R15	$OH + NO_2 (+ M) \rightarrow HNO_3 (+ M)$	$k_{15} = \left\{ \left[4.2 \times 10^{-22} \exp(-170/T)(M) \right] \sigma^{-1} \right.$
R16	$HNO_3 + h\nu \rightarrow OH + NO_2$	$\lambda < 546$ nm $\quad \left. \sigma = 4 \times 10^{-11} (M) + 1.6 \times 10^{-2T} \right\}$
R17	$HO_2 + HO_2 \rightarrow H_2O_2 + O_2$	$k_{17} = 3.0 \times 10^{-11} \exp(-500/T)$
R18	$H_2O_2 + h\nu \rightarrow OH + OH$	$\lambda < 565$ nm
Production and Loss Reactions for Odd Hydrogen		
R19a	$H_2O + O(^1D) \rightarrow OH + OH$	$k_{19a} = 3.0 \times 10^{-10}$
R19b	$CH_4 + O(^1D) \rightarrow CH_3 + OH$	$k_{19b} = 4.0 \times 10^{-10}$
R19c	$H_2 + O(^1D) \rightarrow H + OH$	$k_{19c} = 3.0 \times 10^{-10}$
R20	$H + HO_2 \rightarrow H_2 + O_2$	$k_{20} = 10^{-11}$
R21	$OH + HO_2 \rightarrow H_2O + O_2$	$k_{21} = 5.0 \times 10^{-11}$
R22	$OH + H_2O_2 \rightarrow H_2O + HO_2$	$k_{22} = 1.7 \times 10^{-11} \exp(-900/T)$
R23	$OH + HNO_3 \rightarrow H_2O + NO_3$	$k_{23} = 9 \times 10^{-14}$

TABLE 3. (continued)

Methane Oxidation Reactions		
R24	$OH + CH_4 \rightarrow H_2O + CH_3$	$k_{24} = 2.5 \times 10^{-12} \exp(-1660/T)$
R25	$CH_3 + O_2 + M \rightarrow CH_3O_2 + M$	$k_{25} = 2.6 \times 10^{-31}$
R26	$CH_3O_2 + NO \rightarrow CH_3O + NO_2$	$k_{26} = 1.5 \times 10^{-12} \exp(-500/T)$, assumed
R27	$CH_3O_2 + HO_2 \rightarrow CH_3O_2H + O_2$	$k_{27} = 3.0 \times 10^{-11} \exp(-500/T)$, assumed
R28	$CH_3O_2H + h\nu \rightarrow CH_3O + OH$	$J_{CH_3O_2H} = J_{H_2O_2}$, assumed
R29	$CH_3O + O_2 \rightarrow CH_2O + HO_2$	$k_{29} = 4.2 \times 10^{-13} \exp(-3000/T)$
R30a	$CH_2O + h\nu \rightarrow H_2 + CO$	$\lambda \lesssim 350$ nm, $J_{30a} = 1.1 \times 10^{-4}$
R30b	$CH_2O + h\nu \rightarrow H + CHO$	$\lambda \lesssim 350$ nm, $J_{30b} = 3.3 \times 10^{-5}$
R31	$CH_2O + OH \rightarrow H_2O + CHO$	$k_{31} = 1.4 \times 10^{-11}$
R32	$CHO + O_2 \rightarrow HO_2 + CO$	$k_{32} = 1.7 \times 10^{-13}$
Odd Nitrogen Reactions		
R33	$NO + O_3 \rightarrow NO_2 + O_2$	$k_{33} = 9.0 \times 10^{-13} \exp(-1200/T)$
R34	$NO_2 + O \rightarrow NO + O_2$	$k_{34} = 9.2 \times 10^{-12}$
R35	$NO_2 + h\nu \rightarrow NO + O$	$\lambda < 400$ nm
R36	$N + O_3 \rightarrow NO + O_2$	$k_{36} = 3.0 \times 10^{-11} \exp(-1200/T)$
R37	$N + O_2 \rightarrow NO + O$	$k_{37} = 1.1 \times 10^{-14} \exp(-3150/T)$
R38	$N + OH \rightarrow NO + H$	$k_{38} = 5.3 \times 10^{-11}$
R39	$N + HO_2 \rightarrow NO + OH$	$k_{39} = 2.0 \times 10^{-10}$
R40	$NO + h\nu \rightarrow N + O$	$\lambda < 191$ nm
R41	$N + NO \rightarrow N_2 + O$	$k_{41} = 2.7 \times 10^{-11}$
R42	$N_2O + h\nu \rightarrow N_2 + O$	$\lambda < 337$ nm
R43a	$N_2O + O(^1D) \rightarrow NO + NO$	$k_{43a} = 1.1 \times 10^{-10}$
R43b	$N_2O + O(^1D) \rightarrow N_2 + O_2$	$k_{43b} = 1.1 \times 10^{-10}$
R44	$NO_2 + O_3 \rightarrow NO_3 + O_2$	$k_{44} = 1.23 \times 10^{-13} \exp(-2470/T)$
R45	$NO_3 + h\nu \rightarrow NO_2 + O$	Johnston & Graham (1974)
R46	$NO_3 + NO \rightarrow 2\ NO_2$	$k_{46} = 8.7 \times 10^{-12}$
R47	$NO_3 + NO_2 + M \rightarrow N_2O_5 + M$	$k_{47} = [1.2 \times 10^{-21}\ (M)] / [2 \times 10^{8} + 1.7 \times 10^{-10}\ (M)]$
R48	$N_2O_5 + M \rightarrow NO_2 + NO_3 + M$	$k_{48} = [4000\ (M) \exp(-9650/T)] / [2 \times 10^{8} + 1.7 \times 10^{-10}(M)]$
R49	$N_2O_5 + h\nu \rightarrow NO_2 + NO_3$	Johnston & Graham (1974)

*Notes: two-body reactions, cm^3 *molecules*$^{-1}$ s^{-1}; *three-body reactions*, cm^6 *molecules*$^{-2}$ s^{-1}.

The underlined reactions (R7, 13, 14, 15, 21) are most important for the effect of SST flight on atmospheric ozone.

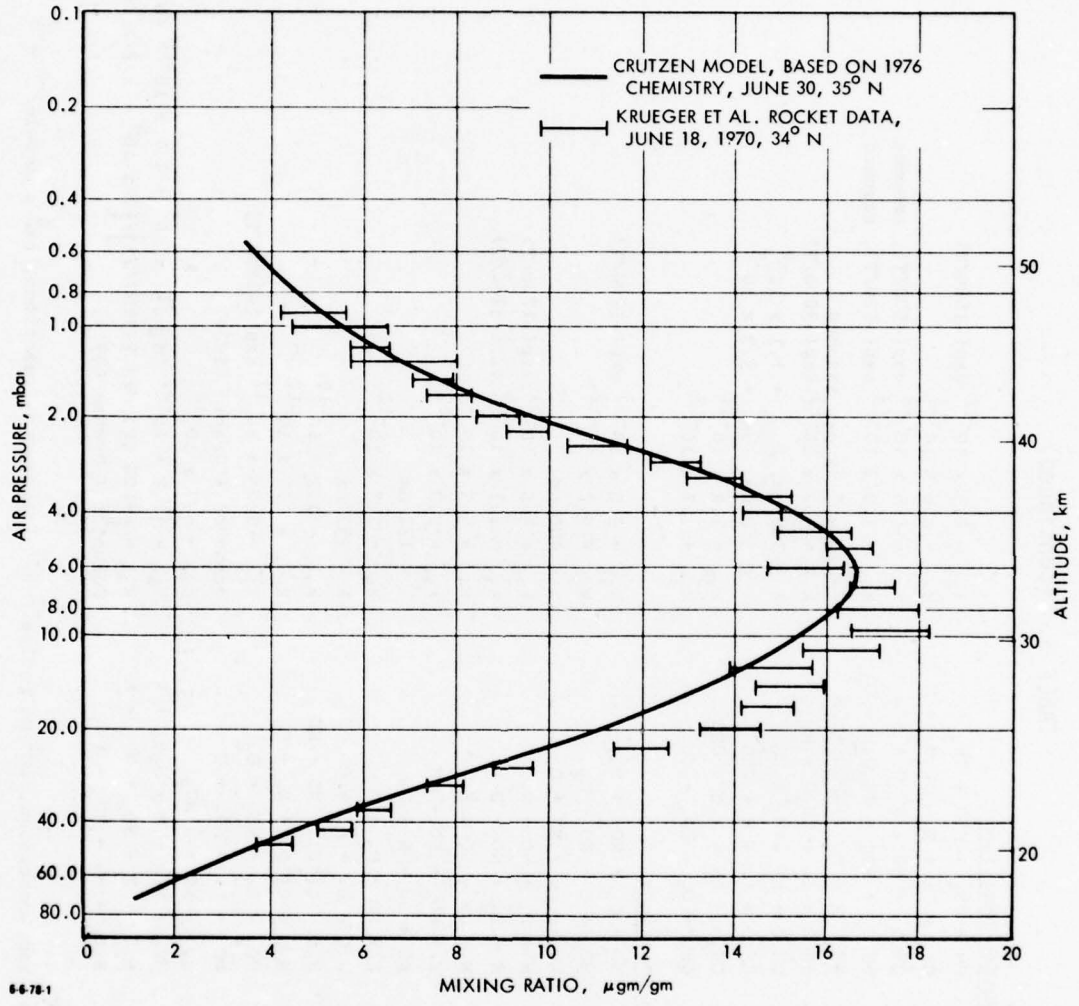

FIGURE 8. Comparison of simulated and observed ozone mixing ratio at 35°N during June. The simulated values in the lower and middle stratosphere were constrained by their use in the parameterization of the eddy transports. The observations are given by the data of Krueger et al. (1973). (Source: Hidalgo and Crutzen, 1977)

on (a) extrapolations to the stratosphere, up to latitudes of 50°N, by Luther (1973) of the tropospheric transports *of heat* (Oört and Rasmusson, 1971), and (b) matching of parts of the time history in the dispersion by the stratosphere of excess C-14 that resulted from the 1961-1962 nuclear weapon detonations in the atmosphere at approximately 70°N. This 2-D parameterization of the dynamics was then tested by reproduction of segments of the time history of the dispersion of other atmospheric radioactive debris; i.e., W-185 and Zr-95. Furthermore, the ozone distributions in the reference atmosphere were calculated utilizing 1976 chemistry; these results indicated good agreement with observations as a function of both altitude, latitude, and season (Widhopf et al., 1977). It must then be noted that this parameterization of the eddy transports in the reference stratosphere is independent of the ozone chemistry.

The chemistry in the two models was, in general, equivalent; especially since the adoption of the tropospheric ozone production mechanisms in the Widhopf model was based on earlier experience with the Crutzen model. However, it is of interest to indicate some differences in the important reaction rates in the stratosphere as used in these two models.

Five reaction rates in the stratospheric HO_x-NO_x cycles have been identified as being the most important ones of those in Table 3 for changes of the ozone column by SSTs. These results are based on the use of a 1-D model and on considerations of the uncertainty in the magnitude of the calculated changes in the ozone column by SSTs due to the uncertainty in the magnitude of the reaction rate coefficients (Duewer et al., 1977). With the notation in Table 3, these reactions are:

R(21) $OH + HO_2 \rightarrow H_2O + O_2$

R(14) $HO_2 + NO \rightarrow OH + NO_2$

R(13) $O_3 + HO_2 \rightarrow OH + 2\ O_2$

R(7) $O_3 + OH \rightarrow HO_2 + O_2$

R(15) $OH + NO_2(+M) \rightarrow HNO_3(+M)$

A comparison of the reaction rate coefficients for the foregoing reactions, as used in the Crutzen and Widhopf 2-D models, is as follows:

Reaction	Crutzen Model	Widhopf Model
R(21)	5.0×10^{-11}	2.0×10^{-11}
R(14)	2.2×10^{-13}	2.3×10^{-13}
R(13)	$1.0 \times 10^{-13} \exp(-1250/T)$	same
R(7)	$1.6 \times 10^{-12} \exp(-1000/T)$	same
R(15)	$\frac{4.2 \times 10^{-22} \exp(-170/T)(M)}{4(10)^{-11}(M) + 1.6(10)^{-2}T}$	$\frac{2.76 \times 10^{-13} \exp(880/T)}{1.166 \times 10^{18} \exp(220/T)+[M]}$

Besides the different formulation of the eddy motions and difference in reaction rate coefficients in the Widhopf and Crutzen models, other significant sources of differences between these models are: (a) the formulation of the H_2O distributions in the troposphere and stratosphere, which were either specified (Widhopf) or parameterized (Crutzen), (b) the magnitude of the removal rates for the tropospheric rainout sinks, (c) the use of the height (Widhopf) instead of the pressure (Crutzen) as the vertical coordinate, the latter being in better accord with airline flight practice, and (d) the numerical integrations of the continuity equations for the conservation of the chemical species. While the Widhopf model solves for each continuity equation, the Crutzen model utilizes a family concept that must invoke chemical equilibrium among short-lived species. Some of the possible limitations introduced by the latter approximations are described by Chang (1977).

Table 4 and Fig. 9 show results for the reference atmosphere, similar to those described above for the Crutzen model, that were obtained from the Widhopf model. However, in contrast with the daylight averages of the Crutzen results (Table 2 and Fig. 6), the corresponding Widhopf values (Table 4 and Fig. 9) are for a

TABLE 4. 24-HOUR, ZONAL AVERAGE OF SPECIES IN THE REFERENCE ATMOSPHERE AS SIMULATED BY WIDHOPF, et al. (1977) AT 40°N DURING LATE SUMMER (AUGUST 15)*

Z (km)	O_3	O_3	N_2O	NO_x	HNO_3	H_2O	H_2O_2	OH	CO	CH_4
50.0	6.94(10)	3.25(-6)	1.43(-8)	2.00(-8)	1.01(-11)	4.39(-6)	7.82(-10)	7.17(-10)	1.29(-8)	2.21(-7)
47.5	1.29(11)	4.42(-6)	2.13(-8)	1.94(-8)	3.83(-11)	4.47(-6)	1.07(-9)	6.40(-10)	1.31(-8)	2.52(-7)
45.0	2.48(11)	6.06(-6)	2.76(-8)	1.90(-8)	1.41(-10)	4.43(-6)	1.36(-9)	5.01(-10)	1.29(-8)	2.80(-7)
42.5	4.69(11)	8.09(-6)	3.47(-8)	1.86(-8)	4.56(-10)	4.43(-6)	1.77(-9)	3.33(-10)	1.25(-8)	3.15(-7)
40.0	8.21(11)	9.88(-6)	4.25(-8)	1.79(-8)	1.08(-9)	4.40(-6)	2.41(-9)	1.77(-10)	1.20(-8)	3.52(-7)
37.5	1.30(12)	1.08(-5)	4.99(-8)	1.67(-8)	1.91(-9)	4.34(-6)	3.48(-9)	8.07(-11)	1.14(-8)	3.84(-7)
35.0	1.93(12)	1.09(-5)	5.78(-8)	1.52(-8)	3.13(-9)	4.32(-6)	4.81(-9)	3.54(-11)	1.07(-8)	4.14(-7)
34.0	2.19(12)	1.07(-5)	6.07(-8)	1.43(-8)	3.74(-9)	4.27(-6)	5.11(-9)	2.56(-11)	1.03(-8)	4.23(-7)
33.0	2.48(12)	1.03(-5)	6.43(-8)	1.34(-8)	4.48(-9)	4.24(-6)	5.30(-9)	1.85(-11)	9.94(-9)	4.34(-7)
32.0	2.79(12)	9.90(-6)	6.82(-8)	1.22(-8)	5.37(-9)	4.22(-6)	5.31(-9)	1.36(-11)	9.61(-9)	4.46(-7)
31.0	3.10(12)	9.45(-6)	7.31(-8)	1.10(-8)	6.42(-9)	4.22(-6)	5.17(-9)	1.01(-11)	9.36(-9)	4.62(-7)
30.0	3.43(12)	8.95(-6)	7.89(-8)	9.62(-9)	7.63(-9)	4.24(-6)	4.89(-9)	7.51(-12)	9.15(-9)	4.81(-7)
29.0	3.72(12)	8.34(-6)	8.47(-8)	8.10(-9)	8.81(-9)	4.23(-6)	4.44(-9)	5.62(-12)	8.88(-9)	4.98(-7)
28.0	4.03(12)	7.72(-6)	9.13(-8)	6.64(-9)	9.96(-9)	4.24(-6)	3.94(-9)	4.24(-12)	8.68(-9)	5.18(-7)
27.0	4.31(12)	7.07(-6)	9.84(-8)	5.28(-9)	1.10(-8)	4.25(-6)	3.41(-9)	3.18(-12)	8.50(-9)	5.39(-7)
26.0	4.53(12)	6.36(-6)	1.05(-7)	4.07(-9)	1.17(-8)	4.25(-6)	2.85(-9)	2.39(-12)	8.29(-9)	5.59(-7)
25.0	4.71(12)	5.66(-6)	1.13(-7)	3.09(-9)	1.22(-8)	4.26(-6)	2.34(-9)	1.79(-12)	8.15(-9)	5.81(-7)
24.0	4.84(12)	4.96(-6)	1.21(-7)	2.33(-9)	1.24(-8)	4.27(-6)	1.88(-9)	1.34(-12)	8.08(-9)	6.07(-7)
23.0	4.89(12)	4.27(-6)	1.30(-7)	1.76(-9)	1.23(-8)	4.27(-6)	1.48(-9)	1.01(-12)	8.08(-9)	6.33(-7)
22.0	4.86(12)	3.06(-6)	1.42(-7)	1.34(-9)	1.26(-8)	4.29(-6)	1.15(-9)	6.08(-13)	8.31(-9)	6.71(-7)
21.0	4.67(12)	2.97(-6)	1.59(-7)	1.02(-9)	1.09(-8)	4.30(-6)	8.92(-10)	5.76(-13)	8.89(-9)	7.24(-7)
20.0	4.10(12)	2.22(-6)	1.86(-7)	7.38(-10)	9.13(-9)	4.31(-6)	6.95(-10)	4.41(-13)	1.03(-8)	8.16(-7)
19.0	3.33(12)	1.54(-6)	2.21(-7)	5.07(-10)	6.96(-9)	4.34(-6)	5.99(-10)	3.55(-13)	1.28(-8)	9.31(-7)
18.0	2.53(12)	9.99(-7)	2.55(-7)	3.29(-10)	4.79(-9)	4.37(-6)	6.03(-10)	3.04(-13)	1.63(-8)	1.05(-6)
17.0	1.70(12)	5.75(-7)	2.86(-7)	2.02(-10)	2.87(-9)	4.39(-6)	6.82(-10)	2.73(-13)	2.10(-8)	1.15(-6)
16.0	1.02(12)	2.94(-7)	3.08(-7)	1.26(-10)	1.50(-9)	6.09(-6)	7.98(-10)	2.46(-13)	2.61(-8)	1.23(-6)
15.0	5.43(11)	1.34(-7)	3.21(-7)	8.49(-11)	6.82(-10)	7.34(-6)	9.44(-10)	2.06(-13)	3.17(-8)	1.28(-6)
14.0	2.49(11)	5.26(-8)	3.26(-7)	5.97(-11)	2.58(-10)	1.03(-5)	1.16(-9)	1.69(-13)	3.84(-8)	1.30(-6)
13.0	1.05(11)	1.89(-8)	3.26(-7)	4.42(-11)	8.97(-11)	1.66(-5)	1.48(-9)	1.44(-13)	4.53(-8)	1.30(-6)
12.0	6.81(10)	1.05(-8)	3.21(-7)	3.43(-11)	5.59(-11)	3.04(-5)	1.88(-9)	1.32(-13)	5.14(-8)	1.29(-6)
11.0	7.13(10)	9.40(-9)	3.12(-7)	2.91(-11)	5.89(-11)	6.06(-5)	2.20(-9)	1.22(-13)	5.52(-8)	1.25(-6)
10.0	7.82(10)	9.10(-9)	3.10(-7)	2.83(-11)	6.49(-11)	1.29(-4)	2.50(-9)	1.12(-13)	6.01(-8)	1.25(-6)
9.0	9.40(10)	9.68(-9)	3.08(-7)	2.69(-11)	7.24(-11)	2.69(-4)	2.76(-9)	9.96(-14)	6.63(-8)	1.25(-6)
8.0	1.09(11)	1.00(-8)	3.06(-7)	2.63(-11)	7.66(-11)	5.18(-4)	3.09(-9)	9.03(-14)	7.47(-8)	1.25(-6)
7.0	1.26(11)	1.03(-8)	3.06(-7)	2.60(-11)	7.97(-11)	9.31(-4)	3.54(-9)	8.43(-14)	8.46(-8)	1.25(-6)
6.0	1.43(11)	1.04(-8)	3.05(-7)	2.80(-11)	8.85(-11)	1.62(-3)	4.16(-9)	7.99(-14)	9.60(-8)	1.26(-6)
5.0	1.61(11)	1.05(-8)	3.06(-7)	3.38(-11)	1.12(-10)	2.74(-3)	4.92(-9)	7.94(-14)	1.08(-7)	1.27(-6)
4.0	1.87(11)	1.10(-8)	3.07(-7)	4.80(-11)	1.66(-10)	4.39(-3)	5.79(-9)	7.90(-14)	1.21(-7)	1.28(-6)
3.0	2.30(11)	1.22(-8)	3.08(-7)	8.21(-11)	2.93(-10)	6.42(-3)	6.79(-9)	8.27(-14)	1.35(-7)	1.29(-6)
2.0	3.05(11)	1.46(-8)	3.10(-7)	1.73(-10)	5.49(-10)	9.12(-3)	7.76(-9)	8.98(-14)	1.52(-7)	1.31(-6)
1.0	4.20(11)	1.82(-8)	3.12(-7)	4.81(-10)	9.49(-10)	1.26(-2)	8.27(-9)	1.03(-13)	1.76(-7)	1.34(-6)
0	5.00(11)	1.96(-8)	3.15(-7)	2.06(-9)	8.45(-10)	1.68(-2)	7.61(-9)	1.61(-13)	2.10(-7)	1.37(-6)

*First ozone column is the concentration (molecule/cm^3), whereas the remaining columns are the volume mixing ratio. Numbers in parentheses represent powers of 10; e.g., 1.02(12) equals to 1.02×10^{12}. In contrast with the corresponding values in Table 2, the volume mixing ratio for species with a short life are based on a 24-hour average.

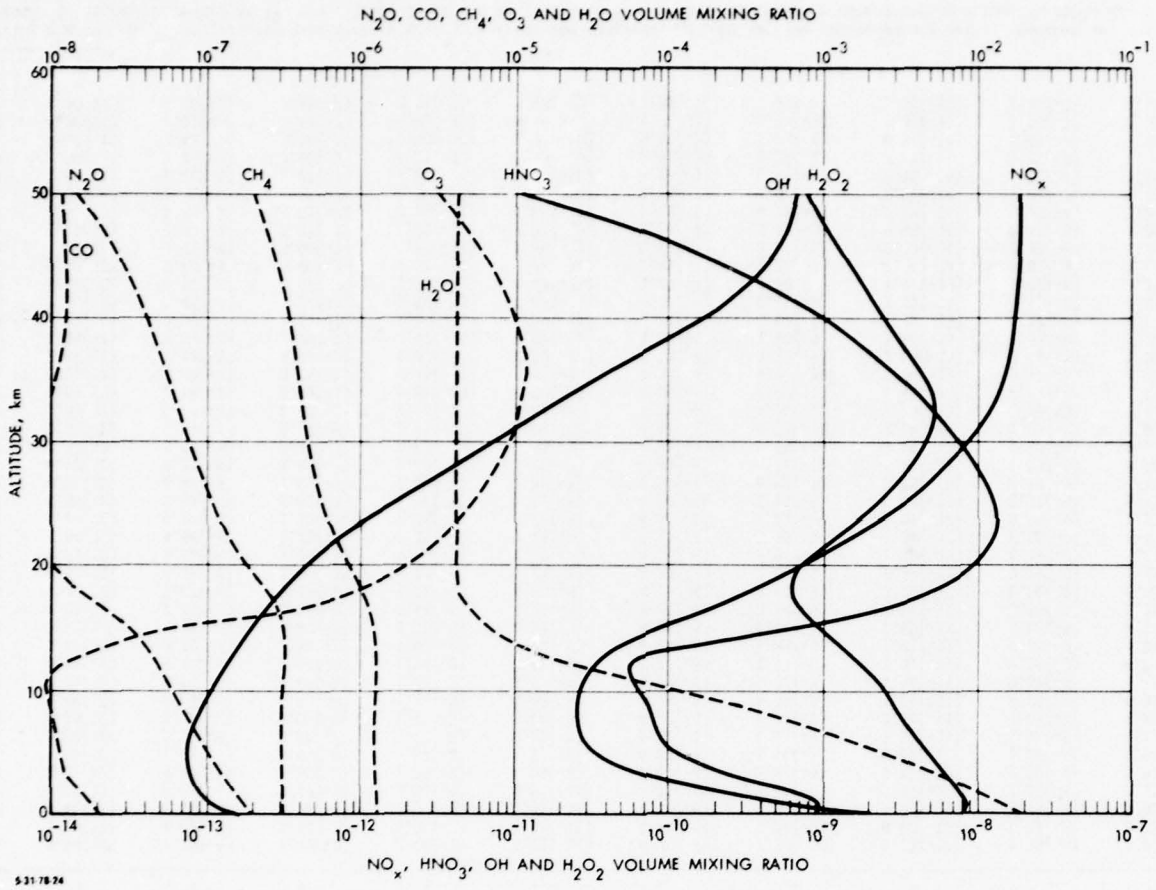

FIGURE 9. Simulated vertical profiles of 24-hour, zonal average of the volume mixing ratio of indicated species in the reference atmosphere at 40°N during summer (August 15) by the Widhopf model with 1976 chemistry. (Source: Widhopf, 1978)

24-hour average; a difference that becomes important for species with a short life relative to the diurnal cycle (i.e., NO, NO_2, N_2O_5, NO_3, H_2O_2, and OH). Therefore, a comparison of the results in Figs. 6 and 9 must be limited to the species with a relatively longer life. However, even then, the interpretation of any difference in such results must take into account the difference in the chemistry as illustrated previously by the reactions R15 and R21. These results indicate the following:

- The 1976 Widhopf HNO_3 profiles are somewhat higher than the Crutzen values above about 15 km altitude. For example, at 24 km altitude, the Widhopf HNO_3 is higher than the Crutzen value by about 11 percent.
- In spite of the higher Widhopf HNO_3 concentrations, the chemistry used in this model tends to give slightly higher ozone concentrations than the Crutzen values above 35 km altitude.
- The Widhopf ozone concentrations in the troposphere are significantly lower than the Crutzen values by a factor as low as approximately 0.15 at 10 km altitude. As indicated subsequently, the 2-D Crutzen ozone concentration for these conditions is lower than observations by about 40 percent (Fishman and Crutzen, 1978), which means that the Widhopf tropospheric ozone values are also significantly lower than observations.
- The Widhopf CO concentrations in the stratosphere are lower than the Crutzen values by a factor of approximately 0.3 at 30 km altitude.

A further comparison of the Widhopf and Crutzen results is given in a subsequent section, which includes the Fishman-Crutzen 2-D results for the troposphere based on the Howard-Evenson rate coefficient and the three-body component for the rate coefficient of the reaction $CO + OH (+M) \rightarrow CO_2 + H + (M)$.

Figure 10 shows results for a combined fleet of subsonics and SSTs as were obtained from the Widhopf model utilizing 1976 chemistry (Widhopf et al., 1977). The total NO_x emissions used in these results were 2.81×10^9 kg of NO_2 per year, which was distributed in altitude and latitude. The bulk of the NO_x emissions (97 percent) was assumed to take place at altitudes below 15 km, so that the SST component of the NO_x emissions in the altitude range $15 \leq z \leq 19$ km was a relatively small fraction of the total NO_x emissions. The latitudinal distribution of the NO_x emissions (Fig. 7) was similar to that of the subsonics for the Crutzen model.

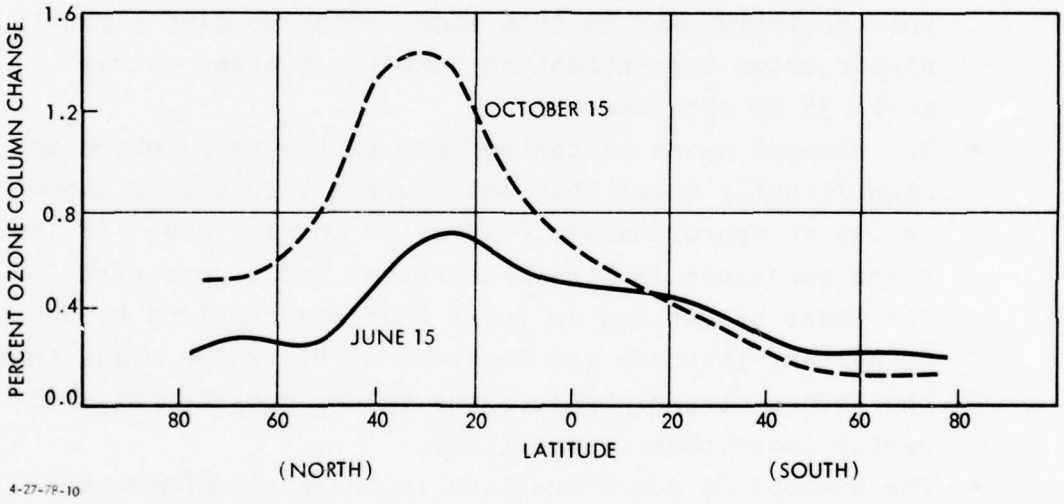

FIGURE 10. Effects of a combined fleet of subsonic and supersonic aircraft on the atmospheric ozone column during summer (June 15) and fall (October 15) after five years of fleet operations. NO_x emissions were for projected fleets assumed to operate in the 1990-time frame. (Source: Widhopf, et al., 1977)

It should be noted that, based on 1-D experience (e.g., Oliver et al., 1977; Broderick, 1977), the above slower rate for R(21) in the Widhopf (as compared with that of the Crutzen) model would tend to decrease the corresponding perturbations of the reference ozone column by SSTs.

Even without consideration of the subsequent 1977 revision of the 1976 chemistry by the Howard-Evenson measurement of the reaction rate for R14, important caveats in regard to the results in Figs. 7 and 10 are as follows: (1) they omitted the simulation of chlorine chemistry in the atmosphere; i.e., of the interactions among the HO_x - NO_x - ClO_x cycles in an oxygen-hydrogen-nitrogen-chlorine atmosphere; (2) they could not, at the time, incorporate the simultaneous effect of the aircraft H_2O effluents, which could again play a significant role in the coupling of the stratospheric HO_x - NO_x - ClO_x cycles; and (3) they had to omit consideration of the peroxynitric acid (HO_2NO_2) molecule or reaction $HO_2 + NO_2 \rightarrow HO_2NO_2$. Although it was considered likely that this reaction takes place in the atmosphere, virtually nothing was known of its kinetics (Hidalgo and Crutzen, 1977). Furthermore, it should be noted that no sensitivity analysis is yet available concerning the effect of subsonics on the calculated change of the ozone column from the uncertain knowledge of the reaction rate coefficients, and even some of the chemical mechanisms, in the troposphere.

3. IMPACT OF CHANGES IN OZONE CHEMISTRY ON 2-D MODELING

Table 3 identified the 1976 photochemistry and chemical kinetics of the troposphere and stratosphere that has been used in 2-D models for an oxygen-hydrogen-nitrogen (O-H-N) atmosphere. This formulation must not only be extended to include chlorine chemistry (i.e., M2, M17, Table 1) and molecules such as HO_2 NO_2, but the complexity of some of the chemical cycles in this table is such as to produce significant uncertainties on their mechanisms and/or rates. These complexities have prevented direct measurements of some of these reaction rate coefficients, which had then to be estimated theoretically from appropriate ratios involving other reactions with better known rate coefficients. As indicated in the previous section, it has been possible to identify the most important reactions in Table 3 (i.e., R7, 13, 14, 15, 21) for the effects of SSTs on ozone for an O-H-N atmosphere. Ongoing research has recently achieved direct measurements of most of these important rate coefficients. Nevertheless, because of the remaining uncertainty in the knowledge of the tropospheric and stratospheric chemistry, as well as the empirical 2-D formulation of the essentially unknown stratospheric dynamics, it is important to indicate that experience with photochemical models has brought out their rather severe inherent limitations due to the availability of a significant number of degrees of freedom for the tuning of a limited set of observations.* Using a reversed chronological order, a brief summary of this experience is as follows:

*Because of the four types of basic limitations indicated previously (Section 1.0), it is important to emphasize that most of these inherent limitations would also be applicable to 3-D and 1-D models.

- The recent development of a laser-magnetic resonance detection technique has allowed direct measurements of HO_2 in the reactions $HO_2 + NO \rightarrow OH + NO_2$ (R14) and $O_3 + HO_2 \rightarrow OH + 2\ O_2$ (R13). This technique has yielded the new (1977, 1978) rate coefficients for these reactions as described before. The 1977 result for R14 is a factor of about 40 faster than the 1976 values used in the Crutzen (2.2×10^{-13}) and Widhopf (2.3×10^{-13}) 2-D models. The 1977 direct measurement of the rate coefficient for R14 significantly upset previous results, which had implied an accurate, model-independent matching of, for example, either vertical ozone profiles at various latitudes and seasons (Widhopf, Glatt, and Kramer, 1977) or those of methane and nitric acid (Hidalgo and Crutzen, 1977). It then becomes evident that artificial combinations of reaction rate coefficients have yielded an adequate matching between the calculated and observed distributions of chemical species in the reference atmosphere.
- Initial experimental results (Burrows et al., 1977) and upper limit considerations (Chang and Kaufman, 1977; Howard, 1977) for the rate coefficient of $OH + HO_2 \rightarrow H_2O + O_2$ (R21), have led to a recommended value of 3.0×10^{-11} cm^3/ molecule-sec for this coefficient (NASA, 1977). This recommended value is nearly an order of magnitude slower than the 1974 value (2.0×10^{-10}) used in the Climatic Impact Assessment Program (CIAP). The revision of this rate coefficient had a significant impact on the previous CIAP results for the probable effects of high-altitude flight on the ozone column (Grobecker et al., 1974; National Academy of Sciences, 1975). Based on 1-D model results, the revision of this rate coefficient produced a significant downgrading of the CIAP assessment of the

potential effects of SSTs on the reference ozone column (Broderick, 1977; Oliver et al., 1977).

- Inclusion of the reaction OH + NO_2(+M) → HNO_3(+M) (R15), in the CIAP assessment of the effects of SST on the ozone column brought about a downgrading, by a factor of about 2, of a previous 1-D assessment of such effects; which had been made without the use of this reaction (Chang, Hidalgo, and Johnston, 1975).
- A pioneering effort on the 2-D modeling of atmospheric ozone found it even feasible to match the ozone column as a function of latitude and season through the use of only the O_x Chapman cycle (R1 to R5, Table 3) and suitable parameterization of the eddy motions (Prabhakara, 1963). The emphasis of this effort was to bring out the role of the dynamics in the stratospheric distribution of ozone.

The foregoing experience indicates that, although significant progress has been made during recent years in measuring important reaction rates for an O-H-N atmosphere, the quantitative 2-D assessment of high-altitude flight on the ozone column has yet to meet satisfactorily the rigorous standards of science, a result that is a consequence of the basic constraints indicated in Section 1. This experience also indicates that consensus of expert human judgment unsupported by critical experiments has not been able to resolve the very complex geophysical puzzles involved in the consideration of the ozone (and climate) change problems. Had such an approach been used, for example in the time of Copernicus, a most probable consensus would have been that the earth did not move.

3.1 UNDERDESTRUCTION OF OZONE WITH 1977 CHEMISTRY

The original O_x cycle (R1-R5, Chapman 1930) was proposed to explain the characteristics of the ozone column. However,

the subsequent gathering of more accurate ozone data developed a need for ozone destruction mechanisms (i.e., M2, Table 1) so as to reduce the calculated Chapman ozone column to the observed values (Johnston, 1975). The evolution of these ozone sinks started with the introduction of the HO_x catalytic cycle (i.e., χ = OH in M2) and has proceeded with the subsequent advents of the NO_x and ClO_x catalytic cycles in the stratosphere.

Prior to the direct measurement by Howard and Evenson of the rate coefficient for the reaction $HO_2 + NO \rightarrow OH + NO_2$, the ozone sinks had been adjusted in the Crutzen 2-D model with the HO_x and NO_x cycles in Table 3. Likewise, the Widhopf 2-D model had used these same cycles, but with some modification in the rate coefficients. However, preliminary results using the Howard and Evenson rate coefficient in the Widhopf model for an O-H-N atmosphere yield ozone columns that are significantly larger than the observed values at all latitudes in the Northern Hemisphere. Figure 11 shows some results from preliminary investigations using the Widhopf model that gave the results in Fig. 10, except for the following modifications (Widhopf and Glatt, 1978): (a) change to the faster Howard-Evenson rate coefficient, (b) changes of other reaction rates to the 1977 NASA recommended values, (c) incorporation of the N_2O_5 and NO_3 species, (d) modifications of the radiation calculations to include multiple scattering and the long wavelength absorption by H_2O_2, (e) change from the 24-hour diurnal to the daylight-night average of the concentration of chemical species, (f) extrapolations of the 2-D vertical eddy coefficients in the middle and upper stratosphere based on the Hunten (1975) instead of the previous McElroy et al. (1974) 1-D vertical eddy coefficients, the former being about a factor of two smaller than the latter, and (g) calculation, instead of specification, of the water vapor distribution.

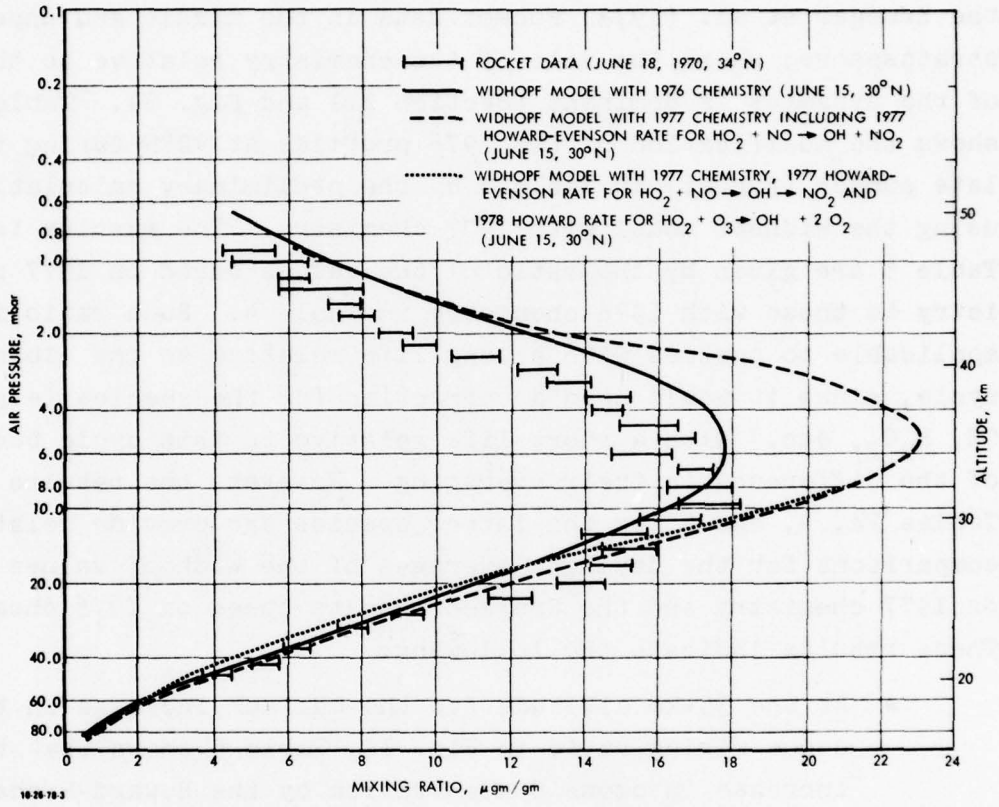

FIGURE 11. Illustration of the impact of the Howard-Evenson reaction rate coefficient on the simulated ozone mixing ratio for the reference atmosphere. Data in Table 5 shows an increase of about 28% on the ozone concentration at 35 km altitude from use of the Howard-Evenson reaction rate coefficient for $HO_2 + NO \rightarrow OH + NO_2$ instead of that used for the results shown in the previous figure. The use of the 1978 Howard rate for $HO_2 + O_3 \rightarrow OH + 2O_2$ does not correct the ozone imbalance above about 30 km altitude. Note the use of a linear, instead of a logarithmic scale so as to display the mismatch in the ozone profile above 30 km. (Source: Widhopf, 1978)

Figure 11 shows that the Howard-Evenson rate coefficient yields significantly higher ozone concentrations than, for example, the Krueger et al. (1973) rocket data in the middle and upper stratosphere; where the role of the chemistry relative to that of the dynamics is dominant (Section 2.1 and Fig. 5). Table 5 shows the modification of the 1976 profiles at 40°N during the late summer (August) in Table 4 by the preliminary calculations using the Widhopf model with 1977 chemistry. The results in Table 5 are given by the ratio of the values based on 1977 chemistry to those with 1976 chemistry in Table 4. Such ratio is applicable to species with a long life relative to the diurnal cycle, since it would need a correction for the species (e.g., OH, H_2O_2, etc.) with a short life relative to this cycle because of the difference in their averaging. However, the results in Tables 2a, 4, and 5 for the latter species can provide relative comparisons for the daylight averages of the Widhopf values based on 1977 chemistry and the Crutzen results based on 1976 chemistry. These results indicate the following:

- At the 35-km altitude for the maximum increase in the ozone mixing ratio in Fig. 11, Table 5 shows that the increase in ozone concentration by the Howard-Evenson rate coefficient in the Widhopf model is about 28 percent. The tropospheric ozone has been increased by factors of better than 2. The corresponding increase in the total ozone columns is 16.5 percent; i.e., from 8.1×10^{18} molecules/cm^2 (Table 4) to 9.5×10^{18} molecule/cm^2 (Tables 4 and 5).*

*At the other latitudes and time of the year, this increase in the ozone column can be 20 to 30 percent higher than either the observed or calculated value with the 1976 chemistry (Widhopf and Glatt, 1978).

TABLE 5. RATIO OF VALUES BASED ON HOWARD-EVENSON RATE (DAILY AVERAGES) TO THOSE CORRESPONDING IN TABLE 4 (24-HOUR AVERAGE) AT 40°N DURING LATE SUMMER.
(Source: Widhopf, 1978)

Z (km)	O_3	N_2O	NO_x	HNO_3	H_2O	H_2O_2	OH	CO	CH_4
50.0	0.926	0.425	1.115	0.426	1.143	0.424	1.261	0.736	0.408
47.5	0.948	0.462	1.060	0.525	1.145	0.391	1.288	0.712	0.431
45.0	1.012	0.494	1.066	0.467	1.150	0.363	1.383	0.641	0.456
42.5	1.121	0.549	1.051	0.569	1.143	0.311	1.527	0.581	0.489
40.0	1.196	0.599	1.022	0.783	1.180	0.242	1.794	0.540	0.521
37.5	1.202	0.631	0.990	0.914	1.203	0.173	2.166	0.511	0.540
35.0	1.277	0.656	0.672	0.783	1.231	0.158	2.398	0.490	0.558
34.0	1.258	0.671	0.654	0.804	1.240	0.139	2.512	0.482	0.570
33.0	1.235	0.691	0.640	0.824	1.248	0.123	2.649	0.479	0.585
32.0	1.214	0.719	0.628	0.844	1.257	0.109	2.745	0.480	0.605
31.0	1.192	0.756	0.620	0.860	1.263	0.097	2.829	0.488	0.632
30.0	1.171	0.798	0.617	0.870	1.267	0.088	2.904	0.502	0.662
29.0	1.151	0.846	0.630	0.876	1.270	0.080	3.012	0.520	0.697
28.0	1.131	0.897	0.647	0.881	1.272	0.072	3.082	0.541	0.735
27.0	1.115	0.946	0.670	0.879	1.273	0.067	3.128	0.563	0.772
26.0	1.100	0.988	0.701	0.878	1.275	0.062	3.173	0.580	0.805
25.0	1.087	1.018	0.738	0.876	1.278	0.058	3.212	0.592	0.832
24.0	1.078	1.037	0.782	0.874	1.287	0.054	3.252	0.598	0.854
23.0	1.078	1.053	0.825	0.871	1.311	0.045	3.313	0.603	0.877
22.0	1.083	1.074	0.852	0.861	1.364	0.049	3.361	0.609	0.907
21.0	1.082	1.104	0.850	0.829	1.461	0.050	3.633	0.614	0.951
20.0	1.071	1.120	0.834	0.765	1.564	0.047	3.915	0.601	0.998
19.0	1.082	1.099	0.842	0.702	1.529	0.038	3.997	0.561	1.013
18.0	1.101	1.068	0.881	0.637	1.334	0.025	3.818	0.524	0.737
17.0	1.159	1.039	0.901	0.567	1.058	0.017	3.510	0.504	1.008
16.0	1.277	1.020	0.806	0.466	0.537	0.014	3.142	0.525	1.005
15.0	1.453	1.010	0.546	0.282	0.269	0.015	2.601	0.565	1.004
14.0	1.647	1.007	0.283	0.096	0.268	0.018	1.943	0.609	1.006
13.0	1.838	1.007	0.121	0.125	0.513	0.023	1.511	0.626	1.007
12.0	2.014	1.007	0.071	0.093	1.047	0.031	1.796	0.620	1.006
11.0	2.184	1.006	0.071	0.116	1.179	0.044	2.413	0.619	1.004
10.0	2.386	1.007	0.079	0.171	1.035	0.061	3.174	0.642	1.003
9.0	2.365	1.008	0.092	0.305	0.932	0.092	4.147	0.680	1.003
8.0	2.397	1.009	0.112	0.536	0.907	0.129	5.162	0.722	1.002
7.0	2.416	1.009	0.143	0.932	0.926	0.174	6.056	0.767	1.002
6.0	2.472	1.009	0.169	1.449	0.940	0.219	6.779	0.816	1.002
5.0	2.531	1.008	0.178	1.873	0.934	0.263	7.028	0.880	1.004
4.0	2.519	1.007	0.164	1.955	0.932	0.300	6.907	0.945	1.006
3.0	2.392	1.005	0.140	1.636	0.970	0.321	6.345	1.000	1.008
2.0	2.100	1.003	0.131	1.232	0.993	0.318	5.744	1.034	1.009
1.0	1.693	1.002	0.152	0.932	1.001	0.300	5.756	1.038	1.007
0	1.200	1.000	0.202	1.088	1.000	0.314	14.181	1.000	1.000

- Table 5 for the Widhopf model shows that the HNO_3 profiles based on 1977 chemistry have decreased significantly in the stratosphere and upper troposphere, whereas those of H_2O in the middle and upper stratosphere have increased appreciably. The reason for the former effect must take into account the corresponding changes in the chemistry, including the consideration of NO_3 species as described previously, whereas the latter effect is due to the calculation, instead of the 1976 specification, of the water vapor distribution.
- The results for NO_x in Table 5, together with those in Tables 2a and 4 indicate that the (daylight) NO_x concentrations in the upper troposphere have decreased by more than an order of magnitude from the 1976 Crutzen value (Table 2a) to the Widhopf value based on 1977 chemistry (Table 5). This Widhopf result, which is of interest for subsonic flights, is a trend toward the Noxon observed values.

The underdestruction of ozone from the use of the Howard-Evenson rate coefficient with 1977 chemistry, as indicated in Fig. 11, becomes important through the following effects (Crutzen and Howard, 1978): (a) a faster rate for $HO_2 + NO \rightarrow OH + NO_2$ (R14) produces a larger production of OH radicals below about 35 km than before. This implies a more efficient conversion of NO_x into the HNO_3 sink through the reaction $OH + NO_2(+M) \rightarrow HNO_3(+M)$ (R15), and (b) the weakening of the ozone destruction by the reaction $OH + O_3 \rightarrow HO_2 + O_2$ (R7) in the HO_x catalytic cycle M3b (Table 1). This latter result is a consequence of the last three reactions (R14, R35, R2) in M4b, which produce as a net the reaction $HO_2 + O_2 \rightarrow OH + O_3$ (R13); a result that, in turn, is opposite to that of R7 in M3b.

Relative results from a 1-D model by S.C. Liu, utilizing the 1977 Howard-Evenson rate coefficient for $HO_2 + NO \rightarrow OH + NO_2$

indicated a decrease by about 9 percent in the ozone column when using the 1978 instead of the 1977 NASA rate coefficient for $HO_2 + O_3 \rightarrow OH + 2\ O_2$ (Zahniser and Howard, 1978). Similar preliminary considerations using the Widhopf 2-D model also indicate the same effects, i.e., the 1978 rate coefficient for $HO_2 + O_3 \rightarrow OH + 2\ O_2$ reduces the imbalance in the *ozone column* to about 10 percent above the observed value for the conditions shown in Fig. 11. However, this effect on the ozone column is caused by an ozone decrease in the lower stratosphere, which is a region where the mass transports become important (Section 2.1, Fig. 5) and the ozone concentrations are relatively high (Table 4). Hence, the calculated imbalance in the ozone mixing ratio in the middle and upper stratosphere caused by the 1977 rate coefficient for $HO_2 + NO \rightarrow OH + NO_2$ is almost unaffected by the more recent measurement of the rate coefficient for $HO_2 + O_3 \rightarrow OH + 2\ O_2$ (Fig. 11). These preliminary results suggest a need for a reassessment of the remaining reaction rate coefficients for an O-H-N atmosphere as well as considerations of the chlorine chemistry for the middle and upper stratosphere.

3.2 ESTIMATES OF TROPOSPHERIC NO_x AND H_2O_2 RAINOUT SINKS

Section 2 presented qualitative considerations which indicated that the results in Fig. 7, for the effect of subsonic flight at 10.8 km on the ozone column, will be increased as a consequence of the faster Howard-Evenson rate coefficient; which yields also a lower calculated tropospheric NO_x background. To provide quantitative considerations of this effect, it is of interest to describe now some relevant results based on 1977 chemistry as obtained by a global, tropospheric, non-dynamical, chemical 2-D model (Fishman and Crutzen, 1978). From the point of view of aircraft effects on the ozone column, emphasis here is on the Northern Hemisphere as well as on (a) the indirect assessments of the amount of NO_x background in

the troposphere, (b) a qualitative assessment of the direction of the change of the ozone column by subsonic flight in the upper troposphere from the revision of the 1976 chemistry by both the Howard-Evenson and Noxon NO_x data, and (c) assessments of the magnitude of the heterogenous removal rates of chemical species in the tropospheric sinks.

The basic approach used in the Fishman-Crutzen (1978) 2-D investigations consists in examining the compatibility of assumed NO_x backgrounds in the troposphere with the corresponding O_3 and CO budgets in the Northern and Southern Hemispheres. Figure 2 indicated that these budgets are essentially controlled by mechanisms M3(a, b, c) and M4(a, b), while Table 1 showed that these mechanisms involve the HO_x (i.e., OH, HO_2), NO_x (NO and NO_2), and CH_4 species. From Table 3, the considerations of the O_3 and CO budgets put emphasis on the odd hydrogen HO_x species (R6 to R23), NO_x (R33, 35), and the methane oxidation reactions (R24 to R32). Two important considerations in these 2-D calculations in the troposphere are the short lifetimes of the HO_x species and their consequent equilibrium with a prescribed background of O_3, CO, H_2O, CH_4 and the unknown NO_x. These considerations allow the calculation of the HO_x species by using a quasi-steady state or equilibrium 2-D model with prescribed tropospheric distributions of O_3, CO, H_2O, CH_4, and NO_x as a function of season in both hemispheres. Other important consequences of these considerations are the lack of requirements for both time-dependent calculations for a given season and parameterizations of the tropospheric 2-D dynamics.

Because of the current lack of adequate statistical data for NO_x and HO_x species, the basic aim in these calculations is then to examine the sensitivity of the tropospheric O_3 and CO budgets as a function of prescribed levels of NO_x. The most probable values of NO_x (and HO_x) in the troposphere would then be given by the assumed NO_x amount that is most consistent with the balancing of the O_3 and CO budgets. The emphasis on con-

sistency instead of exact matching of these budgets stems from the rather significant uncertainties in the current knowledge of these budgets. It is important to emphasize that these 2-D calculations utilized 1977 chemistry as given by:

- The 1977 Howard-Evenson rate coefficient for R14
- The three-body component for the CO and OH reaction, which becomes important in the troposphere. Hence, in addition to the two-body reaction R8 in Table 3, these tropospheric calculations used the reaction $CO + OH(+M) \rightarrow CO_2 + H(+M)$ with a three-body rate coefficient given by $7.3 \times 10^{-33}[M]$ cm^3/molecule-sec (Chan et al., 1977).
- The photolysis rate (J) for $O_3 + h\nu \rightarrow O_2 + O(^1D)$ (R3a) that includes a temperature dependence in its quantum yield $\phi(\lambda)$. This latter parameter is defined by

$$J = \int_{290}^{320} Q\sigma\phi d\lambda \ ,$$

  where Q is the solar flux, σ the ozone cross section, and λ the wavelength in the range $290 \leq \lambda \leq 320$ nm. The temperature dependence of the quantum yield can alter the calculated production rate of $O(^1D)$ by as much as 20 percent over the range of tropospheric temperatures.
- The NASA (1977) revisions of the other rate coefficients in Table 3.
- The heterogenous removal of H_2O_2 and CH_3O_2H.

In addition, these 2-D calculations included the reaction of methyl chloroform (CH_3CCl_3) with OH; i.e., $CH_3CCl_3 + OH \rightarrow H_2O + CH_2\ CCl_3$. Other modifications of the reactions in Table 3 for this tropospheric model were as follows: the dropping of R1, R3b and R4 in the oxygen reactions; the dropping of R6, R10, R12, and R20 for the hydrogen species; and the replacement of R26 with $CH_3O_2H + OH \rightarrow CH_3O_2 + H_2O$.

Figure 12 defines the assumed input levels of NO_x used in these 2-D calculations. The profile A is representative of unpolluted conditions and it is consistent with both the Noxon (1977) and the surface observations of Drummond (1977) for clean air in Wyoming. This profile gives a tropospheric column density of 2.1×10^{14} molecules/cm^2. The profile B is assumed to represent polluted conditions with a corresponding column density of 4.6×10^{14} molecules/cm^2. Profile A is used at latitudes $\theta \leq 15°N$ and in the entire Southern Hemisphere, whereas profile B is used at $\theta \geq 45°N$. Intermediate profiles are used in the latitude range $15°N \leq \theta \leq 45°N$. These 2-D calculations utilized four assumed levels of NO_x which were given by:

- A low, constant vertical profile of the volume mixing ratio at every latitude given by a value of 10^{-12} or a tropospheric column density of 0.2×10^{14} molecules/cm^2
- The profiles A and B or corresponding column densities of 2.1×10^{14} and 4.6×10^{14} molecules/cm^2 with latitudinal distributions as described before. The average NO_x column density in the Northern Hemisphere is then 3.4×10^{14} molecules/cm^2
- Twice those of profiles A and B
- A high, constant vertical profile of the volume mixing ratio at every latitude given by a value of 10^{-10} or a tropospheric column density of 22.9×10^{14} molecules/cm^2.

Hence, the assumed NO_x distributions in the troposphere of the two hemispheres varied by about two orders of magnitude.

3.2.1 Assessment of Tropospheric NO_x in the Northern Troposphere

Table 6 shows the sensitivity of the tropospheric ozone production (M4a, b, Table 1) and destruction (M3a, b, c) mechanisms in the Northern Hemisphere to the foregoing assumed amounts of NO_x. The ozone production by mechanisms 4a and 4b

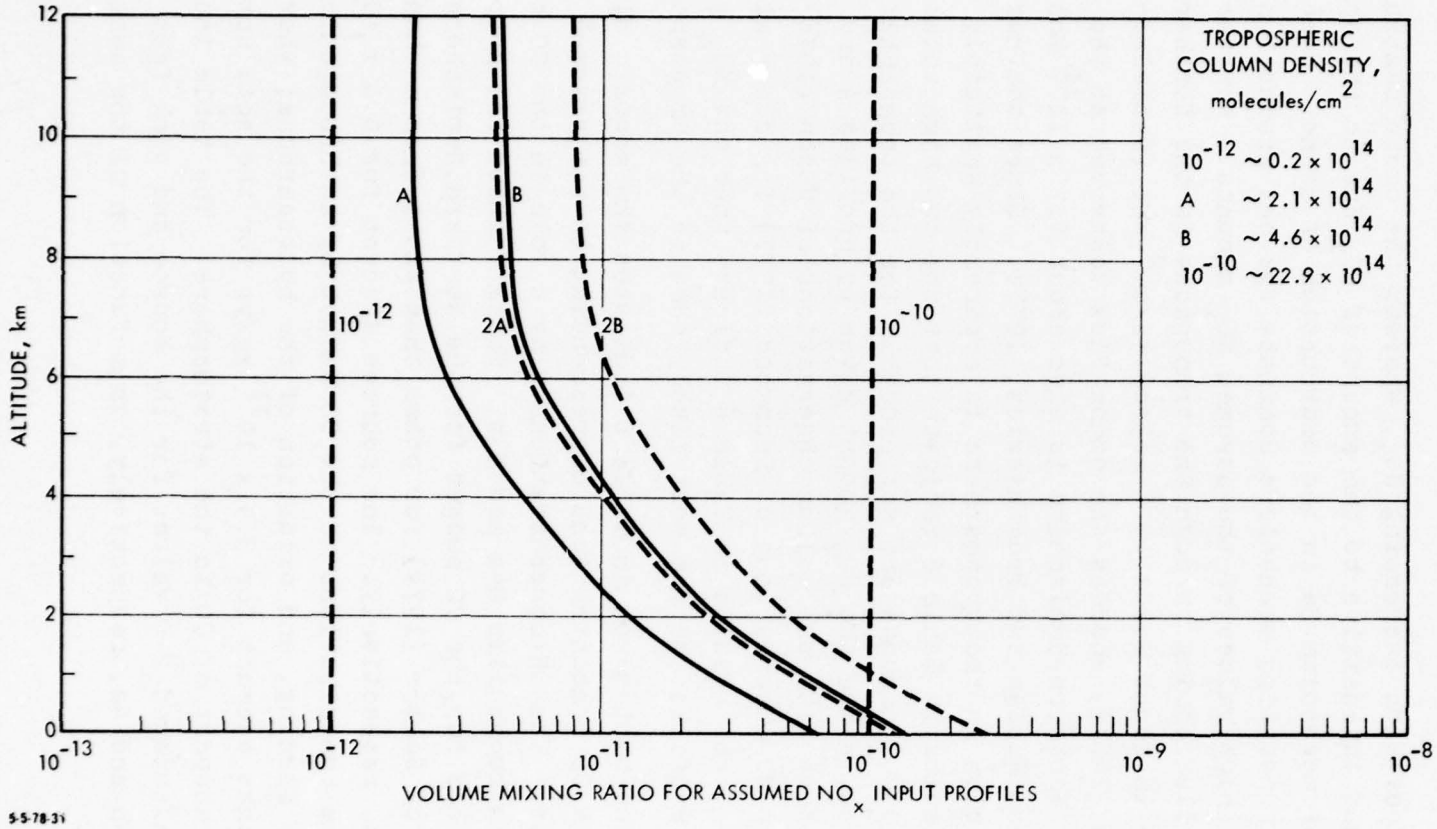

FIGURE 12. Assumed tropospheric NO_x profiles for sensitivity analysis of the tropospheric ozone and CO budgets to NO_x and HO. (Source: Fishman and Crutzen, 1978)

increases with increasing NO_x, whereas the ozone destruction is somewhat insensitive to the amount of NO_x due to the dominant role of mechanism 3a in the destruction of ozone. Hence, the ozone production mechanisms dominate the net production of ozone at the high values of the assumed NO_x amounts. However, the ozone flux coming through the tropopause in the Northern Hemisphere is about 0.7×10^{11} molecules/cm^2-sec (Danielsen and Mohnen, 1977), whereas the ozone flux destroyed at the ground in the Northern Hemisphere is also about 0.7×10^{11} molecules/cm^2-sec (Fabian and Pruchniewicz, 1977). Since the net ozone production in the troposphere is apparently negligibly small, the results in Table 6 indicate that the two high values of the assumed NO_x amounts are not probable for the troposphere. Furthermore, since the NO_x amount given by profiles A and B are consistent with the column observations of Noxon (1978) and the surface NO observations of Drummond (1977) for clean air in Wyoming, the results in Table 6 indicate that the NO_x given by these profiles are the most likely ones in the troposphere.

The bottom row in Table 6 indicates the annual, diurnal average OH concentrations corresponding to the assumed NO_x amounts. The OH concentrations play a role in the CO budget through mechanisms M4a and M4b. Table 7 shows the sources and sinks for the CO budget for the Northern Hemisphere as given by Seiler (1974) for other than those from mechanisms 4b and 4a, respectively. The sources account for 6.6×10^{11} kg/yr for the contributions to the CO budget by anthropogenic, oceans, forest burning, and oxidation of the hydrocarbons; whereas the sinks account for 3.9×10^{11} kg/yr for the soil uptake and the transport of CO to the stratosphere. The table includes the calculated 2-D values for the source and sink from mechanisms 4b and 4a, respectively, as a function of the assumed NO_x

TABLE 6. SENSITIVITY OF OZONE BUDGET TO PRESCRIBED NO_x CONCENTRATIONS FOR THE NORTHERN HEMISPHERE (Source: Fishman and Crutzen, 1978)

	Assumed NO_x (10^{14} molecules/cm^2)			
	0.2	3.4	6.8	22.9
Ozone Production (M4a, b) (10^{11} molecules/cm^2 sec)	0.1	1.8	3.3	10.0
Ozone Destruction (M3a, b, c) (10^{11} molecules/cm^2 sec)	1.2	1.2	1.2	1.4
Net Ozone Production (10^{11} molecules/cm^2 sec)	-1.1	0.6	2.1	8.6
Annual Diurnal Average OH Concentration in Northern Hemisphere (10^5 molecules/cm^3)	2.9	3.3	3.9	9.5

TABLE 7. SENSITIVITY OF CO BUDGET TO PRESCRIBED NO_x CONCENTRATIONS FOR THE NORTHERN HEMISPHERE* (Sources: Seiler, 1974; Fishman and Crutzen, 1978)

	Assumed NO_x (10^{14} molecules/cm^2			
Sources (10^{11} kg/year)	0.2	3.4	6.8	22.9
Anthropogenic	5.4	5.4	5.4	5.4
Oceans	0.4	0.4	0.4	0.4
Forest Burning	0.4	0.4	0.4	0.4
Oxidation of Hydrocarbons	0.4	0.4	0.4	0.4
CH_4 oxidation (M4b)	1.7	1.7	2.2	3.7
Total Sources	8.3	8.3	8.8	10.3
Sinks (10^{11} kg/year)				
Soil uptake	3.0	3.0	3.0	3.0
Transport to Stratosphere	0.9	0.9	0.9	0.9
CO Oxidation (M4a)	6.7	8.9	11.2	31.8
Total Sinks	10.6	12.8	15.1	35.7
Imbalance (10^{11} kg/year)	-2.3	-4.5	-6.3	-25.4

*For the Southern Hemisphere and NO_x amount of 3.4×10^4 molecules/cm^2, for example, the corresponding source and sink total values are 3.6 and 7.7 (in units of 10^{11} kg/yr), respectively (Fishman and Crutzen, 1978).

amounts. The results in this table indicate that the imbalance between the total sources and sinks is aggravated significantly as the assumed NO_x amount increases, an effect that is due to the resulting increase in the average OH concentration (bottom row, Table 6) and overdestruction of CO. Therefore, as in the case of the ozone budget, the two higher values of the assumed NO_x amounts are again not probable for the troposphere. In regard to the new, significantly lower estimate of the annual, diurnal average of the OH concentrations in the northern troposphere ($\sim 3.3 \times 10^5$ molecules/cm^3, Table 6), it should be noted that it implies more reasonable magnitudes for mechanisms 4b and 4a than before. As indicated by Seiler (1974), previous estimates for the source M4b were in the excessive range from 15×10^{11} to 40×10^{11} kg/yr, and for the sink M4a from 19.4×10^{11} to 50×10^{11} kg/yr. The significantly lower values for the CH_4 and CO oxidations in Table 7 stem from the new revisions in the chemistry. Nevertheless, the still significant imbalance of the CO budget for the lower NO_x amounts in Table 7 suggests that (a) each of the Seiler sources and sinks may have to be reevaluated, and (b) the tropospheric OH must be much better known as a function of latitude and season. It is important to note that because of the high variability of OH, such data should be accompanied by simultaneous measurements of H_2O_2, O_3, H_2O, etc.

3.2.2 Ozone Change Due to Subsonics with 1977 Chemistry

The results in Fig. 7 for the effects of subsonic flight at 10.8 km at 45°N latitude during summer were based on an NO_x background given by a volume mixing ratio of 6.5×10^{-11} (Table 2a), a result that is a factor of about 16 larger than that of the polluted profile B in Fig. 12 ($\sim 4 \times 10^{-12}$). Therefore, in order to examine qualitatively the direction of the ozone effect shown in Fig. 7 as a consequence of the Howard-Evenson

and Noxon data, it becomes of interest to return to the results for the ozone production mechanism in Table 6. As indicated by mechanisms 4a and 4b in Table 1, the oxidations of CO and CH_4 produce one O_3 molecule for each CO and four O_3 for each CH_4 molecule. However, a limiting step in the CH_4 oxidation is the photolysis of CH_2O. Consideration of the photolysis rates in the photochemical reactions R30a, b, reduces the efficiency of the methane oxidation to the production of only 2.5 molecules of O_3 for each molecule of CH_4. Thus, an upper limit for the production of O_3 is given by the sum of the CO oxidation and 2.5 times that of CH_4. However, from the actual model results, it becomes possible to determine a corresponding true "O_3 efficiency production factor" for each of the four assumed NO_x distributions. Table 8 gives a summary of these results, which include the magnitude of the CO and CH_4 oxidations, the upper limit O_3 production, the actual ozone production that was given in Table 6, and the O_3 efficiency production factor. Thus, for the NO_x profiles A and B (second column), the upper limit O_3 production of 3.5×10^{11} molecules/cm^2-sec is given by the CO oxidation and 2.5 times that of methane. This upper limit O_3 production, together with the actual ozone production of 1.8×10^{11} molecules/cm^2-sec yield, then, an efficiency factor of 0.5. Important results in Table 8 are (a) the dominant role of the CO relative to the CH_4 oxidation and (b) the increase in both the upper-limit O_3 production and O_3 efficiency production factor with increasing NO_x amounts.

TABLE 8. SENSITIVITY OF TROPOSPHERIC OZONE PRODUCTION TO PRESCRIBED NO_x CONCENTRATIONS FOR THE NORTHERN HEMISPHERE

(Source: Fishman and Crutzen, 1978)

	Assumed NO_x (10^{14} molecules/cm^2)			
	0.2	3.4	6.8	22.9
CO oxidation (M4a) (10^{11} molecules/cm^2sec)	1.8	2.4	3.0	8.5
CH_4 oxidation (M4b) (10^{11} molecules/cm^2sec)	0.4	~ 0.4	~ 0.6	~ 1.0
Upper Limit O_3 Production (M4a, b) (10^{11} molecules/cm^2sec)	2.8	~ 3.5	~ 4.4	~ 10.9
Ozone Production (M4a, b) (10^{11} molecules/cm^2sec)	0.1	1.8	3.3	10.0
O_3 Efficiency Production Factor (M4a, b)	0.03	0.5	0.75	0.92

The relative importance of the Howard-Evenson and Noxon data in the ozone production by NO_x effluents in the upper troposphere may then be assessed by examining the reactions in mechanisms M4a; i.e.,

(R8) $CO + OH\ (+M) \rightarrow CO_2 + H\ (+M)$

(R11) $H + O_2 + M \rightarrow HO_2 + M$

(R14) $HO_2 + NO \rightarrow OH + NO_2$

(R35) $NO_2 + h\nu \rightarrow NO + O$

(R2) $O + O_2 + M \rightarrow O_3 + M$

$$CO + 2\ O_2 \rightarrow CO_2 + O_3$$

where (R8) includes the two-body reaction with (+M) = 0. The production of ozone takes place from the reaction of molecular oxygen with atomic oxygen (R2), the latter being produced by photolysis of NO_2 (R35). The role of NO_x and the Howard-Evenson

reaction rate takes place through the formation of NO_2 from HO_2 (R14); which is produced in the above chain from every H in (R8), through (R11). The relative fraction of the HO_2 molecules that become involved in R14 may be determined by examining the competing reactions for HO_2 in Table 3; i.e., R13, 14, 17, 21, and 27:

(R13) $O_3 + HO_2 \rightarrow OH + 2\ O_2$

(R14) $HO_2 + NO \rightarrow OH + NO_2$

(R17) $HO_2 + HO_2 \rightarrow H_2O_2 + O_2$

(R21) $OH + HO_2 \rightarrow H_2O + O_2$

(R27) $CH_3O_2 + HO_2 \rightarrow CH_3O_2H + O_2$

This relative fraction is then given from the normalized values of $k_i[\chi_i]/\Sigma k_i[\chi_i]$, where k_i is the rate constant, $[\chi_i]$ the concentration of the reactants for HO_2, and i the reactions R13, 14, 17, 21, and 27.

Table 9 shows results for these relative fractions for the 2-D model conditions of the subsonic flight in Fig. 7, and those given by the Howard-Evenson and representative NO_x profile B (Fig. 12). The former includes conditions for both the reference and perturbed tropospheres as determined from the Crutzen tropospheric-stratospheric 2-D model with 1976 chemistry. The latter are those from the Fishman-Crutzen 2-D model calculations for the reference troposphere including the Howard-Evenson rate coefficient, the modified R8 reaction to include the three-body component, the revisions in the quantum yield for the photolysis of $O(^1D)$, and the modified reaction rates as given by NASA (1977). The [NO] concentration in Table 9 for the Fishman-Crutzen 2-D calculations corresponds to that of profile B (Fig. 12) at 10.8 km and 45°N latitude. The results in Table 9 for the

TABLE 9. COMPETITION OF REACTIONS INVOLVING THE HO_2 RADICAL FOR IMPORTANT SUBSONIC FLIGHT CONDITIONS (~ 10.8 km, 45°N, August 30)

2-D Model	Reaction	Ambient Temperature °K	Rate Constant* k_i	Reactant Concentration** $[\chi_1]$	$[\chi_1]$	$k_i[\chi_1]$ (sec^{-1})	$\frac{k_i[\chi_1]}{\Sigma k_i[\chi_1]}$
Crutzen, Reference Atmosphere (1976 chemistry)	R13	227.2	4.1×10^{-16}	$[O_3]$	5.2(11)	2.1(-4)	0.29
	R14	--	2.2×10^{-13}	[NO]	4.1(8)	9.0(-5)	0.12
	R17	227.2	3.3×10^{-12}	$[HO_2]$	7.7(7)	2.5(-4)	0.35
	R21	--	5.0×10^{-11}	[OH]	8.5(5)	4.3(-5)	0.06
	R27	227.2	3.3×10^{-12}	$[CH_3O_2]$	3.9(7)	1.3(-4)	0.18
Crutzen, Atmosphere Perturbed by Aircraft NO_x Effluents (1976 chemistry)	R13	227.2	4.1×10^{-16}	$[O_3]$	5.8(11)	2.4(-4)	0.26
	R14	--	2.2×10^{-13}	[NO]	1.7(9)	3.7(-4)	0.39
	R17	227.2	3.3×10^{-12}	$[HO_2]$	5.4(7)	1.8(-4)	0.19
	R21	--	5.0×10^{-11}	[OH]	1.2(6)	6.0(-5)	0.06
	R27	227.2	3.3×10^{-12}	$[CH_3O_2]$	2.7(7)	9.0(-5)	0.10
Fishman-Crutzen, Reference Troposphere	R13	227.2	1.2×10^{-16}	$[O_3]$	8.1(11)	9.7(-5)	0.09†
	R14	--	8.0×10^{-12}	[NO]	3.0(7)	2.4(-4)	0.21
	R17	227.2	5.5×10^{-12}	$[HO_2]$	9.0(7)	5.0(-4)	0.44
	R21	--	5.0×10^{-11}	[OH]	8.8(5)	4.4(-5)	0.04
	R27	227.2	5.5×10^{-12}	$[CH_3O_2]$	4.5(7)	2.5(-4)	0.22

*cm^3/molecule - sec

**molecule/cm^3

†This contribution will be increased when using the 1978 reaction rate coefficient for R13.

$[CH_3O_2]$ concentrations are based on the approximation $[CH_3O_2] \simeq 0.5\ [HO_2]$, results that are further constrained by the significant uncertainty (unmeasured) in the reaction rate for (R27) involving HO_2 and CH_3O_2. The results for the reference and perturbed atmospheres with 1976 chemistry indicate the shift in the competition from R14 for HO_2 due to the increased NO_x by subsonic aircraft. These shifts indicate (a) an enhancement in the competition of (R14) for HO_2 by a factor of 3.3 as a result of the NO_x effluents, which produced the local ozone increase of 12 percent, and (b) a suppression of the R17 competition of HO_2 for itself by a factor of 1.8 as a consequence of the NO_x effluents. The results in Table 9 for the reference tropospheres indicate an enhancement in the competition from R14 for HO_2 by a factor of 1.8 as a result of the revision of the 1976 to the 1977 chemistry. Hence, the increased role of R14 in the competition for HO_2 in the reference troposphere within the dominant M4a mechanism, coupled with the weakening of the stratospheric NO_x catalytic cycle by R14, indicates that the change of the ozone column given in Fig. 7 for the 1976 chemistry should be enhanced by the 1977 chemistry. The direction of this effect is somewhat corroborated by preliminary results from the Widhopf model using the Howard-Evenson (1977) rate coefficient, which indicate that the previous peak enhancement of the ozone column in Fig. 10 increases from a value of about 1.4 percent to about 3.5 percent, even though the SST component of the combined fleet was increased by a factor of about 3 in the later calculations; which, however, included the effect of simultaneous injections of NO_x and H_2O engine effluents (Widhopf and Glatt, 1978).

3.2.3 Heterogeneous Removal Rates of H_2O_2 in Tropospheric Sinks

A fundamental unknown in tropospheric chemistry is the removal rate of water-soluble atmospheric gases by processes other than gas-phase reactions (e.g., M9, Table 1, and Fig. 2).

Estimates of these removal rates have been obtained by Fishman and Crutzen (1978) from the sensitivity of the imbalance of the CO budget (Table 7) to OH through the heterogeneous removal rates of H_2O_2. These 2-D calculations used the reactions

$$H_2O_2 \rightarrow \text{heterogeneous removal}$$
$$CH_3O_2H \rightarrow \text{heterogeneous removal},$$

both of which were assumed to have the same removal rate given by

$$k(z)_{het} = k^{\circ}_{het} \exp\,[-0.46(z-5)], \quad z > 5 \text{ km}$$

where $k^{\circ}_{het}(sec^{-1})$ is a constant for the heterogeneous removal rate below 5 km altitude. The exponential decay at altitudes above 5 km reproduces the observations of Davidson et al. (1966) for removal of radioactive debris. Table 10 gives results of these sensitivity analyses for a specified NO_x amount with an average column density of 3.4×10^{14} molecules/cm^2 (Table 7); which is given by profiles A or B (Fig. 12), depending on the latitude, as indicated previously. This table shows three values for k°_{het}, the largest one being the rate used in all the previous results (Tables 6 to 8). This table includes corresponding values of H_2O_2 in the lower (1 km) and upper (10 km) troposphere as well as the corresponding annual, diurnal average of OH in the Northern Hemisphere.

TABLE 10. SENSITIVITY OF OH TO REMOVAL RATES OF H_2O_2 FOR THE ASSUMED NO_x PROFILES A AND B IN THE NORTHERN HEMISPHERE

(Source: Fishman and Crutzen, 1978)

k°_{het} sec^{-1}	$(k^{\circ}_{het})^{-1}$	H_2O_2 (ppb), 1 km	H_2O_2 (ppb), 10 km	(OH) ave 10^5 molecules/cm^3
2.0×10^{-5}	13.9 hr	0.34	0.23	3.3
5.0×10^{-6}	2.3 days	1.40	0.62	4.8
2.4×10^{-6}	4.8 days	2.46	0.78	5.7

From the results in Tables 7 and 10, it can be seen that the two slower heterogeneous rates in Table 10 would increase the average OH concentration and aggravate significantly the imbalance of the CO budget. Hence, an estimate for the heterogeneous removal rate of H_2O_2 below 5 km is given by $k°_{het} \geq 2 \times 10^{-5}$ per second or $(k°_{het})^{-1} \leq 13.9$ hour.

3.3 COMPARISON OF 2-D MODEL TROPOSPHERIC RESULTS

Section 2.0 presented some comparisons between the Crutzen and Widhopf 2-D models. These considerations are now extended to include the following: (a) NO_x concentrations in the upper troposphere, (b) heterogenous removal rates of water soluble species, and (c) the parameterization of the water vapor in the reference stratosphere.

Figure 13 shows a comparison between (a) the tropospheric NO_x profiles at middle northern latitudes during summer calculated by the Crutzen and Widhopf 2-D models with 1976 chemistry, as well as the corresponding preliminary Widhopf 2-D result based on 1977 chemistry; and (b) profiles A and B which were found to be more consistent with the balancing of the ozone and CO budgets. It is noted that the Crutzen and Widhopf profiles based on 1976 chemistry are closer to 10^{-10}, which was the extreme high value used in the Fishman-Crutzen calculations (Fig. 12). Hence, the calculated NO_x concentrations in the upper troposphere at middle northern latitudes based on 1976 chemistry were significantly larger than the estimated profile B at this latitude. Figure 13 includes the 1976-Crutzen NO_x profile at 15°N to show the effect of latitude on it, and which is to be compared with profile A of the Fishman-Crutzen 2-D calculations. Again, the profile at 15°N is significantly larger than profile A. However, the result at 40°N from the preliminary Widhopf calculations based on 1977 chemistry shows rather good agreement with profiles A and B, which are applicable to latitudes

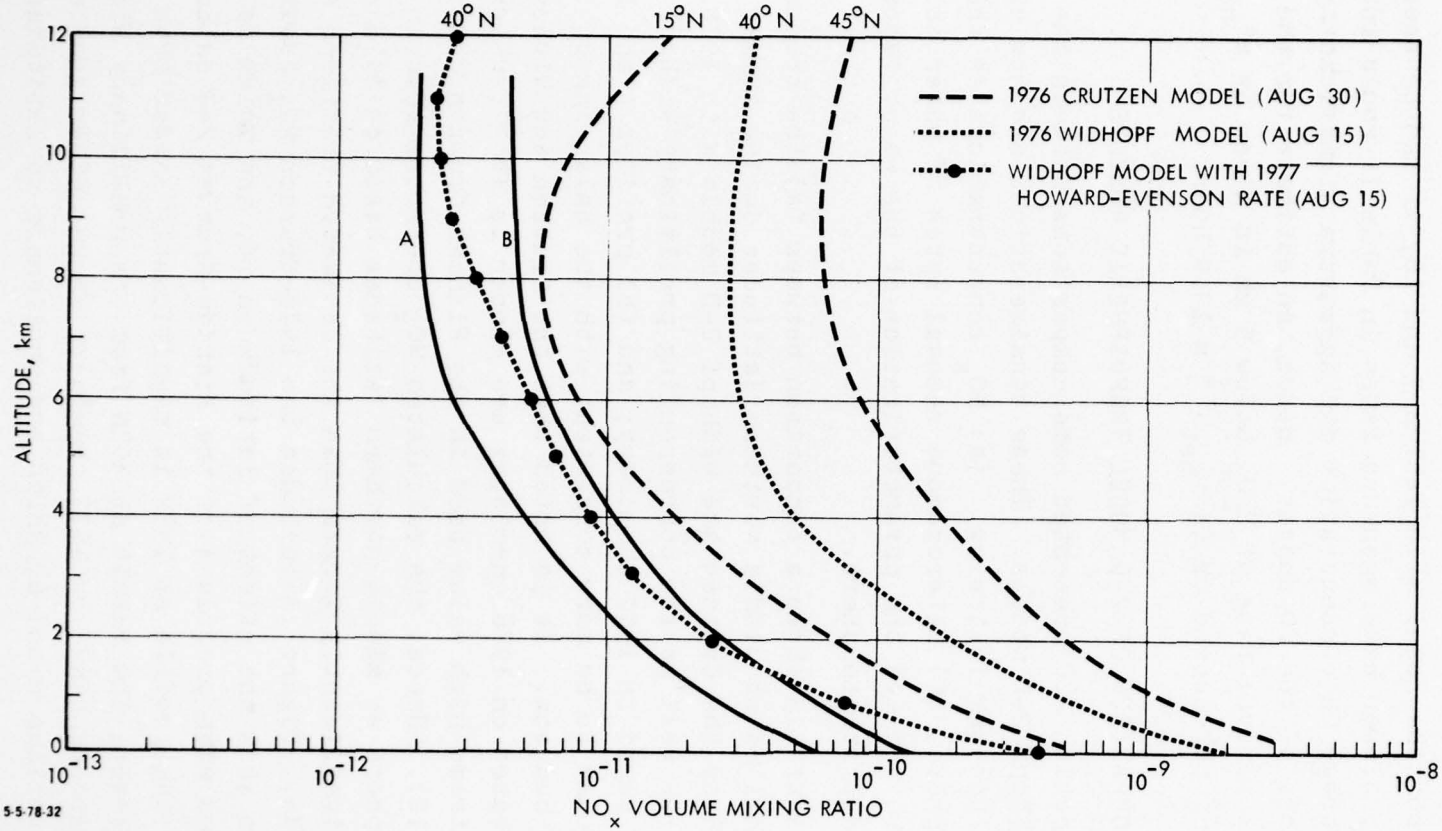

FIGURE 13. Comparison of NO_x calculations in the troposphere by 2-D models utilizing 1976 (Crutzen and Widhopf) and revised (Widhopf and Fishman-Crutzen) chemistries.

$\theta \leq 15°N$ and $\theta \geq 45°N$, respectively. It should be noted that the NO_x volume mixing ratio at the surface for these preliminary calculations has dropped by a factor of about five from the corresponding 1976 Widhopf value. The reason for this effect is a change in the eddy coefficient at the surface, which had to be modified by a revision of the modeling of the rainout sink. Therefore, the use of the 1977 Howard-Evenson rate coefficient and the revised rainout in the Widhopf 2-D model of the stratosphere and troposphere yield NO_x values that are in relatively good agreement with the average NO_x amount based on the O_3 and CO budgets, which is, in turn, consistent with the available limited Noxon data.

Other basic parameters of interest for 2-D photochemical models are the heterogeneous removal rates, not only of H_2O_2 (Table 10), but also those for NO_x, HNO_3, N_2O_5, and CH_3O_2H. These mechanisms have been parameterized differently in the Crutzen and Widhopf 2-D models. The former utilized crude estimates as given in Hidalgo and Crutzen (1977), while the latter did so using as a reference the removal of water vapor in the lower troposphere.

The parameterization of the water vapor distribution in the reference stratosphere is of primary concern for the effect of H_2O effluents on ozone, because of the relatively dry stratospheric medium in the regions of significant ozone production (Figs. 5, 6). Because of the water vapor transports between the stratosphere and troposphere, the parameterization of the water vapor in the stratosphere has to consider the lower atmosphere ($0 < z < 50$ km) as a whole. The parameterization of the tropospheric water vapor in the Crutzen 2-D model is based on statistical data for the 2-D dynamics as well as the mean temperature [T] and its standard deviation [$\sqrt{\overline{T^{*2}}}$] as derived from observations by Oört and Rasmusson (1971) and Louis (1974). The distribution of water vapor in the troposphere is

dependent on condensation processes and water removal by rainfall. The basic procedure consists in the calculation of a local probability of cloud formation, $[P_c]$, at each grid point so as to allow rainfall anywhere within the lower troposphere. The procedure is as shown schematically in Fig. 14 and it consists of the following steps (Crutzen, 1975): (a) calculation of the humidity [q] from the continuity equation for H_2O subject to appropriate boundary conditions at the earth's surface and the stratopause, (b) consideration of the saturation humidity $[q_s]$, as a function of pressure and the saturation temperature $[T_s]$ as given, for example, by the Smithsonian meteorological tables, and (c) a Gaussian distribution for the temperature at each grid point based on the mean temperature and its standard deviation. From the intersection of the calculated humidity, [q], with the saturation humidity, $[q_s]$, it is possible to determine the saturation temperature $[T_s]$. Hence, for all temperatures $[T] << [T_s]$, the air will be supersaturated. The probability of cloud formation $[P_c]$ can then be determined from the Gaussian temperature-distribution function at each grid-point, as indicated in Fig. 14. By this method, it is also possible to determine the rate of precipitation at each grid point. With knowledge of the probability of cloud formation, it becomes possible to estimate the loss rate $[L_r]$ of water-soluble gaseous compounds in the tropospheric sinks. These estimates were based on the following:

$$[L_r(\chi_i)] = - k^\circ_{het_i} P_c[\chi_i] = - \frac{P_c[\chi_i]}{(k^\circ_{het})_i^{-1}} \quad ,$$

where the $(k^\circ_{het})_i^{-1}$ were assumed to be given by 1.5 days for NO_x and 1/3 day for HNO_3, H_2O_2, N_2O_5, and CH_3O_2H (Hidalgo and Crutzen, 1977). It should be noted that this value for H_2O_2 is consistent with that estimated subsequently from considerations of the CO budget (Table 10).

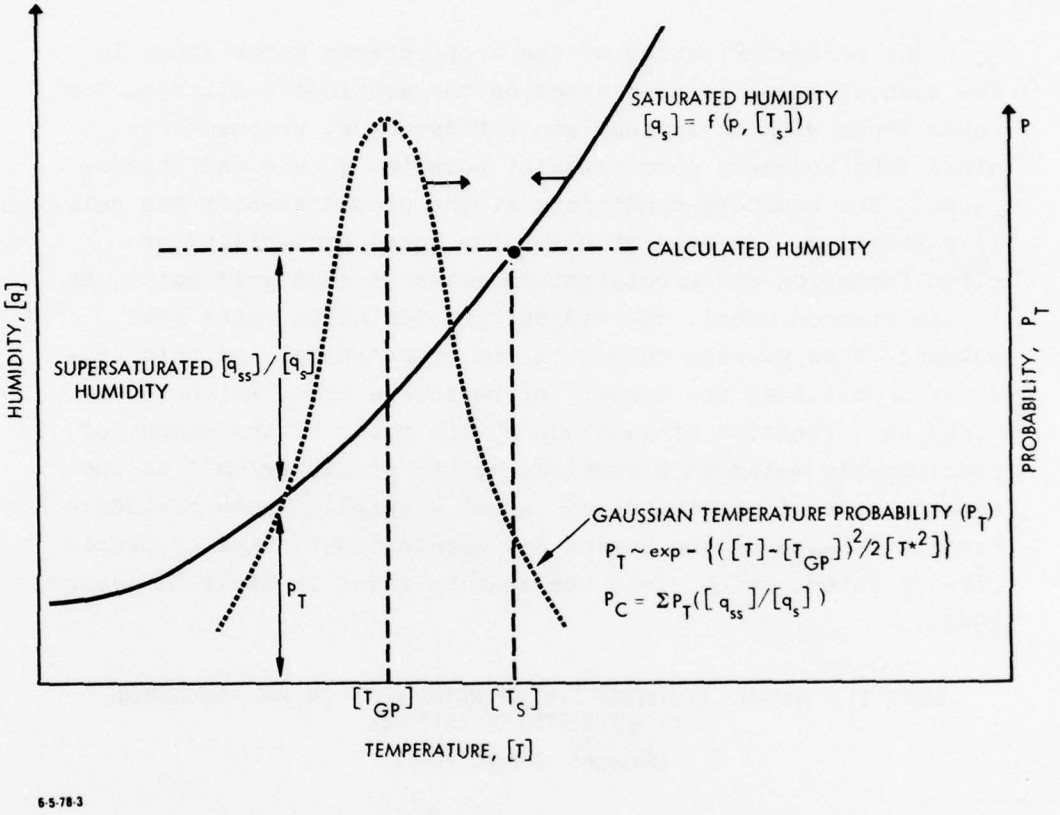

FIGURE 14. Illustration of H_2O parameterization in the Crutzen 2-D model at a grid point ($[T_{GP}]$). Note that the probability of cloud formation can be reduced to an integration over temperature.

The parameterization of the tropospheric water vapor in the Widhopf model is also based on the continuity equation for water vapor with an appropriate 2-D dynamics, tropospheric sinks, and boundary conditions at both the ground and stratopause. The boundary conditions at the ground specify the relative humidity. Instead of using the local probability of cloud formation and precipitation rates at each grid point, as in the Crutzen model, the Widhopf precipitation rates are assumed to be average values in the troposphere, and this calculation utilizes the concept of residence time, which is defined as a function of latitude by the ratio of the amount of precipitable water in a vertical column of air (g/cm^2) to the average rate of precipitation (g/cm^2 - year). These residence times are based on the Bannon and Steele (1957) maps of precipitable water, which yield the results given in Table 11 (Junge, 1963):

TABLE 11. AVERAGE RESIDENCE TIME OF WATER VAPOR IN THE TROPOSPHERE AS A FUNCTION OF LATITUDE

(Source: Junge, 1963)

	Latitude (degrees)								
	80-90	70-80	60-70	50-60	40-50	30-40	20-30	10-20	0-10
Residence Time (days)	(15.0)	(13.4)	8.7	6.2	6.4	8.7	12.0	11.2	8.1

The results in this table are given as a function of latitude, and they indicate that the average residence time of water vapor in the troposphere is about 10 days. The calculation of the precipitation rates in the Widhopf model is then given by the ratio of the local amount of precipitable water to the residence time for the water vapor column as a function of latitude. The parameterization of the heterogeneous removal rates of water-soluble species was assumed to be given in terms of the residence

times for water vapor (Table 11). The residence times for NO_x and H_2O_2 were specified as being ten times that of water vapor, whereas those for HNO_3 and N_2O_5 were assumed to be identical to those of water vapor (Widhopf, 1978).

Figures 15 and 16 show the water vapor distributions as a function of latitude during the fall season as given by the Crutzen and Widhopf models, respectively. The latter figure includes the corresponding Oört and Rasmusson (1971) data for the troposphere and the Harries (1976) data for the stratosphere. These results indicate that either parameterization gives an adequate description of the water vapor distribution in the troposphere. In the reference stratosphere, both models give similar results of a relatively dry and nearly constant vertical gradient of water vapor mass mixing ratio at every latitude. This parameterization of water vapor has so far been tested in an atmosphere perturbed by H_2O effluents only in the Widhopf 2-D model (Widhopf and Glatt, 1978).

3.4 CRITICAL CHEMICAL REACTIONS FOR AVIATION EFFECTS

The previous section identified the five most important reactions involving hydrogen-oxide species for the assessment of SST effects on the ozone column (Duewer et al., 1977). In chronological order of the revision of their reaction rates they are as follows:

(R15)	$OH + NO_2(+M) \rightarrow HNO_3(+M)$	$\log_{10}k = -AT/(B+T) - 0.5 \log_{10}(T/280)$
(R21)	$OH + HO_2 \rightarrow H_2O + O_2$	3×10^{-11}
(R14)	$HO_2 + NO \rightarrow OH + NO_2$	8×10^{-12}
(R13)	$O_3 + HO_2 \rightarrow OH + 2\,O_2$	7.3×10^{-14} exp (-1275/T)
(R 7)	$O_3 + OH \rightarrow HO_2 + O_2$	1.5×10^{-12} exp (-1000/T)

where the corresponding reaction rate coefficients are those recommended most recently by NASA (1977). The parameters A and

AD-A065 472 INSTITUTE FOR DEFENSE ANALYSES ARLINGTON VA F/G 4/1
STATUS OF REPRESENTATIVE TWO-DIMENSIONAL MODELS OF THE STRATOSP--ETC(U)
OCT 78 H HIDALGO DOT-FA-77WA-3965
UNCLASSIFIED P-1341 FAA-AEE-78-23 NL

2 OF 3
AD A065472

END
DATE FILMED
4-79
DDC

CONT

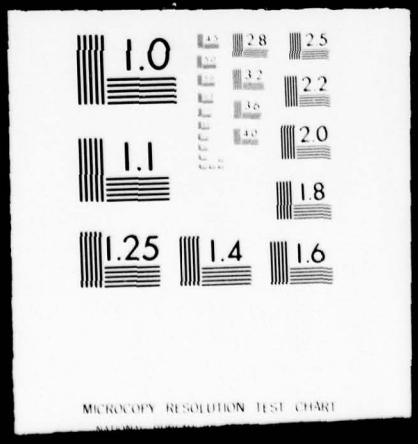

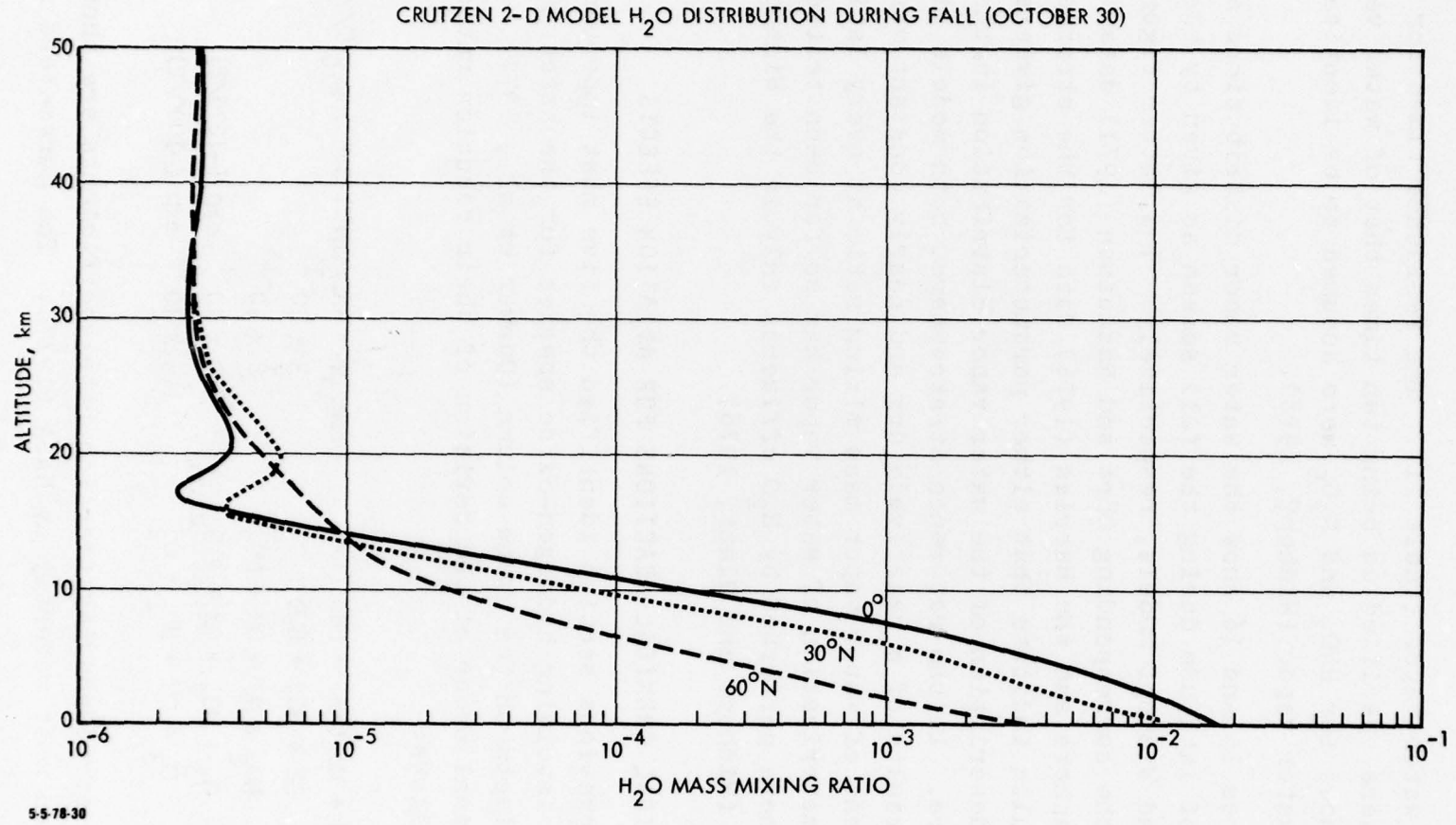

FIGURE 15. Simulation of water vapor distribution in the reference atmosphere by the Crutzen model as a function of latitude in the Northern Hemisphere (Source: Hidalgo and Crutzen, 1977)

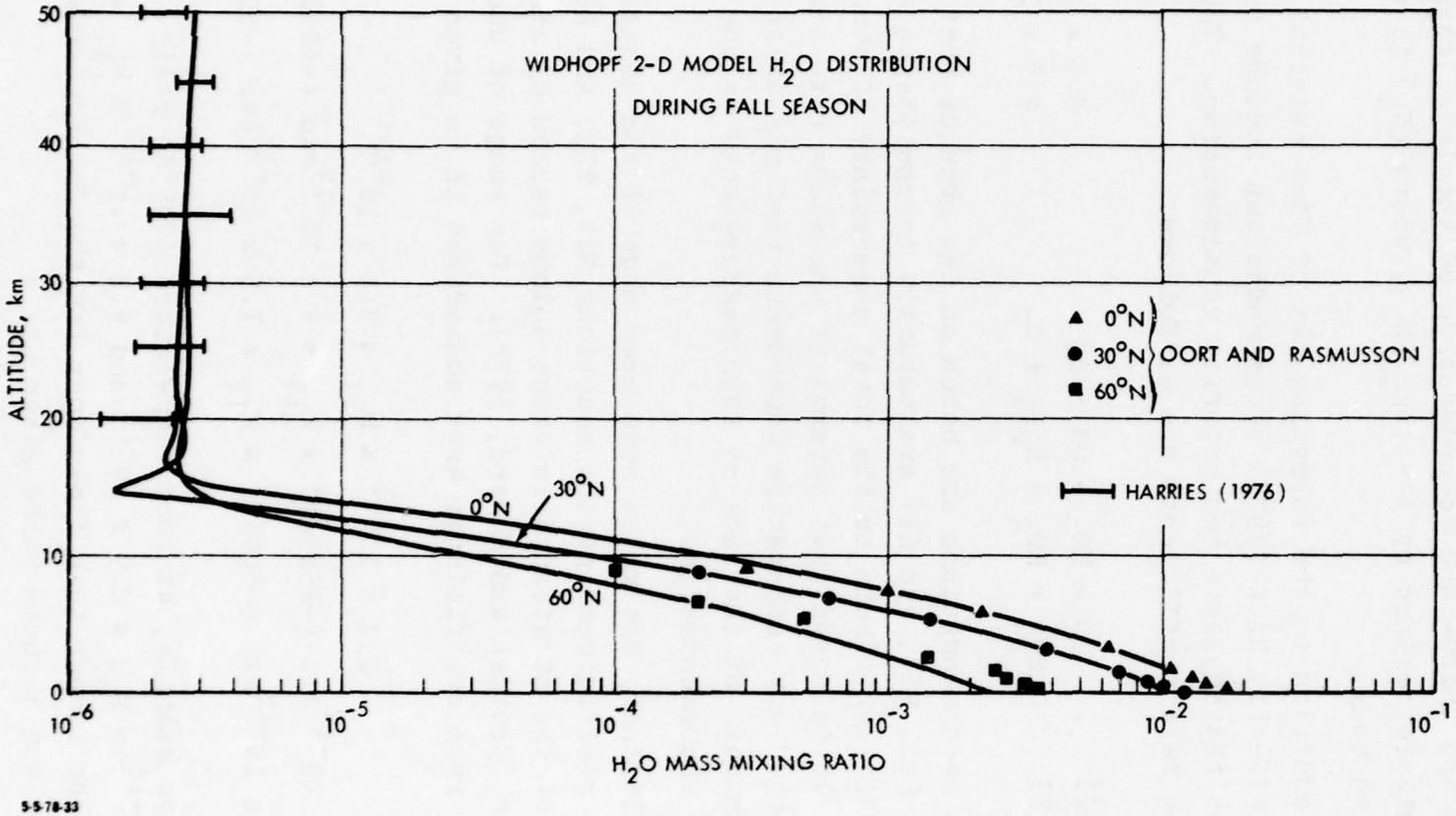

FIGURE 16. Simulation of water vapor distribution in the reference atmosphere by the Widhopf model as a function of latitude in the Northern Hemisphere. (Source: Widhopf, 1978)

B in R15 are third- and second-degree polynomials, respectively, of a variable defined by $Z = \log_{10}[N_2]$, where $[N_2]$ is nitrogen as a third body.

In addition to the foregoing set of five critical reactions for SST effects, NASA (1977) recommendations include two other reactions that deserve top priority consideration. These reactions and rate coefficients are as follows:

(R12)	$O + HO_2 \rightarrow OH + O_2$	3.5×10^{-11}
(R17)	$HO_2 + HO_2 \rightarrow H_2O_2 + O_2$	2.5×10^{-12}

The NASA recommendations are based on the grounds that existing data for R21, R14, and R17 are mutually inconsistent; while R13, R7, and R12 contribute to the total uncertainty of stratospheric models. It is noted that several of the above rate coefficients have omitted any temperature dependence that may exist in such rates, because of the lack of such measurements at the time of the NASA recommendations.

Preliminary estimates have been made of the sensitivity of the rate coefficients of the reactions R21, R13, and R17 for changes of the stratospheric ozone column caused by aircraft effluents (Crutzen and Howard, 1978). The range of uncertainty in these rate coefficients were considered to be given by

$$2.1 \times 10^{-11} \leq k_{21} \leq 5.1 \times 10^{-11}$$

$$10^{-13}\exp(-1525/T) \leq k_{13} \leq 2 \times 10^{-13}\exp(-1250/T)$$

$$5 \times 10^{-12}\exp(-500/T) \leq k_{17} \leq 1.5 \times 10^{-11}\exp(-500/T)$$

which, for example, at room temperature (296°K) yield $5.8 \times 10^{-16} \leq k_{13} \leq 2.9 \times 10^{-15}$ and $9.2 \times 10^{-13} \leq k_{17} \leq 2.8 \times 10^{-12}$. The temperature dependency for the Howard-Evenson reaction rate was assumed to be given by

$$k_{14} = 3 \times 10^{-11} \exp(-390/T) \quad .$$

These sensitivity estimates considered combinations of the above end values for each range using (a) a steady-state, one-dimensional model that did not include the troposphere, (b) an oxygen-hydrogen-nitrogen stratosphere, and (c) assumed NO_x and H_2O emissions of 10^3 and 2×10^5 molecules/cm^3-sec, respectively, at altitudes of either 16 or 20 km. Although these preliminary investigations could not overcome the problem of underdestruction of ozone in the reference stratosphere (Section 3.1), the results indicated that the sign of the change of the ozone column by SST flight at 16 km or 20 km depended mainly on the relative magnitudes of the rate coefficients for R21 and R13. These results are summarized in Table 12. The fourth column in this table shows that the sign in the change of the ozone column by the assumed NO_x and H_2O effluents at either 16 km or 20 km changes from negative to positive for a combination of the lower (2.1×10^{-11}) value for R21 with the higher value (2.9×10^{-15}) of R13. The higher value of R13 is an upper limit derived in the original sensitivity analysis by Duewer et al., 1977. This table includes also the NASA recommended values for these rates, where the room temperature value has again been used for R13 to provide a reference when comparing it with the values in these preliminary investigations. In spite of the NASA recommendations for the rate coefficient of R13, recent (1978) experimental results by Howard indicate that this rate is actually closer to the higher value used in these calculations.*

*As indicated earlier, recent measurements of the temperature dependence of the reaction rate coefficient of R13 is $k_{13} = (1.4 \pm 0.4)\ 10^{-14} \exp[-(580 \pm 100)/T]$ cm^3 $molecule^{-1}$ sec^{-1} (Howard, 1978). At 296°K, this rate coefficient yields $k_{13} \simeq 20 \times 10^{-16}$.

TABLE 12. SENSITIVITY OF THE SIGN OF THE OZONE CHANGE TO RATE COEFFICIENTS OF R21 and R13
(Source: Crutzen and Howard, 1978)

Flight Altitude (km)	Reaction	Reaction Rate at 296°K	Sign of O_3 Column Change	NASA (1977) Recommended Rates	Ratio of Crutzen (1978) to NASA Rates
16	R21	5.1(-11)	-1.03	3.0(-11)	1.7
16	R13	5.8(-16)		9.8(-16)	0.6
16	R21	2.1(-11)	-0.37	3.0(-11)	0.7
16	R13	5.8(-16)		9.8(-16)	0.6
16	R21	2.1(-11)	1.21	3.0(-11)	0.7
16	R13	29.0(-16)		9.8(-16)	3.0
20	R21	5.1(-11)	-2.75	3.0(-11)	1.7
20	R13	5.8(-16)		9.8(-16)	0.6
20	R21	2.1(-11)	-1.55	3.0(-11)	0.7
20	R13	5.8(-16)		9.8(-16)	0.6
20	R21	2.1(-11)	1.11	3.0(-11)	0.7
20	R13	29.0(-16)		9.8(-16)	3.0

It must be emphasized that these preliminary results are subject to the additional constraints of a lack of coupling between the NO_x and ClO_x cycles in the stratosphere (M2, Table 1) below 35 km through reactions such as $NO_2 + ClO + M \rightarrow ClNO_3 + M$ and $NO + ClO \rightarrow Cl + NO_2$. Furthermore, a current open question in the chlorine chemistry is the difference by an order of magnitude between the higher observed and (1-D) ClO_x values in the reference atmosphere (Crutzen et al., 1978). It is currently unknown if this difference is due to experimental errors in the observations or to an unknown source of ClO_x in the stratosphere.

4. ASSESSMENT OF THE 2-D FORMULATION OF THE ATMOSPHERIC DYNAMICS

The previous section emphasized considerations of the chemical mechanisms in Fig. 2 and Table 1 for the reference and perturbed stratospheres and tropospheres. Because of the empiricism in the 2-D formulation of the dynamics for the reference atmosphere, it becomes necessary to (a) review the basic assumptions in the available 2-D parameterizations of the dynamics for the reference upper troposphere and stratosphere, (b) assess the applicability of such formulation to extensions of such parameterizations to an atmosphere assumed to be perturbed by large continuous injections of aircraft effluents in the flight corridors, and (c) explore newer concepts for a more correct theoretical 2-D formulation of the dynamics for the reference and perturbed upper tropospheres and lower stratospheres.

4.1 BASIC ASSUMPTIONS IN THE 2-D PARAMETERIZATIONS OF THE DYNAMICS

A basic aim in the 2-D formulation of the dynamics of photochemical models is to describe the mass transports of trace chemical species in the reference lower atmosphere ($0 < z < 50$ km) as well as the enhanced mass transports of engine effluents for assumed large aircraft traffic in the flight corridors of the perturbed upper troposphere and lower stratosphere. It should be noted that, because of the relatively long-time scales in Fig. 3 (i.e., months), the interest is on the eddy mass transports by the large-scale motions. The available 2-D parameterizations of the atmospheric dynamics have utilized two basic assumptions which are (a) the decoupling of the temperature and dynamics from the chemistry, and (b) the extension of the mixing length

hypothesis for momentum transports in microscale turbulent flow to the mass transports in the macroscale turbulence of the stratosphere. Each of these assumptions is described below.

4.1.1 Decoupling of Temperature and Dynamics from the Chemistry

A first basic approximation in the 2-D formulation of the Crutzen and Widhopf 2-D models is to decouple the conservation of the chemical species from the so-called primitive equations for the general circulation of air in the reference troposphere and stratosphere. Since the primitive equations for the reference atmosphere essentially describe the temperature and dynamics, a fundamental assumption in these 2-D models is then that anthropogenic changes in the distributions of radiative and chemically active trace gases (e.g., Fig. 6) will not produce first-order effects on the initial temperature field and air motions of the reference atmosphere. Hence, such decoupled formulation cannot consider feedback effects on the calculated ozone changes from any change in the background stratospheric temperature and dynamics which would result from the changes in both the absorption of solar radiation and emission of infrared radiation that would be induced by the calculated changes of ozone (Figs. 7, 10). These feedback effects on the ozone change would take place through (a) the temperature dependence of the reaction rate coefficients (e.g., Table 3), (b) the coupling between the temperature changes and changes in the air motions, and (c) changes in the distributions of chemical species due to the changes in the dynamics. Obviously, the validity of the decoupling of the temperature and dynamics from the chemistry becomes increasingly open to question as the magnitude of the changes in ozone by all anthropogenic effects becomes large, a condition that stems from the fact that such anthropogenic effects on the temperature and dynamics would become part of the atmospheric background for the aircraft effluents. In this context, it is of interest to note that current assessments, based on 1977 chemistry, of the effect on

the global (1-D) ozone column from recent release rates of chlorofluoromethanes at the earth's surface (Fig. 2 as well as M17 and M2 in Table 1) forecast an eventual decrease of the 1-D ozone column by as much as about 14 percent by the first quarter of the next century (e.g., NASA, 1977).

The coupling between the temperature field and dynamics with the chemistry in the primitive equations for the reference stratosphere is taken into account by a parameterization of the net heating of the stratospheric air. Hence, the remaining coupling between the temperature and dynamics can be illustrated by considering the change in the magnitude of the vertical eddy transports in the tropopause region, which are of crucial importance in the assessment of the magnitude of aviation effects on ozone. The change in the vertical eddy transports in the tropopause region becomes important because engine effluents deposited above the tropopause are then trapped and allowed eventually to propagate upwards to the ozone production regions in the middle and upper stratosphere (Fig. 5).

The change in the magnitude of the vertical eddy transports in the tropopause region depends on the change in atmospheric stability, which depends, in turn, on the change in the sign of the vertical temperature gradient in this region. The latter change is due to the vertical distribution of the ozone mixing ratio in the stratosphere (Fig. 6) and the consequent absorption of UV solar radiation by ozone. As indicated by the U.S. Standard Atmosphere (1976), for example, the undisturbed ambient temperature (a) decays with increasing altitude in the troposphere, (b) becomes constant at the tropopause (z_t) and in the lower stratosphere ($z_t < z < 20$ km), and (c) increases with increasing altitude in the middle and upper stratosphere ($20 < z < 50$ km). A fundamental problem in the 2-D description of the dynamics is then the formulation of the eddy transports of chemical species between the lower stratosphere and upper troposphere. However, basic difficulties in such formulation

are (a) the lack of observations for the statistics of the very small, vertical transports in the tropopause and lower stratosphere regions (Oört and Rasmusson, 1971), and (b) *the complex three-dimensional dynamics of the tropopause gaps produced by the jet streams at the northern middle latitudes which are important for aviation effects (Fig. 7).*

The most general approach for the simulation of the interactions of the temperature field, the dynamics and chemical processes in the reference and perturbed atmospheres, would be based on the coupling of the 3-D primitive equations for atmospheric motions with those for the conservation of chemical species. This coupled system of equations would yield solutions for the vertical and horizontal transports of chemical species as a function of time and the three space coordinates of the atmosphere (latitude, altitude, longitude). However, the complexity of such a system, coupled with the basic limitations given in Section 1, has so far prevented the practical application of such a system to either the reference stratosphere or the study of the effects of high-altitude subsonic and SST flight on atmospheric ozone. Nevertheless, it is of interest to describe such a system in order to bring out the subsequent 2-D approximations.

The 3-D or primitive equations for the air motions without chemical interactions, in a frame of reference fixed to the rotating earth, are as follows (e.g., Lorenz, 1967):

$$d\vec{U}/dt = - f\vec{k} \times \vec{U} - g\vec{\nabla}z + \vec{F} \qquad (1)$$

$$dT/dt = \kappa T\omega/p + Q/c_p \qquad (2)$$

$$\vec{\nabla} \cdot \vec{U} + \partial\omega/\partial p = 0 \qquad (3)$$

$$\partial z/\partial p = -RT/gp \qquad (4)$$

Equation (1) represents the conservation of momentum for the quasi-horizontal motions ($\vec{U}$) and contains two scalar equations for the eastward (u) and northward (v) air velocities. This

equation gives the total or individual acceleration, defined by $d\chi/dt = \partial\chi/\partial t + \vec{V} \cdot \chi \vec{U} + \partial(\chi\omega)/\partial p$, in terms of the Coriolis acceleration due to the earth's rotation ($-f\vec{k} \times \vec{U}$), that due to the geopotential (gz) gradients along surfaces of constant pressure (p), and the acceleration due to friction ($\vec{F}$). Equation (2) represents the conservation of energy and gives the total time rate of change of the air temperature (T) on the left-hand side, whereas the variables $\omega(\equiv dp/dt)$ and Q are related to the vertical winds and the net heating of air per unit mass, respectively. In the relatively dry stratosphere (Fig. 6), the net heating is the result of (a) absorption of solar radiation by ozone, carbon dioxide, and water vapor; and (b) emission of IR radiation by O_3, CO_2, and H_2O, which is a mechanism dominant in the lower stratosphere. Equation (3) represents the conservation of air mass and Eq. (4) the condition of vertical hydrostatic equilibrium, which allows conversion of the altitude to the pressure coordinate. The condition of hydrostatic equilibrium filters out sound waves that are unimportant for the macroscale motions, whereas the condition of geostrophic equilibrium [i.e., balance of the Coriolis acceleration with those from pressure gradients in Eq. (1)] at middle and high latitudes filters out the unimportant gravity waves (Lorenz, 1967).

The interactions of the stratospheric temperature and dynamics with the chemistry are given by the conservation of the chemical species; i.e.,

$$\frac{dR_i}{dt} = P_i - L_i \qquad (5)$$

where R_i denotes the mixing ratio for any of the given i species, and P_i as well as L_i the production and loss chemical mechanisms in Table 1. It should be noted that Eq. (5) is also applicable to phase changes such as those of H_2O in the troposphere, and that the production term P_i for aviation effects must include the engine effluents. The dynamic terms in Eq. (5) may be identified

through the expansion of dR_i/dt, which in pressure coordinates becomes (Lorenz, 1967):

$$\frac{dR_i}{dt} = \frac{\partial R_i}{\partial t} + \vec{\nabla} \cdot R_i \vec{U} + \frac{\partial \omega R_i}{\partial p} \qquad (6)$$

where

$$\vec{\nabla} \cdot R_i \vec{U} = \frac{1}{a \cos\theta}\left[\left(\frac{\partial u R_i}{\partial \lambda}\right)_p + \left(\frac{\partial R_i v \cos\theta}{\partial \theta}\right)_p\right] \qquad (7)$$

and "a" denotes the earth's radius.

The primitive equations (1 through 4), without the use of the conservation of chemical species, are the basis for the available general circulation models (GCMs) of the stratosphere and troposphere. The GCMs must consider the conservation equation for H_2O and extend the parameterization of the net heating (Q) to include the heating by condensation of H_2O in the lower and middle troposphere. The GCMs must incorporate further parameterizations for the effect of clouds on the incoming solar radiation as a function of season, the H_2O sinks in the troposphere, and appropriate boundary conditions at both the earth's surface and stratopause.

Either observations or solutions of the primitive equations provide data for the foregoing dependent variables $\chi(\lambda, \theta, p, t)$ as a function of longitude (λ), latitude (θ), pressure level (p), or height (z), and the time (t). However, such variables may be expressed as $\chi = [\chi] + \chi^*$, where the operation [ ] denotes longitudinal or zonal averages and χ^* deviations from such averages. Hence, the zonal mean is given by $[\chi] = f(\theta, p, t)$; whereas $\chi^* = g(\lambda, \theta, p, t)$ but $[\chi^*] = 0$. Similarly, the dependent variables may also be expressed in terms of time averages $\chi = \overline{\chi} + \chi'$, where $\overline{\chi}$ and χ' are associated with the so-called standing and transient motions, respectively. Hence, any dependent variable such

as the northward wind (v) may be expressed as $v = [\bar{v}] + [v]' + \bar{v}^* + v^{*\prime}$. The poleward transport of χ (say O_3) is then given by (Lorenz, 1967):

$$[\overline{\chi v}] = [\bar{\chi}][\bar{v}] + \overline{[\chi]'[v]'} + [\bar{\chi}^*\bar{v}^*] + \overline{[\chi^{*\prime}v^{*\prime}]} \qquad (8)$$

where the first two terms on the right side are the standing and transient transports by the meridional circulation, and the latter two the corresponding standing and transient eddy transports. This split of the atmospheric motions considers a zonal symmetric flow plus eddy or wave motions superposed on the zonal symmetric flow. The wave motions are characterized by a spectrum of (for example) zonal wave numbers, i.e., number of wavelengths in a latitudinal circle around the earth's axis of rotation.

A general 2-D formulation of the couplings of the temperature, dynamics and chemistry would involve taking the time and zonal averages of the system of Eqs. (1) through (5). However, from the decoupling of the chemistry from the temperature and dynamics, the basic 2-D equation for the conservation of species may then be obtained by (a) performing the zonal average of only Eq. (5), (b) using Eq. (8) to split the transports into the zonal mean and eddy components, and (c) using the zonal average of the continuity Eq. (3). The result is as follows:*

$$\frac{\partial[R_i]}{\partial t} + \frac{[v]}{a}\frac{\partial[R_i]}{\partial\theta} + [\omega]\frac{\partial[R_i]}{\partial p} + \frac{1}{a\cos\theta}\frac{\partial}{\partial\theta}[v^*R_i^*]\cos\theta +$$

$$\frac{\partial[\omega^*R_i^*]}{\partial p} = [P_i] - [L_i] \quad . \qquad (9)$$

The decoupling of the chemistry from both the air temperature and motions, as used in the Crutzen and Widhopf 2-D models, eliminates the need to consider the time and zonal averages of the primitive equations (1) through (3) for the reference and

*The time-averaging notation in Eq. (8) is subsequently dropped for simplicity. Likewise, the difference between standing and transient eddies is omitted.

perturbed atmospheres. These 2-D models must instead specify as a function of month or season, the meridional air temperature (so as to determine the reaction rate coefficients, e.g., Table 3) and motions for the reference stratosphere and troposphere. The role of the 2-D formulation of the dynamics is therefore defined by the second to fifth terms in the left-hand side of Eq. (9). The second and third terms involve the transports of mixing ratio by the meridional circulation, whereas the fourth and fifth are, respectively, the poleward and vertical mass transports by the eddy motions. Hence, the first term in the left-hand side of Eq. (9) is the net local rate of change of the mixing ratio of any of the i species as a result of the transports by the dynamics as well as the chemical mechanisms in the right-hand side of the equation. It is important to note that the determination of the meridional profiles of ozone and related i species (e.g., Fig. 6) requires, in general, the simultaneous numerical solution of a set of i equations (9). While the Widhopf 2-D model solves for each individual Eq. (9), the Crutzen model utilizes equilibrium approximations for species with relatively short characteristic times so as to reduce the number of equations. These simultaneous solutions must utilize appropriate boundary conditions at the earth's surface and stratopause, and include the heterogenous mechanisms in the tropospheric sinks (M9, Table 1) in the term L_i for the lower troposphere.

4.1.2 Hypothesis of Large-Scale Diffusion in the Stratosphere

The decoupling of the chemistry from the air temperature and motions allows the simultaneous solution of the system of Eq. (9) with specified meridional temperature profiles and dynamics for the reference atmosphere as a function of month or season. The dynamics is given by (a) the meridional circulation, given in Fig. 17, which was determined by Louis (1974) and Louis et al. (1974) from temperature observations and the use of the energy equation as well as the conservation of air mass; and (b) the poleward and vertical eddy mass transports, which

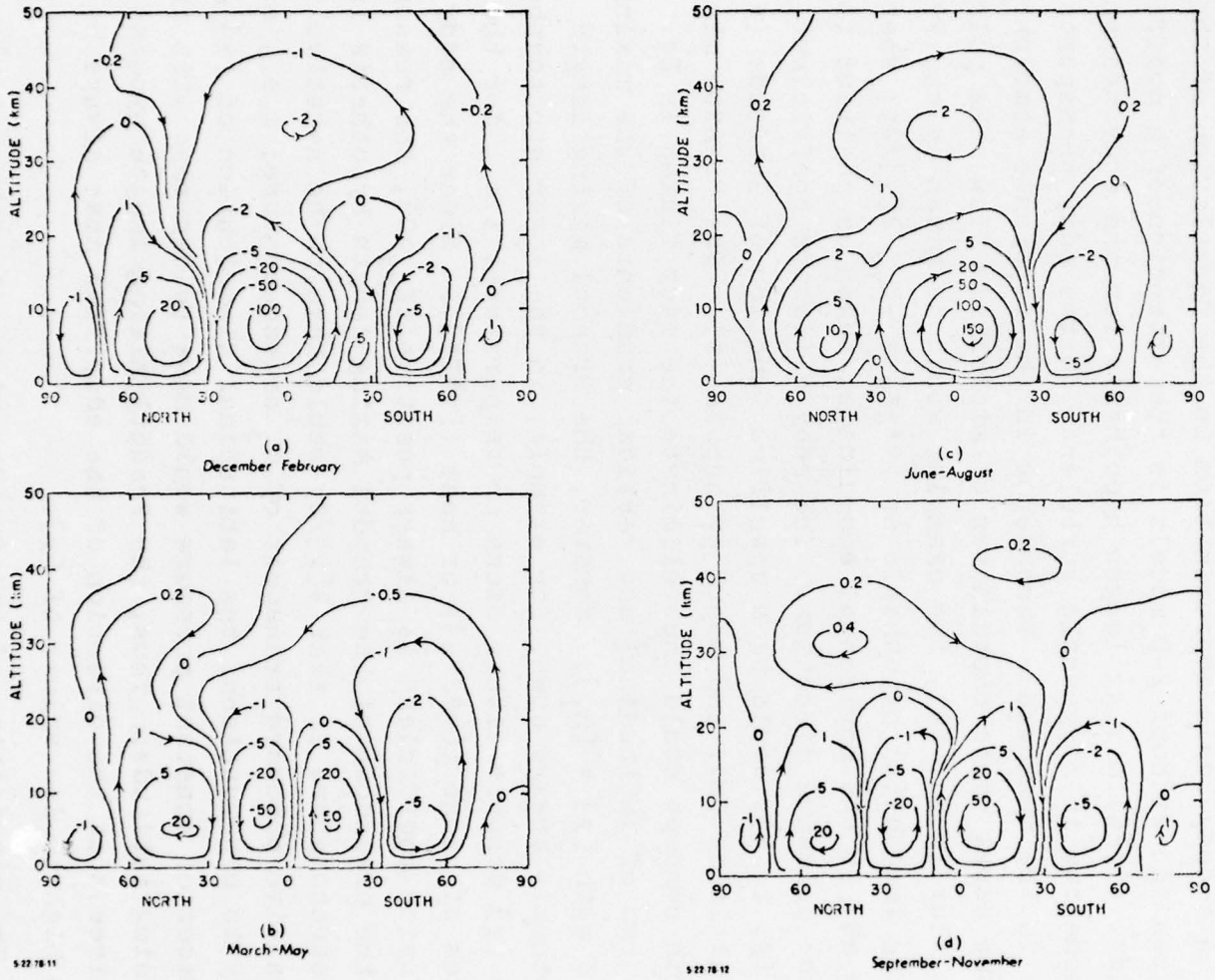

FIGURE 17. Meridional Circulation as a function of season. (Source: Louis in CIAP Monograph 3, 1975; Chapter 4).

are essentially unknown in the stratosphere due to the lack of observations for the statistics of such motions (Oört and Rasmusson, 1971).

A second basic approximation in the formulation of the Crutzen and Widhopf 2-D models is the extension of a modified Prandtl (1925) mixing length hypothesis for the eddy transports of momentum in microscale turbulence to the eddy transports of mass in the macroscale turbulence in the reference atmosphere. In the usual space coordinates of microscale flow, the poleward eddy flux in Eq. (9), for example, would be given by the Prandtl mixing length (ℓ) hypothesis as $[v^*\chi^*] = -K_{yy}\, \partial[\chi]/\partial y$; where y ($= a\theta$) is the horizontal coordinate, taken as positive ($\Delta y > 0$) in the poleward direction. The eddy diffusion coefficient, K_{yy} (y, z, t), would be a specified function of latitude (y or θ), altitude (z), and month or season (t). The Prandtl mixing length concept would thus eliminate the eddy fluxes in Eq. (9) in terms of latitudinal and vertical gradients of the mixing ratio with $[\chi] = [R_i]$. However, the Prandtl mixing length hypothesis breaks down, for example, in the lower stratosphere when $[\chi]$ denotes either ozone or temperature; i.e., for the eddy fluxes of ozone ($[v^*O^*_3]$) or heat ($[v^*T^*]$). Since the eddy diffusion coefficient is always positive ($K_{yy} > 0$), the reason for the breakdown of the Prandtl mixing length hypothesis in the stratosphere is that $\partial[\chi]/\partial y$ would have to be negative for a positive poleward transport of O_3 or temperature; i.e., contrary to observations, the latitudinal distribution of $[\chi]$ along surfaces of constant pressure would have to decrease with increasing latitude. Thus, the Prandtl mixing length hypothesis requires that the direction of the eddy flux must always be from high to low values of $[\chi]$.

The application of the Prandtl mixing length concept had then to be modified if it was to take into account poleward countergradient eddy fluxes in a direction from low to high

values of $[\chi]$. The countergradient eddy fluxes in the lower stratosphere were explained by Newell (1964) and formulated analytically by Reed and German (1965). The compression of the atmosphere with increasing latitude towards the cold polar regions produces a downward inclination in the poleward slopes of constant pressure surfaces. Because the temperature is constant in the relatively dry (Fig. 6) undisturbed lower stratosphere, the slope of constant entropy tends then to be the same as the downward, poleward slopes of the isobaric surfaces. The crux of the argument to explain countergradient eddy fluxes of heat in the lower stratosphere was that the subsiding air parcels moving northward from the cold (altitude-wise) tropical regions do so along inclined paths with a downward slope larger than those of the undisturbed isentropic surfaces. Similarly, ascending air parcels would be transported southward along paths with inclinations similar to those of the subsiding parcels.

The foregoing concept for countergradient eddy fluxes is illustrated in Fig. 18 for the heat flux, where $[\chi]$ denotes the potential temperature as defined by an assumed isentropic compression from the parcel temperature and pressure to a standard pressure (1000 mbar). The use of the potential temperature separates the effects of adiabatic and nonadiabatic heating during the displacement of the air parcels across a mixing length distance (approximately 100 km). The figure shows (1) a downward slope α for both subsiding and ascending parcels arriving at the point defined by the origin of the horizontal and vertical axes, and (2) the smaller slope β for the isentropes. The local gradient vector $\vec{\nabla}[\chi]$ in the figure gives $\partial[\chi]/\partial y>0$ along the horizontal axis; i.e., if the eddy flux is poleward, it will take place from low to high values of $[\chi]$. The countergradient flux of potential temperature at the origin becomes evident by considering the net eddy transport of $[v^*\chi^*]$. If the eddy fluxes of heat are quasi-isentropic, the northward subsiding parcels arriving at the origin will be anomalously

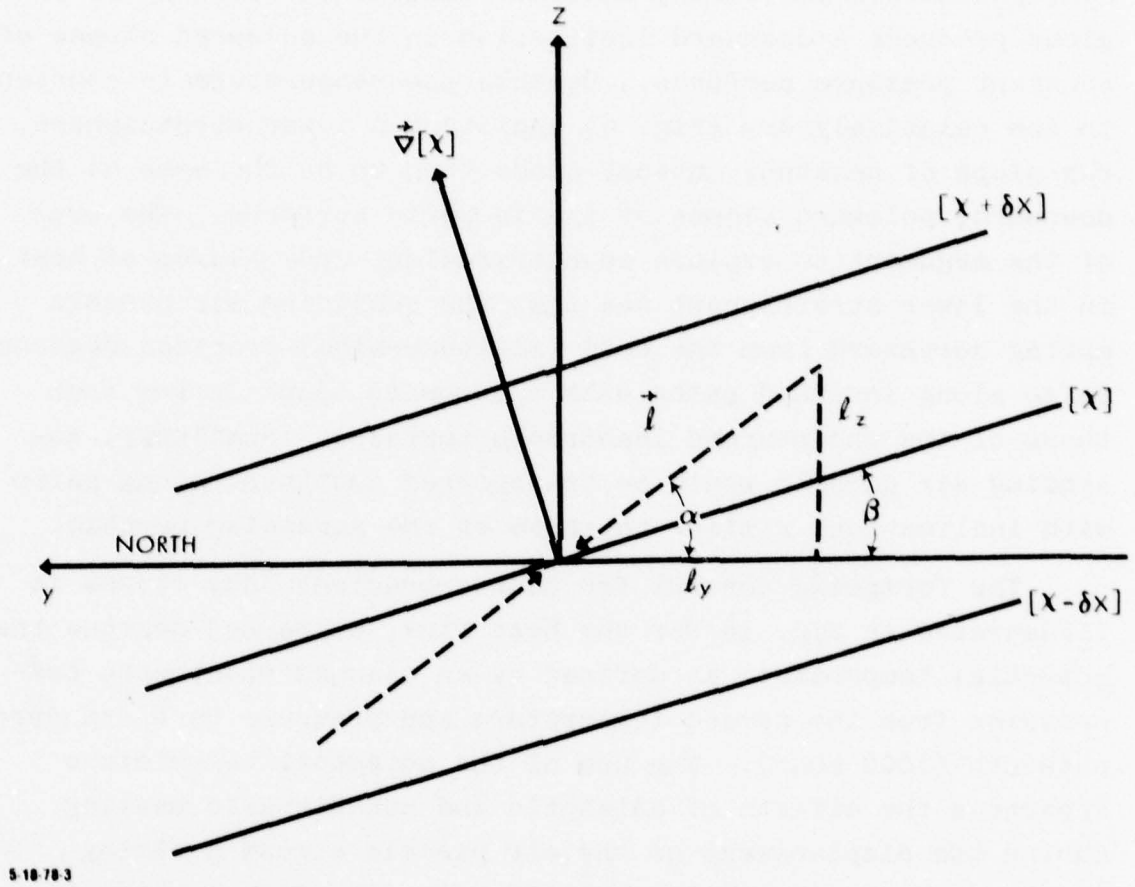

FIGURE 18. Schematic representation of the slope (α) of the mixing length path necessary for countergradient eddy fluxes in the Prandtl mixing length hypothesis. (Source: Reed and German, 1965)

warm; whereas the southward ascending particles arriving at the same point will be anomalously cold. Hence, the net eddy transport of heat in the subsequent mixing of the air parcels will be northward in spite of the fact that $\partial[\chi]/\partial y>0$; i.e., the poleward eddy transports of heat become countergradient when $\alpha > \beta$. Similar consideration indicates that when $\alpha = \beta$, the eddy fluxes tend to vanish, and when $\alpha = 0$ the poleward eddy flux becomes as in the Prandtl mixing length hypothesis. These results are, therefore, a function of α for the fixed condition of $\partial[\chi]/\partial y>0$ along the y-axis. Hence, the magnitude of the slopes $\alpha(y,z,t)$ of the eddy motions as well as the corresponding variability (i.e., variance $[\alpha^{*2}]$) of such slopes determine the nature (with or countergradient) as well as the magnitude of the horizontal and vertical eddy fluxes in Eq. (9). The modification of the Prandtl mixing length hypothesis must then take into account the slopes α and β of the mixing length and isentropic surfaces.

The formulation of the eddy horizontal and vertical transports in Eq. (9) are usually given in the space coordinates (y,z) instead of those in Eq. (9). Hence, the concepts illustrated in Fig. 18 indicate that

$$\chi^* = -\vec{\ell} \cdot \vec{\nabla}[\chi] = -\left(\ell_y \frac{\partial[\chi]}{\partial y} + \ell_z \frac{\partial[\chi]}{\partial z}\right) , \qquad (10)$$

where $\vec{\ell}$ is the mixing length vector with horizontal and vertical components given by ℓ_y and ℓ_z. The horizontal and vertical eddy fluxes are then given by

$$[v^*\chi^*] = -\left(K_{yy} \frac{\partial[\chi]}{\partial y} + K_{yz} \frac{\partial[\chi]}{\partial z}\right) \qquad (11a)$$

and

$$[w^*\chi^*] = -\left(K_{zy} \frac{\partial[\chi]}{\partial y} + K_{zz} \frac{\partial[\chi]}{\partial z}\right) , \qquad (11b)$$

where $K_{yy} \equiv [\ell_y v^*]$, $K_{yz} \equiv [\ell_z v^*]$, $K_{zy} \equiv [\ell_y w^*]$ and $K_{zz} \equiv [\ell_z w^*]$. Using the approximation that the mixing length components (ℓ_z, ℓ_y) are proportional to the respective air velocities (w, v) and the fact that the magnitude of α is small (approximately 10^{-4}), then

$$\begin{aligned} v^* &= V \cos \alpha \simeq V \\ \ell_y &= \ell \cos \alpha \simeq \ell \\ w^* &= V \sin \alpha \simeq V\alpha \\ \ell_z &= \ell \sin \alpha \simeq \ell\alpha \quad , \end{aligned} \tag{12}$$

where V is the wind along the mixing length direction. With Eqs. (12), the eddy coefficients K_{yy}, K_{yz}, K_{zy}, and K_{zz} in the Cartesian coordinates of Fig. 18 can be expressed in the principal axes given by $\vec{\ell}$ and $\vec{\nabla}\chi$ as follows:

$$\begin{aligned} K_{yy} &\equiv [\ell_y v^*] = [V\ell] = K \\ K_{yz} &\equiv [\ell_z v^*] = [V\ell\alpha] = [V\ell([\alpha] + \alpha^*)] \simeq [\alpha]\, K \\ K_{zy} &\equiv [\ell_y w^*] = [V\ell\alpha] = K_{yz} \\ K_{zz} &\equiv [\ell_z w^*] = [V\ell\alpha^2] = [V\ell([\alpha] + \alpha^*)^2] \simeq ([\alpha]^2 + [\alpha^{*2}])\, K, \end{aligned} \tag{13}$$

where it is assumed that $[\alpha]$ and α^* are independent of V and ℓ. The results in Eqs. (13) indicate a coupling among K_{yz}, K_{yy}, and K_{zz}. Substitution of Eqs. (13) into (11a) and (11b), and using $[\beta] \simeq [\tan \beta] = -(\partial[\chi]/\partial y)/(\partial[\chi]/\partial z)$, alternative expressions for the eddy fluxes are given by

$$\begin{aligned} [v^*\chi^*] &= -K_{yy}\left(1 - \frac{[\alpha]}{[\beta]}\right)\frac{\partial[\chi]}{\partial y} \\ [w^*\chi^*] &= -K_{zz}\left(1 - \frac{[\alpha][\beta]}{[\alpha]^2 + [\alpha^{*2}]}\right)\frac{\partial[\chi]}{\partial z}\,. \end{aligned} \tag{14}$$

Equation (14) indicates that when $[\alpha] = [\beta]$, the horizontal eddy fluxes vanish, and when $[\alpha] = 0$, the horizontal and vertical eddy fluxes are as in the Prandtl formulation. The Crutzen 2-D model utilized Eqs. (13) in the form (Crutzen, 1975):

$$K_{yy} = K_{11}$$
$$K_{yz} = [\alpha]\, K_{11} \qquad (15)$$
$$K_{zz} = K_{22} + [\alpha]^2\, K_{11},$$

where $K_{22} = [\alpha^{*2}]\, K_{11}$. The Crutzen model used the seasonal distributions of ozone and water vapor in the lower stratosphere, where the effects of chemistry are not dominant (Section 2.1 and Fig. 5), so as to determine the eddy parameters K_{11}, $[\alpha]$, and K_{22}. A test of this parameterization of eddy coefficients was made by simulating the late-time history of the dispersion of gaseous tracers deposited in the lower stratosphere by nuclear detonations. The results indicated depletions of the stratospheric burdens of such tracers that were faster than observations by about 30 percent (Crutzen, 1978). This discrepancy was not considered to be significant in view of the uncertainty associated with the accuracy of this type of tracer data.

The Widhopf 2-D model utilizes the height coordinate and Eqs. (11a) and (11b). As indicated earlier, the Widhopf parameterization of the eddy coefficients K_{yy}, K_{yz}, and K_{zz} was based on (a) extrapolations to the stratosphere by Luther (1973), of the Oört and Rasmusson (1971) data for the eddy transports of heat in the upper troposphere up to latitudes of 50°N. Such extrapolations have to take into account directly the complex 3-D dynamics of the tropopause gaps (Section 4.1.1) at the important middle latitudes for aviation effects (e.g., Fig. 7), and (b) the matching of segments of the time history of excess C-14 data from the 1961-1962 nuclear detonations in the atmosphere at approximately 70°N latitude, a procedure that is constrained by the accuracy and scope of the C-14 data. More specifically, this procedure consisted in the reproduction of the C-14 profiles at 30°N between April 1963 and January 1966 with adequate accuracy (Widhopf et al., 1977). Subsequent independent tests of this parameterization included numerical simulations of the distributions of other tracers in the stratosphere such as W-185 from

a nuclear detonation at approximately 11°N latitude in the summer of 1958 (Friend et al., 1961) and radioactive Zr-95 from a nuclear detonation at approximately 40°N in the summer of 1967 (Telegadas, 1974). These tests of the parameterization of eddy transports also gave adequate results when compared with these observations of limited accuracy. Since the Widhopf parameterization of the eddy coefficients is thus independent of the chemistry, the subsequent successful simulation of the meridional ozone distributions could be assumed to be a consistency test of the formulation of the 1976 chemistry.

The magnitude of the eddy coefficients is illustrated in Table 13, which shows the eddy coefficients for the Crutzen model for the lower stratosphere and upper troposphere during summer and winter in the Northern Hemisphere. The results in Table 13 indicate that the horizontal eddy coefficient (K_{yy}) is of the order of 10^{10} cm^2/sec, and its magnitude at every latitude is significantly larger during winter than in summer. The slope of the mean diffusion axis ($[\alpha]$) is of the order of 10^{-4}, and it is, in general, negative, as indicated in Fig. 18. The eddy coefficient K_{zz} is of the order of 10^4 cm^2/sec in the lower stratosphere, and its increase with decreasing altitude near the tropopause is as expected from the previous considerations of the relative stabilities of the lower stratosphere and upper troposphere.

Table 14 illustrates the eddy coefficients for the Widhopf model, which are given as a function of month instead of season, as in the Crutzen model. Because of the poorer data base for the Southern Hemisphere, the eddy coefficients are taken to be there the same as in the Northern Hemisphere; but shifted by 6 months to take into account the corresponding shift in the solar inclination as a function of latitude (Widhopf, et al., 1977). Although the sample data in Table 14 are given in the model for the month of August in both hemispheres, the winter southern latitudes for August have been changed in this table

TABLE 13. SAMPLE EDDY PARAMETERS FOR CRUTZEN MODEL DURING SUMMER AND WINTER IN NORTHERN HEMISPHERE* (Source: Hidalgo and Crutzen, 1977)

Altitude (km)	Summer, Latitude (deg.)					Winter, Latitude (deg.)				
	80°N	60°N	40°N	20°N	0°N	80°N	60°N	40°N	20°N	0°N
Eddy Transport Coefficient K_{yy}, (10^{10} cm^2/sec)										
19.8	1.44	1.12	0.80	0.43	0.30	4.40	4.40	3.80	1.18	0.31
18.0	1.44	1.12	0.80	0.47	0.36	4.40	4.40	3.80	1.22	0.37
16.3	1.44	1.12	0.80	0.54	0.45	4.40	4.40	3.80	1.29	0.45
14.5	1.44	1.12	0.91	0.59	0.48	4.40	4.43	4.52	1.46	0.48
12.7	1.44	1.28	1.13	0.64	0.48	4.48	5.42	5.65	1.72	0.48
10.8	1.66	1.61	1.28	0.68	0.48	5.46	6.82	6.08	1.88	0.48
Slope of Mean Diffusion Axis, $[\alpha](10^{-4})$										
19.8	-7.42	-12.14	-13.96	-5.00	-0.30	-5.03	- 9.24	-12.15	-4.29	-0.27
18.0	-7.85	-12.74	-14.71	-1.28	-0.25	-5.85	-10.24	-12.96	-0.43	-0.24
16.3	-8.30	-13.22	-12.40	-0.40	-0.19	-6.66	-11.14	- 9.74	0.41	-0.18
14.5	-8.34	-10.75	- 4.52	-0.18	-0.17	-7.24	-11.21	- 0.21	-0.67	-0.08
12.7	-6.77	- 3.13	0.95	-0.82	-0.15	-6.85	- 8.29	2.57	0.04	-0.04
10.8	-1.84	1.17	1.09	-1.68	-0.09	-4.56	0.29	2.51	-0.67	-0.04
Eddy Transport Coefficient, K_{zz}, (10^4 cm^2/sec)										
19.8	1.71	2.16	1.77	0.36	0.12	2.30	4.34	4.79	0.58	0.12
18.0	1.60	2.20	1.85	0.29	0.12	2.56	4.97	5.17	0.39	0.12
16.3	1.57	2.12	1.56	4.23	15.70	2.90	5.61	1.57	4.31	16.13
14.5	1.44	1.38	0.81	5.26	14.10	3.11	5.08	1.62	5.37	14.44
12.7	0.93	0.83	0.61	6.41	12.52	2.63	2.92	0.80	6.49	12.73
10.8	0.45	1.45	1.98	8.88	22.00	1.26	1.74	3.09	9.00	22.00

*Eddy parameters are given as a function of season (instead of month) in the Crutzen model.

TABLE 14. SAMPLE EDDY PARAMETERS FOR WIDHOPF MODELS DURING SUMMER (AUGUST) IN NORTHERN HEMISPHERE AND WINTER IN SOUTHERN HEMISPHERE* (Source: Widhopf, 1978)

Altitude (km)	Summer (August), Latitude (deg.)					Winter (February), Latitude (deg.)				
	80°N	60°N	40°N	20°N	0	80°N	60°N	40°N	20°N	0
Eddy Transport Coefficient K_{yy} (10^{10} cm^2/sec)										
20	0.29	0.28	0.19	0.12	0.17	3.76	2.97	0.83	0.27	0.17
18	0.34	0.38	0.39	0.21	0.21	3.37	2.90	1.17	0.70	0.21
16	0.42	0.52	0.63	0.30	0.25	2.99	2.87	1.61	1.18	0.25
14	0.63	1.03	1.27	0.42	0.34	2.77	3.22	2.91	2.13	0.34
12	0.85	1.54	1.90	0.55	0.43	2.54	3.57	4.21	3.09	0.43
10	1.61	2.20	1.71	0.40	0.32	3.21	4.94	5.62	2.67	0.32
Slope of Mixing Axis, $\lvert\alpha\rvert$(10^{-4})										
20	-4.66	-14.57	- 9.63	-2.86	- 2.53	1.62	6.23	14.70	0.73	- 2.53
18	-5.97	-16.18	-15.95	-4.90	- 4.33	1.81	6.38	12.39	4.37	- 4.33
16	-6.60	-16.17	-15.87	-5.70	- 6.08	2.04	6.45	10.31	4.40	- 6.08
14	-6.92	-12.82	- 6.94	-5.36	- 9.65	2.89	7.52	5.53	3.10	- 9.65
12	-7.14	-11.95	- 3.99	-5.07	-11.74	3.90	8.40	3.68	-0.32	-11.74
10	0.62	0.16	0.58	2.50	- 1.89	-0.31	0.16	-0.18	-0.37	- 1.89
Eddy Transport Coefficient K_{zz} (10^4 cm^2/sec)										
20	0.42	0.42	0.22	0.06	0.07	1.01	1.01	1.59	0.07	0.07
18	0.43	0.43	0.84	0.14	0.15	0.80	0.80	1.69	0.26	0.15
16	0.45	0.45	1.45	0.22	0.24	0.66	0.66	1.76	0.45	0.24
14	0.85	0.85	1.33	0.33	0.69	1.05	1.05	1.50	0.55	0.69
12	0.60	1.50	1.20	0.51	1.14	0.40	1.45	1.23	0.78	1.14
10	0.86	1.51	1.80	0.89	1.75	0.59	1.00	3.02	1.27	1.75

*The actual notation for the eddy coefficients in the Widhopf model is $K_{\phi\phi}$, $K_{z\phi}$ and K_{zz} (Widhopf, Glatt and Kramer, 1977). The angle α is given here by the ratio $K_{z\phi}/K_{\phi\phi}$. The eddy coefficients in this model are given as a function of month for both northern and southern latitudes. Above data is applicable for the month of August; i.e., summer in the Northern Hemisphere and winter in the Southern Hemisphere. See text for the shift from southern (August) to northern (February) latitudes for winter.

back to the corresponding winter northern values during February. The reason for this latitudinal shift is to facilitate a comparison of the Widhopf and Crutzen eddy coefficient data for winter in the Northern Hemisphere. This shift from southern (August) back to northern (February) latitudes has required a repetition for winter of the zero latitude column during summer. Although a more consistent comparison of the data in Tables 13 and 14 would require the seasonal averages of the Widhopf data, these tables suggest rather significant differences between these two sets of eddy coefficients for the lower stratosphere in either season.

A third parameterization of the 2-D dynamics, based on the Louis meridional circulation, was given by Danielsen and Louis (1977). This parameterization utilized the observed transports of ozone in the lower stratosphere, based on arguments that *(a) ozone may be considered to be a passive tracer below about 21 km (i.e., Section 2.1 and Fig. 5), and (b) ozone is the best-documented tracer in the lower stratosphere.* The calculations of the K_{yy}, K_{yz}, and K_{zz} coefficients utilized the following assumptions: (1) the horizontal eddy flux of ozone is proportional to its mean flux, and (2) the product $[\alpha]^2 K_{yy}$ in the vertical flux (Eq. 15) must be a minimum so as to avoid large values of $[\alpha]$, which would give vertical fluxes of ozone that are greater than the ozone destruction at the ground. These two assumptions gave two relationships between K_{yy} and K_{yz}. The third coefficient, K_{zz}, was obtained by solving Eq. (9) for ozone in the lower stratosphere. Table 15 illustrates results from these calculations, where the K_{yz} values are given in terms of $[\alpha]$ through the ratio K_{yz}/K_{yy}. These results are for December-February; i.e., for winter in the Northern Hemisphere and summer in the Southern Hemisphere. However, if the eddy coefficients in either hemisphere are assumed to depend only on season (as in the Widhopf model), the December-February summer data for the Southern Hemisphere also becomes applicable

for the summer (June-August) in the Northern Hemisphere. The validity of this assumption for the Danielsen-Louis parameterization may be somewhat constrained by the difference in the ozone distributions in the two hemispheres as reflected by the data in Fig. 3. Based on this assumption, a comparison of the results in Tables 13 and 15 indicates rather drastic differences for either season between the Crutzen and Danielsen-Louis parameterizations of the eddy coefficients, both of which utilized ozone distributions.

The Danielsen-Louis parameterization of the eddy transports was also tested using numerical simulations of segments of time history of the meridional distributions of tracers deposited in the lower stratosphere by nuclear detonations. These tests simulated the transports of Zr-95 from a series of Chinese nuclear tests (1968-1972), and a high-yield 1968 French test as well as the transport of W-185 from the U.S. Hardtack test at 11°N latitude during 1958. The results of these simulations indicated that use of the Louis meridional circulation (Fig. 17) and the eddy coefficients in Table 15 gave depletion rates of the stratospheric burdens of such tracers that were too large compared with observations. Significant improvements in these simulations were obtained by decreasing by a factor of 2 both the air velocities in Fig. 17 and the eddy coefficients in Table 15. This procedure was justified by citing the uncertainty of a factor of about 2 in the derivation of the Louis meridional circulation.

Since Fig. 18 indicates that for countergradient eddy transports (i.e., $[\alpha] >> [\beta]$), $[\alpha] = [w^*R^*]/[v^*R^*]$, which from Eqs. (13) is also given by $[\alpha] = K_{yz}/K_{yy}$, then $K_{yz}/K_{yy} = [w^*R^*]/[v^*R^*]$. Hence, Eqs. (11a,b) yield (Mahlman, 1975):

$$K_{yy} = - \frac{[v^*R^*]^2}{[v^*R^*] \frac{\partial [R]}{\partial y} + [w^*R^*] \frac{\partial [R]}{\partial z}} , \qquad (16)$$

TABLE 15. SAMPLE EDDY PARAMETERS DERIVED FROM POLEWARD TRANSPORT OF OZONE*
(Source: Danielsen and Louis, 1977)

Altitude (km)	Summer/Latitude (deg.)					Winter/Latitude (deg.)				
	80°N	60°N	40°N	20°N	0°	80°N	60°N	40°N	20°N	0°
Eddy Transport Coefficient K_{yy}, (10^{10} cm^2/sec)										
25	0.13	0.17	0.10	0.12	0.15	0.40	0.44	0.20	0.15	0.15
20	0.19	0.43	0.11	0.17	0.25	0.33	0.54	0.24	0.15	0.25
15	0.16	0.25	0.11	0.28	0.61	0.24	0.40	0.33	0.21	0.61
10	0.20	0.21	0.13	0.38	1.04	0.32	0.49	0.34	0.23	1.04
Slope of Mean Diffusion Axis, [α] (10^{-4})										
25	5.15	6.29	2.84	-2.08	0.33	0.65	- 2.45	- 1.45	1.47	0.33
20	5.26	7.14	-12.18	-1.18	0.48	-3.00	-10.33	-20.92	-0.60	0.48
15	-0.38	9.60	11.73	-2.43	0.16	-7.96	-18.55	-29.61	-1.24	0.16
10	-1.25	2.48	1.08	-4.00	-0.16	0.44	- 4.55	- 6.21	4.22	-0.16
Eddy Transport Coefficient, K_{zz}, (10^4 cm^2/sec)										
25	0.13	0.21	0.09	0.12	0.26	0.22	0.20	0.10	0.11	0.26
20	0.14	0.42	0.23	0.13	0.46	0.39	0.84	1.15	0.10	0.46
15	0.09	0.48	0.19	0.15	0.66	0.63	1.27	3.01	0.11	0.66
10	0.23	0.35	0.19	0.55	2.69	0.87	1.14	0.39	0.35	2.69

*Data is applicable to December-February; i.e., for summer in the Southern Hemisphere and winter in the Northern Hemisphere. See text for the switch in summer latitudes from south (December-February) to north (June-August).

and

$$K_{zz} = - \frac{[w^*R^*]^2}{[v^*R^*] \frac{\partial [R]}{\partial y} + [w^*R^*] \frac{\partial [R]}{\partial z}} \quad . \tag{17}$$

Equations (16) and (17) also identify the parameters that would have to be deduced from observations for a reliable 2-D parameterization of the eddy coefficients. These parameters involve the eddy horizontal and vertical mass fluxes as well as the corresponding gradients of the mixing ratio as a function of altitude, latitude, and month or season.

Equations (16) and (17), together with $[\alpha] = [w^*R^*]/[v^*R^*]$, yield $K_{zz} = [\alpha]^2 K_{yy}$, a result that is consistent with Eqs. (13) because the condition $[\alpha] = [w^*R^*]/[v^*R^*]$ also implies from Eqs. (14) that $[\alpha^{*2}]/[\alpha] \ll 1$. The foregoing result can be put in the form

$$\frac{K_{zz}}{[\alpha]^2 K_{yy}} = 1, \tag{18}$$

which is a condition that can be used to test the internal consistency of the parameterizations in Tables 13 through 15. Inspection of these tables at either constant altitude (rows) or constant latitude (columns) indicates that this consistency condition is violated (i.e., $K_{zz}/[\alpha]^2 K_{yy} \neq 1$) whenever there is mainly a rapid change of α alone. This consistency test reveals the following:

(a) The Crutzen 2-D parameterization (Table 13) is consistent within itself only at middle and high latitudes within the stratosphere, since $K_{zz}/[\alpha]^2 K_{yy} \gg 1$ at low latitudes ($20°N \leq \theta \leq 20°S$) in both the lower stratosphere and upper troposphere. Furthermore, $K_{zz}/[\alpha]^2 K_{yy}$ increases rapidly above unity in the upper troposphere at any latitude.

(b) The Widhopf 2-D parameterization (Table 14) is consistent within itself only at middle latitudes within

the stratosphere, because $K_{zz}/[\alpha]^2 K_{yy} > 1$ at high (80°) and low ($\theta < 20°$) latitudes in the lower stratosphere. Again, $K_{zz}/[\alpha]^2 K_{yy}$ increases rapidly above unity in the upper troposphere in the $20° < \theta < 60°$ latitudinal range.

(c) The Danielsen-Louis 2-D parameterization is consistent within itself only at middle latitudes ($40° \leq \theta \leq 60°$) within the stratosphere below 20 km, because $K_{zz}/[\alpha]^2 K_{yy}$ is otherwise either larger (> 1) or much larger (>>1) than unity.

The criterion given by Eq. (18) indicates that the Widhopf parameterization is the most consistent at low latitudes in the stratosphere because $K_{zz}/[\alpha]^2 K_{yy} > 1$ instead of $K_{zz}/[\alpha]^2 K_{yy} >> 1$ as in the other two parameterizations. These consistency tests reveal, then, an extra degree of freedom used in these parameterizations as the result of apparent violations of the interrelationships among the eddy parameters as given by Eqs. (13). Furthermore, the inconsistency at low latitudes becomes important for the proper interpretation of the transport of engine effluents from the Northern to the Southern Hemisphere; i.e., for the impact of high-altitude flight in the flight corridors of the Northern Hemisphere on the ozone column in the Southern Hemisphere.

It is important to indicate that the eddy coefficients (e.g., Tables 13 through 15) are assumed to be properties of the atmosphere which are taken to be the same in the calculation of the eddy transports in Eq. (9) for each of the chemical species.

Equations (9) and (11a, b) also identify *model-dependent* effects in the Crutzen and Widhopf 2-D photochemical models, which involve uncertainties in the magnitudes of the photolysis rates and chemical rate coefficients (e.g., Table 3) as well as eddy coefficients (Tables 13 and 14). These model-dependent

effects are a consequence of the basic constraints indicated previously (Section 1) and they have been responsible for the poor forecast record of aviation effects on ozone (Section 3). For example, since Eqs. (11a, b) with $\chi = R_i$ show that the eddy fluxes in Eq. (9) are proportional to the gradients of the mixing ratio of the i species, it becomes clear that the Howard-Evenson rate coefficient in the revised 1977 chemistry has distorted the previous calculated transports of mixing ratio by the meriodional circulation and eddy motions through distortions of the meridional distributions of the mixing ratios R_i. *Hence, any compensation of the imprecise knowledge of photolysis and chemical kinetic rates through artibrary adjustments in the parameterizations of the eddy transports or vice versa would not necessarily be justified.*

4.2 EVALUATION OF THE EXTENSION OF THE DIFFUSION HYPOTHESIS TO THE PERTURBED ATMOSPHERE

The applicability of arbitrary extensions of the 2-D parameterizations of the dynamics for the reference upper troposphere and lower stratosphere to describe the mass transports of engine effluents from an assumed large, high-altitude aircraft traffic requires considerations of (a) the degree of empiricism in the available 2-D parameterizations of the dynamics as revealed by the dynamic meteorology of the region, and (b) the mass transports of passive tracers in the upper troposphere and lower stratosphere as determined from 3-D solutions of the equations of atmospheric motions for instantaneous (e.g., nuclear detonations) and continuous (i.e., aircraft-like) sources of such material in the upper troposphere and/or lower stratosphere. These considerations are given below.

4.2.1 Dynamic Meteorology of Eddy Transports in the Stratosphere

The foregoing 2-D empirical parameterizations of large-scale eddy transports of mass in the reference stratosphere

(Tables 13 through 15) utilize two basic assumptions: (1) the meridional circulation is independent of the eddy motions, and (2) the eddy components of the mixing ratios (R_i^*) are proportional to the meridional gradients of the zonally averaged mixing ratio (Eq. 10). The validity of these assumptions is not supported by the fundamental primitive equations.

The differential equations for the meridional circulation and eddy motions can be obtained from the primitive Equations (1) through (3) by the following steps: (1) splitting the dependent variables (χ = u, v, w, T) into their zonal mean and eddy components (Eq. 8); (2) taking the zonal average of the primitive equations, and (3) subtracting the zonally averaged equations from each respective primitive equation. Using the altitude instead of the pressure as a vertical coordinate, the results are given in Tables 16 and 17 for the zonal mean circulations and eddy motions, respectively. The equations for the zonal mean circulations consist of four equations for the four dependent variables [v], [w], [u], and [T], while those for the eddies give the corresponding components v*, w*, u*, and T*.

The results in Table 16 indicate that the meridional circulation is driven by the eddy motions through the terms [F_x], [F_y], and [G], whereas those in Table 17 show complex couplings among the eddies and the meridional circulation. Therefore, the system of equations in Tables 16 and 17 implies that the mass transports by the eddies in Eq. (9) are not as assumed by Eqs. (11a, b), since the poleward and vertical eddy velocities are coupled in a very complex way not only with the meridional circulation ([v], [w]), but also with the zonal circulation ([u]) and other eddy variables such as the eddy component of the net heating (Q*). Furthermore, since tracer material in the reference stratosphere is imbedded in the eddy field, the results in Table 17 imply that the eddy mixing ratio (R_i^*) cannot be as is assumed by Eq. 10.

TABLE 16. PRIMITIVE EQUATIONS FOR MERIDIONAL CIRCULATION (Source: e.g., Holton, 1975)

$$\frac{\partial[u]}{\partial t} + [v]\frac{\partial[u]}{\partial y} + [w]\frac{\partial[u]}{\partial z} - \left(2\Omega + \frac{[u]}{a\cos\theta}\right)[v]\sin\theta = -[F_x] \qquad (a)$$

$$\frac{\partial[v]}{\partial t} + [v]\frac{\partial[v]}{\partial y} + [w]\frac{\partial[v]}{\partial z} + \left(2\Omega + \frac{[u]}{a\cos\theta}\right)[u]\sin\theta + \frac{\partial[\phi]}{\partial y} = -[F_y] \qquad (b)$$

$$\frac{\partial[T]}{\partial t} + [v]\frac{\partial[T]}{\partial y} + [w]\frac{\partial[T]}{\partial z} + \left(\frac{dT_o}{dz} + \frac{\kappa T_o}{H}\right)[w] = \frac{[Q]}{c_p} - [G] \qquad (c)$$

$$\frac{1}{\cos\theta}\frac{\partial}{\partial y}([v]\cos\theta) + \frac{1}{\rho_o}\frac{\partial}{\partial z}(\rho_o[w]) = 0 \qquad (d)$$

where the forcing terms $[F_x]$, $[F_y]$ and $[G]$ are given by

$$[F_x] = \frac{1}{\cos^2\theta}\frac{\partial}{\partial y}([u^*v^*]\cos^2\theta) + \frac{1}{\rho_o}\frac{\partial}{\partial z}(\rho_o[u^*w^*])$$

$$[F_y] = \frac{1}{\cos\theta}\frac{\partial}{\partial y}([v^{*2}]\cos\theta) + \frac{1}{\rho_o}\frac{\partial}{\partial z}(\rho_o[v^*w^*]) + \frac{[u^{*2}]\tan\theta}{a}$$

$$[G] = \frac{1}{\cos\theta}\frac{\partial}{\partial y}([v^*T^*]\cos\theta) + \frac{1}{\rho_o}\frac{\partial}{\partial z}(\rho_o[w^*T^*]) .$$

The symbol Ω in Eqs. (a) and (b) denotes the earth's rotation, and $[\phi]$ in Eq. (b) is given by $\partial[\phi]/\partial z = R[T]/H$; where R is the gas constant for dry air and H the scale height ($\equiv RT_s/g$, where T_s is a constant stratospheric mean temperature). T_o in Eq. (c) is a basic state temperature and $\rho_o = \rho_s \exp(-z/H)$ in Eq. (d), where ρ_s is the density at sea level.

TABLE 17. PRIMITIVE EQUATIONS FOR EDDY MOTIONS (Source: e.g., Holton, 1975)

$$\frac{\partial u^*}{\partial t} + [u]\frac{\partial u^*}{\partial x} + [v]\frac{\partial u^*}{\partial y} + [w]\frac{\partial u^*}{\partial z} - \left(2\Omega + \frac{[u]}{a\cos\theta}\right)\sin\theta\, v^* - \frac{[v]u^*\tan\theta}{a} + v^*\frac{\partial [u]}{\partial y} + w^*\frac{\partial [u]}{\partial z} + \frac{\partial \phi^*}{\partial x} = -F_x^* \qquad (a)$$

$$\frac{\partial v^*}{\partial t} + [u]\frac{\partial v^*}{\partial x} + [v]\frac{\partial v^*}{\partial y} + [w]\frac{\partial v^*}{\partial z} + \left(2\Omega + \frac{[u]}{a\cos\theta}\right)\sin\theta\, u^* + \frac{[u]u^*\tan\theta}{a} + v^*\frac{\partial [v]}{\partial y} + w^*\frac{\partial [v]}{\partial y} + \frac{\partial \phi^*}{\partial y} = -F_y^* \qquad (b)$$

$$\frac{\partial T^*}{\partial t} + [u]\frac{\partial T^*}{\partial x} + [v]\frac{\partial T^*}{\partial y} + [w]\frac{\partial T^*}{\partial z} + v^*\frac{\partial [T]}{\partial y} + w^*\frac{\partial [T]}{\partial z} + w^*\left(\frac{dT_o}{dz} + \frac{\kappa T_o}{H}\right) = \frac{Q^*}{c_p} - G^* \qquad (c)$$

$$\frac{\partial u^*}{\partial x} + \frac{1}{\cos\theta}\frac{\partial}{\partial y}(v^*\cos\theta) + \frac{1}{\rho_o}\frac{\partial}{\partial z}(\rho_o w^*) = 0 \qquad (d)$$

where the eddy interaction terms F_x^*, F_y^*, and G^* are given by

$$F_x^* = \frac{\partial u^{*2}}{\partial x} + \frac{1}{\cos^2\theta}\frac{\partial}{\partial y}\{(u^*v^* - [u^*v^*])\cos^2\theta\} + \frac{1}{\rho_o}\frac{\partial}{\partial z}\{\rho_o\,(u^*w^* - [u^*w^*])\}$$

$$F_y^* = \frac{\partial}{\partial x}(u^*v^*) + \frac{1}{\cos\theta}\frac{\partial}{\partial y}\{(v^{*2} - [v^{*2}])\cos\theta\} + (u^{*2} - [u^{*2}])\frac{\tan\theta}{a} + \frac{1}{\rho_o}\frac{\partial}{\partial z}\{\rho_o(v^*w^* - [v^*w^*])\}$$

$$G^* = \frac{\partial}{\partial x}(u^*T^*) + \frac{1}{\cos\theta}\frac{\partial}{\partial y}\{(v^*T^* - [v^*T^*])\cos\theta\} + \frac{1}{\rho_o}\frac{\partial}{\partial z}\{\rho_o(w^*T^* - [w^*T^*])\}$$

It should be noted that results in Table 16 have been used to determine the meridional circulation shown in Fig. 17. Considerations of the scales of the meridional velocities indicate that $[v] \sim 1.5$ m/sec and $[w] \sim 1$ cm/sec. Because of the smallness of the vertical velocity, its magnitude cannot be determined from direct observations. Therefore, the procedure used by Louis consisted of using Eqs. (c) and (d) in Table 16, together with observed temperature fields, and estimates of the eddy fluxes of heat in the term [G], and the net heating rate per unit mass [Q]. The uncertainty in these results depends, then, on the parameterization of the eddy transports of sensible heat as well as the radiation calculations.

The meridional circulation as well as the eddy variables in Table 17 can be determined from solutions of the (unaveraged) primitive equations themselves, which can be solved either by finite difference or spectral numerical techniques. Figure 19 shows solutions of such system of equations based on the latter technique and the assumption of geostrophic equilibrium (Cunnold et al., 1975). Although the analytical results in Fig. 19 resemble those in Fig. 17, which were obtained from observations, this agreement is not surprising; because the model specified the radiative equilibrium temperature distribution and the static stability instead of using only the flux of solar radiation across the outer boundary of the atmosphere.

The splitting of the atmospheric motions into average circulations and eddy components (Eq. 8), as used in the results of Tables 16 and 17, turns out to be more important in the stratosphere than in the troposphere. A main reason for this condition, of course, is the absence in the stratosphere of the topographical and thermal forcings of the troposphere. For example, it has been shown that the annual energy budget of the large-scale eddy transports in the lower stratosphere is driven primarily by planetary waves propagating upwards from the

troposphere during winter (Dopplick, 1971). This mechanism can, surprisingly, be described in terms of linear wave mechanics and requires consideration of the effects of the meridional circulation on the zonal flow [u]. The Coriolis torque exerted by

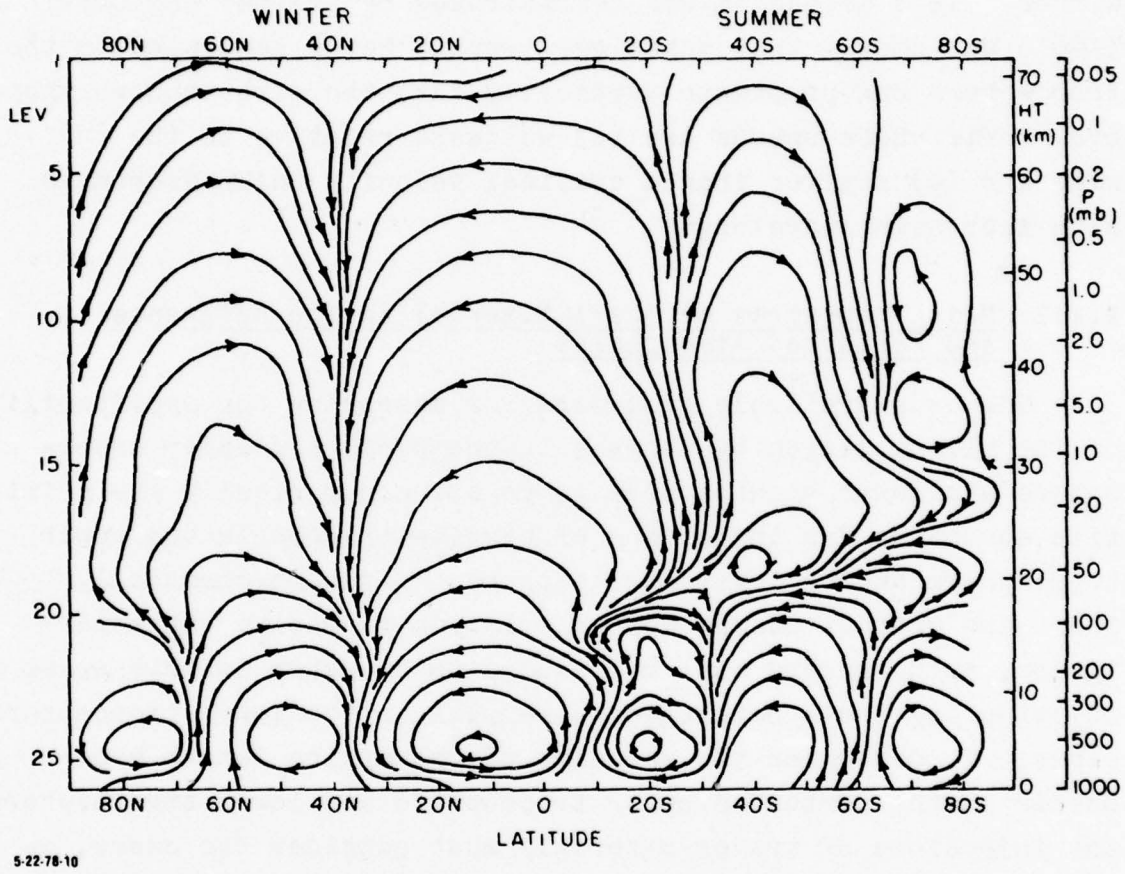

FIGURE 19. Simulation of meridional circulation by a three-dimensional model of the troposphere-stratosphere-mesosphere ($0 < z < 70$ km) utilizing the condition of geostrophic equilibrium and the spectral representation of the dependent variables. Note the simulation of the three cells in the troposphere; i.e., the direct Hadley cell at low latitudes, the indirect Ferrel cell at middle latitudes and the polar cell. Note also the complex downward stratospheric motions at the tropopause gaps between the Hadley and Ferrel cells at about 30° latitude during winter and summer. Corresponding eddy motions are not shown. (Source: Cunnold et al., 1975)

the meridional flow (Fig. 19) generates stratospheric mean zonal winds ([u]) in the westward direction during summer and in the eastward direction during winter. This change in the sign of the stratospheric zonal wind allows, then, vertical propagation of tropospheric planetary waves to the stratosphere during winter. This mechanism was demonstrated by Charney and Drazin (1961) who showed that quasi-geostrophic waves generated in the troposphere can propagate vertically into the stratosphere whenever their phase speeds are (a) westward relative to the [u] wind and (b) smaller than a critical velocity which decreases with increasing wavelength.

4.2.2 Mass Transports of Inert Material in the Reference and Perturbed Atmospheres

The *only* available procedure for assessing the applicability of the mixing length hypothesis to the *perturbed* upper troposphere and lower stratosphere is to solve numerically the primitive equations for injections of passive tracers in the upper troposphere and/or lower stratosphere. Although chemically inert and without absorption or emission radiative characteristics, such tracers must be assumed to be water soluble so as to stimulate their heterogenous removal in the lower tropospheric sinks. To determine the validity of the mixing length hypothesis in the perturbed upper troposphere and lower stratosphere, the injections of tracer materials must consider two cases, as discussed in the following paragraphs.

The first case would involve instantaneous injections at a point in the lower stratosphere to simulate the dispersion of debris from nuclear detonations in the reference upper troposphere and lower stratosphere; i.e., by considering solutions of Eq. (5) for the conservation of the passive tracer mixing ratio, $dR/dt = 0$, subject only to the removal of the tracer material in the tropospheric sinks. These solutions must consider an initial, local distribution of tracer and provide the

subsequent time evolutions of the mixing ratio in the stratosphere and troposphere. More important, these numerical solutions can provide insight into the relative roles of the meridional circulation and eddy motions in the overall transport of tracer mixing ratio in the stratosphere. Another result would include an evaluation of the validity of the mixing length hypothesis itself anywhere in the reference upper troposphere and stratosphere. This latter result would be derived from (a) comparisons of the simulated and observed dispersions, as a function of time, of tracer material from nuclear detonations; and (b) comparisons of the eddy parameters in Tables 13 through 15, with those derived from the eddy transports and gradients of mixing ratio obtained from the primitive equations and the assumption that Eqs. (11a, b) are indeed valid.

The second case would require continuous injections at a typical location of the flight corridors to simulate the dispersion of aircraft engine effluents (NO_x and H_2O) in the perturbed upper troposphere and stratosphere; i.e., by considering solutions of Eq. (5) for the tracer mixing ratio, $dR/dt = S(\lambda, \Theta, z)$, subject to (a) a continuous source (S) in the typical flight corridor as a function of longitude, latitude, and altitude; and (b) the removal of tracer material in the tropospheric sinks. Because of the consideration of a passive tracer, the numerical results are applicable to the conservation of the aircraft NO_x and H_2O species during their dispersion in the atmosphere, i.e., to NO_y (NO_x + HNO_3) as well as to exclusion of H_2O from mechanism M11ab in Fig. 2 for H_2O. These solutions must consider numerical time integrations for a time long enough (several years) to approach equilibrium conditions (i.e., $\partial R_i/\partial t \rightarrow 0$ for a given month or season) between the continuous source and the tropospheric sinks in the Northern and Southern Hemispheres. These solutions can again provide the eddy parameters based on results from the primitive equations together with the mixing length hypothesis [Eqs. (11a, b)] for the perturbed upper tropo-

sphere and stratosphere. These results would thus establish the applicability of the eddy parameters for the reference atmosphere when extended to the perturbed conditions.

Numerical solutions of the above nature have been carried out at the Geophysical Fluid Dynamics Laboratory (GFDL) by Mahlman (1973, 1975) and Mahlman and Moxim (1978). The basic approach consisted of using available GCM solutions for the primitive equations (1 through 4) as inputs to the dynamical terms in the expansion of dR/dt (Eqs. 6 and 7). The numerical solutions of the passive tracer mixing ratio are then based on the use of the 3-D dynamics for one annual cycle in Eqs. (6) and (7); i.e., the tracer integrations proceeded beyond a year by recycling the same input data each year. Although this constraint stemmed from otherwise prohibitive investments in computer time, it should be noted that this procedure did keep all the terms in Tables 16 and 17 unchanged from one annual cycle to the next. The result is, then, a tracer behavior during several annual cycles that is solely due to the tracer itself.

The tracer solutions provide the 3-D distributions of the tracer mixing ratio as a function of time, but they can be reduced to the 2-D form of Eq. (9) by performing their zonal averages. These operations yield, then, each of the four dynamic terms in the left side of Eq. (9), which may be written for the instantaneous injection case as:

$$\frac{\partial [R]}{\partial t} + M_H + M_V + E_H + E_V + \Sigma T = 0 \ , \qquad (19)$$

where M_H and M_V denote the terms related to the horizontal and vertical transports of mixing ratio by the meridional circulation, E_H and E_V the corresponding eddy terms, and ΣT those due to the sinks as well as small-scale (subgrid) diffusion and filling (i.e., a correction to the advective terms whenever

truncation errors lead to a local negative mixing ratio). Hence, it becomes possible to (a) identify the relative roles of each of the above four dynamic terms on the local time evolution of the mixing ratio during any season as a function of time (years) or configurations of the tracer, and (b) calculate the corresponding eddy parameters [α], K_{yy}, and K_{zz} from the ratio of the eddy fluxes as well as the use of Eqs. (16) and (17).

Since the tracer equation may be made dimensionless by dividing each term of the equation by a constant reference value of the mixing ratio, the numerical results may be scalable to any other amplitude or peak value of the initial tracer distribution. Hence, the mixing ratio can be expressed in arbitrary units, denoted as R units. Likewise, the rate of change of mixing ratio can be based on a time characteristic of the zonal averaging (e.g., a day); hence the rate of change of the mixing ratio can be expressed, in general, in terms of R-units/day.

The numerical experiments for the instantaneous injection simulated a nuclear detonation in the lower stratosphere at about mid-latitudes in the Northern Hemisphere. The initial tracer distribution started in January 1 and was centered at 65 mbar (approximately 19 km) and 36°N. The initial distribution had a peak value of about 0.31 R units at 65 mbar and 36°N, a value that decayed exponentially with either increasing or decreasing altitude as well as latitude. The numerical integrations used a time step of 24 minutes for integrations of five annual cycles. The 3-D results were then averaged zonally to obtain the equivalent 2-D values, and monthly to determine the time evolutions of the tracer mixing ratio.

Figure 20 shows the meridional distribution of tracer mixing ratio for January or winter (top) and July or summer (bottom) during the first (left) and third (right) years of integrations. The vertical shape of the mixing ratio for January of the first year near 30°N reflects that of the initial

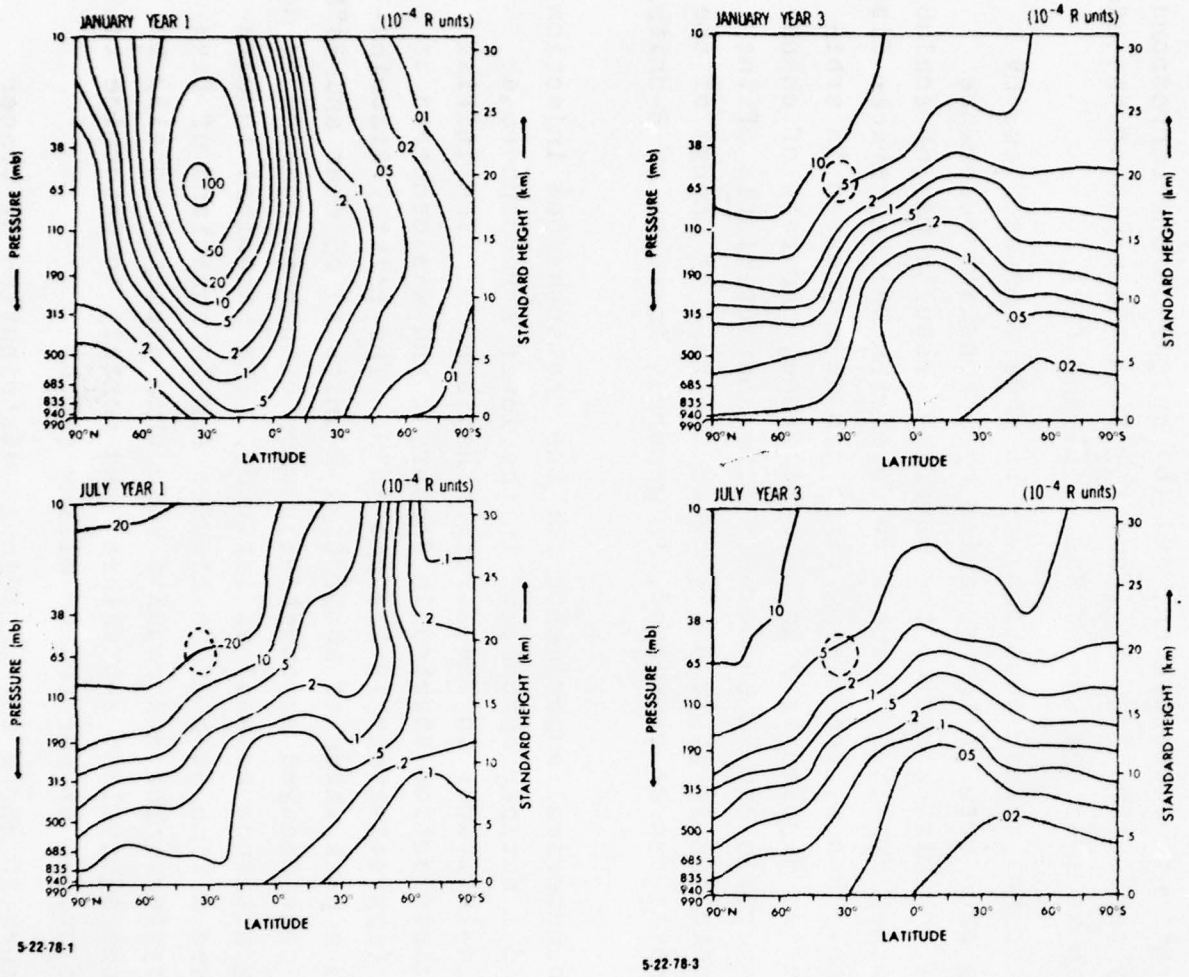

FIGURE 20. Simulation of β-lines (Fig. 18) by a three-dimensional passive tracer model utilizing finite differences of the primitive equations for an instantaneous injection of material at 36°N and 65 mbar during January. The dashed closed contours denote the location of the peak initial distribution. (Source: Mahlman and Moxim, 1978)

profile, which had mixing ratio values at 36°N equal to one-third the 65 mbar peak value at both 10 mbar and 190 mbar. The peak value of 100 (10^{-4} R units) for January of the first year shows that the mixing ratio there has decayed by more than a factor of about 30 from its initial peak value (0.31 R) during the first month after the assumed detonation. The July contours for the first year indicate that this decay of mixing ratio has proceeded by another factor of five after the first half year, when the formation of the [β] lines (Fig. 18) becomes evident. The January and July meridional distributions of mixing ratio during the third year are typical of those for the preceding and subsequent years. Figure 21 shows a cross plot of results for the end of the fourth year similar to those in Fig. 20, for constant pressure levels during winter (December). Figure 21 indicates that the mixing ratio at the location of the peak initial value of mixing ratio has dropped from the value at the beginning of the third year by a factor of about three during the next 2 years.

Figure 22 shows the dynamic interactions (Eq. 19) at the 65 mbar injection level corresponding to the meridional distributions in Fig. 20. The 3-D results shown in Fig. 22 indicate considerable compensation between the mean meridional circulation and the eddy fluxes. As pointed out by Holton (1978), these compensating effects are not accidental, because Andrews and McIntyre (1976) have already shown that the mean meridional circulation can be divided into two parts: a portion due to the diabatic heat sources and a portion driven by the eddies. For stationary eddies, the latter *exactly* cancels the eddy fluxes. Most of the mean meridional circulation is thus driven by the eddies. All of this would be much less confusing if a Lagrangian instead of an Eulerian point of view were to be used. Thus, it is to be expected that eventually McIntyre's "Lagrangian mean formulation" will replace the present awkward parameterizations in 2-D models. As pointed out again by Holton (1978),

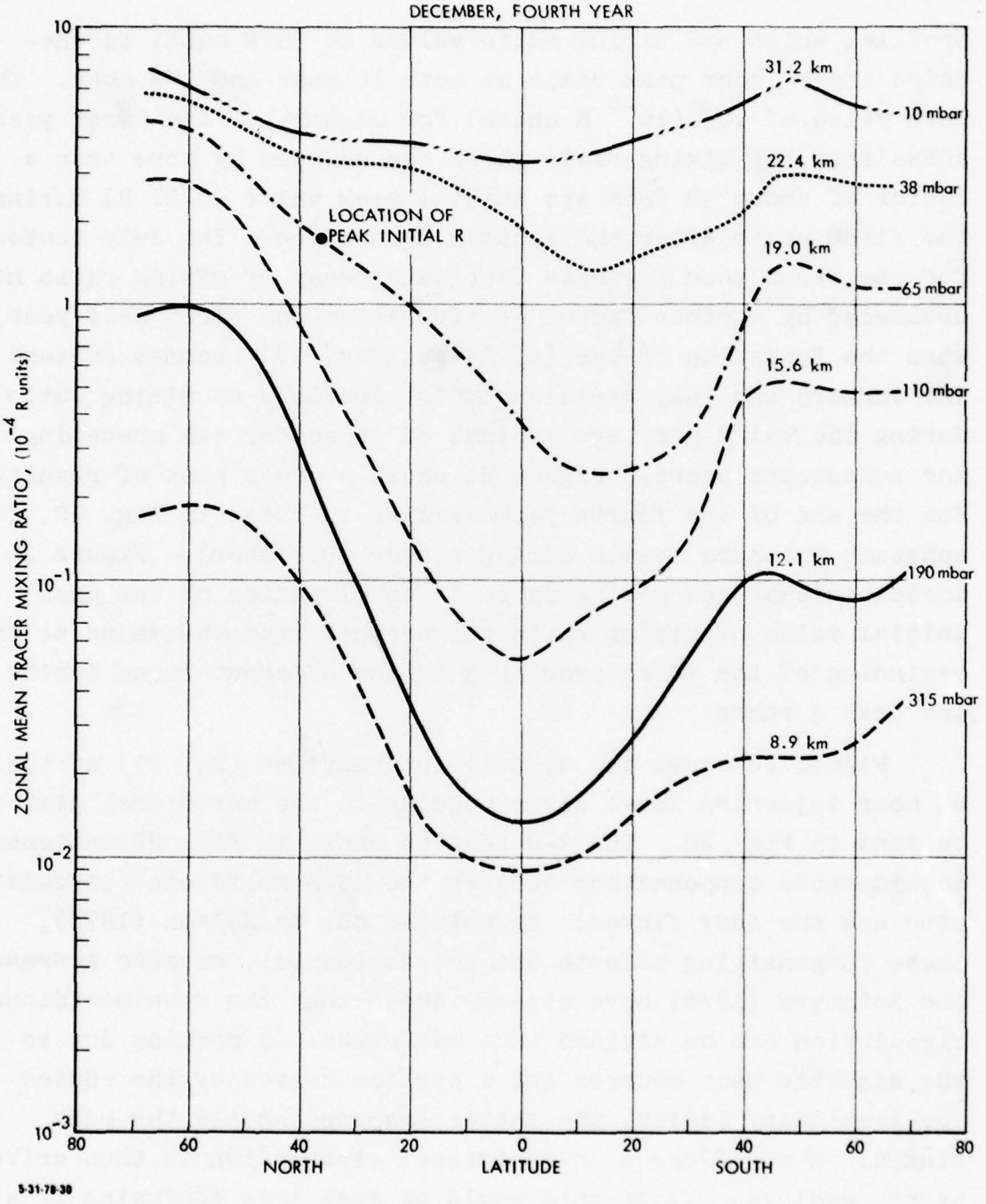

FIGURE 21. Stratospheric tracer mixing ratio as a function of latitude, altitude and season for winter (December) of the fourth year after an assumed instantaneous release of tracer material at 36°N and 65 mbar. (Source: Mahlman and Moxim, 1978)

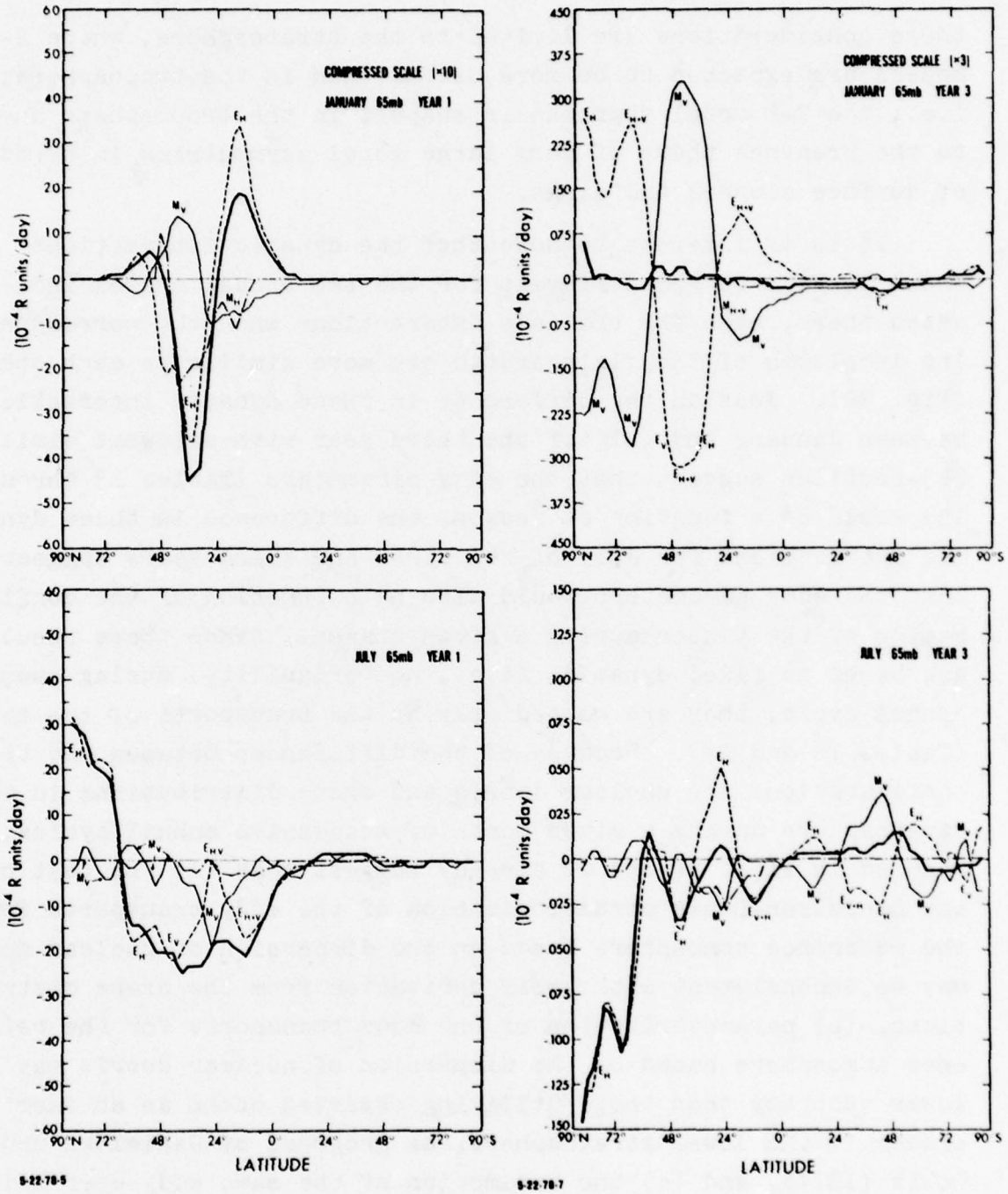

FIGURE 22. Interactions at the injection level (65 mbar) among the eddy and meridional motions in the dispersion of tracer material (Eq. 19) in the stratosphere during winter (top) and summer (bottom) (Source: Mahlman and Moxim, 1978)

these considerations are limited to the stratosphere, where 2-D models are expected to be more useful than in the troposphere; i.e., the 2-D model approach is suspect in the troposphere due to the presence there of very large zonal asymmetries in terms of surface sources and sinks.

It is of interest to note that the dynamic interactions shown in Fig. 22 are different for the two annual cycles indicated there, even for the July interactions when the corresponding isopleths of the mixing ratio are more similar to each other (Fig. 20). Just as the difference in these dynamic interactions between January and July of the third year with somewhat similar [β]-profiles suggest that the eddy parameters (Tables 13 through 15) would be a function of season, the difference in these dynamic interactions for July of the first and third years suggests that the eddy parameters would also be a function of the configuration of the tracer during a given season. Since these results are based on fixed dynamics (i.e., no variability) during each annual cycle, they are caused only by the transports of the tracer (Tables 16 and 17). Because of the differences between the tracer configurations for nuclear debris and ozone distributions in the stratosphere during a given month of successive annual cycles, the results in Figs. 20 and 22 already suggest that (a) the test of the Danielsen-Louis parameterization of the eddy transports for the reference atmosphere based on the dispersion of nuclear debris may be inconsistent with their derivation from the ozone distributions, (b) parameterization of the eddy transports for the reference atmosphere based on the dispersion of nuclear debris may have lower accuracy than those utilizing observed ozone as an inert tracer in the lower stratosphere, as proposed by Danielsen and Louis (1977), and (c) the assumption of the same eddy coefficient for every one of the chemical species with different configurations may be invalid. Furthermore, because of the expected differences between the tracer configurations of aircraft effluents and those of either ozone or nuclear debris in the reference

atmosphere, the available parameterizations of the eddy transports for the reference atmosphere may not be accurate for their extensions to the dispersion of engine effluents in the perturbed stratosphere.

The numerical experiments for the continuous injections simulate SST traffic at middle latitudes in the lower stratosphere of the Northern Hemisphere. The simulation of the aircraft traffic was assumed to be given by a source, S, of mixing ratio given by

$$S = S_o \exp\left[-\left(\frac{\theta - 48°N}{12}\right)^2\right] \exp\left[-\left(\frac{z-16.5}{1.8}\right)^2\right] \qquad (20)$$

i.e., by assuming that the peak source (S_o) from aircraft traffic occurs at θ_o = 48°N and z = 16.5 km. Thus, most of the SST tracer material was deposited at the 110 mbar level and in the altitude range 14 < z < 18.5 km. At either end of this altitude range, the tracer was assumed to drop to zero. The longitudinal (λ) dependence of the SST source was assumed to be unity over the North Atlantic (0°W < λ < 70°W) and East Pacific (130°W < λ < 140°E), and zero otherwise.

The initial conditions for this continuous source experiment utilized available results for the buildup of tracer mixing ratio as obtained from the following assumptions (Mahlman, 1973): (a) the SST problem could be represented, approximately, by a superposition of individual tracer time histories of different age; which are determined from a long series of single sources pulsing with a frequency of once every few hours, and (b) the time history of mixing ratio from each pulse is independent of that of the others, an assumption that was based on the fact that the ultimate global-scale distribution of a given tracer release is nearly independent of the initial (January) meteorological conditions of the single source experiment (e.g., Fig. 20). It is important to indicate that the main motivation

for using these initial conditions is avoidance of prohibitive investments in computer time when reaching the equilibrium tracer distributions given by the eventual balance between the continuous injections and the tropospheric sinks. Since this superposition procedure had been carried out for the first 4 years of assumed SST operation, the subsequent numerical experiments using a continuous source (e.g., Eq. 20) extends currently to 3 additional years (fifth to seventh) of assumed SST operations.

Figures 23 and 24 indicate results for the enhancement in the tracer mixing ratio during winter (December) and summer (August), respectively, from SST-like sources as given by Eq. 20. Since the tracer equation may again be made dimensionless by dividing it by the strength of the source term, these results are expressed in an arbitrary but convenient unit that allows their scaling to any specified source intensity. The units in Figs. 23 and 24 represent the enhancement of mixing ratio from one day's emissions over a *reference* value given by a uniform dilution of the daily tracer injection into the whole atmosphere. For example, for an annual emission rate of 10^9 kg of tracer material per year, one day's emission would be 2.7×10^6 kg per day. The uniform dilution of this daily emission into the mass of the atmosphere (5.1×10^{21} g of air) gives a reference value of 5.4×10^{-13} per day. Since Fig. 24 gives an enhancement of about 3800 over the reference value at 40°N and 65 mbar (19.0 km) during summer, the predicted enhancement in mixing ratio at this location would be 2.0 ppbm. Because the enhancements in Fig. 24 are approaching equilibrium conditions between the continuous source and the tropospheric sinks, this enhancement in mixing ratio at 40°N and 65 mbar is also approaching the maximum perturbation in the tracer mixing ratio for a given intensity of the continuous source. The results in Figs. 21, 23, and 24 indicate the following:

- There is a significant difference in the tracer configurations of the reference and perturbed lower

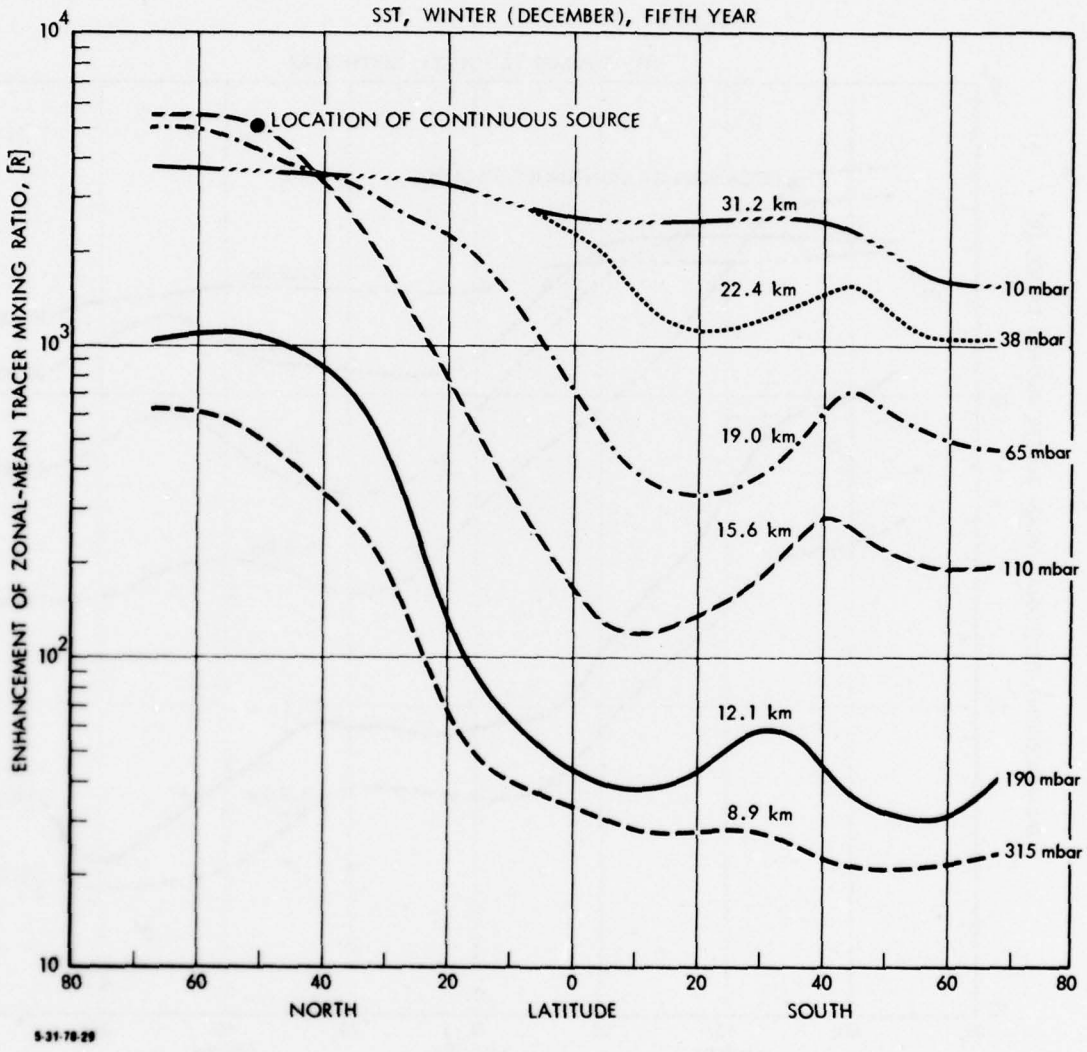

FIGURE 23. Enhancement of tracer mixing ratio as a function of latitude and altitude during winter (December) of the fifth year for a simulated SST-like continuous release of tracer material as per Eq. (20). Note the tendency towards a uniform distribution of tracer mixing ratio between 38 mbar (standard altitude of 22.4 km) and 10 mbar (31.2 km) in the Northern Hemisphere. (Source: Mahlman and Moxim, 1978)

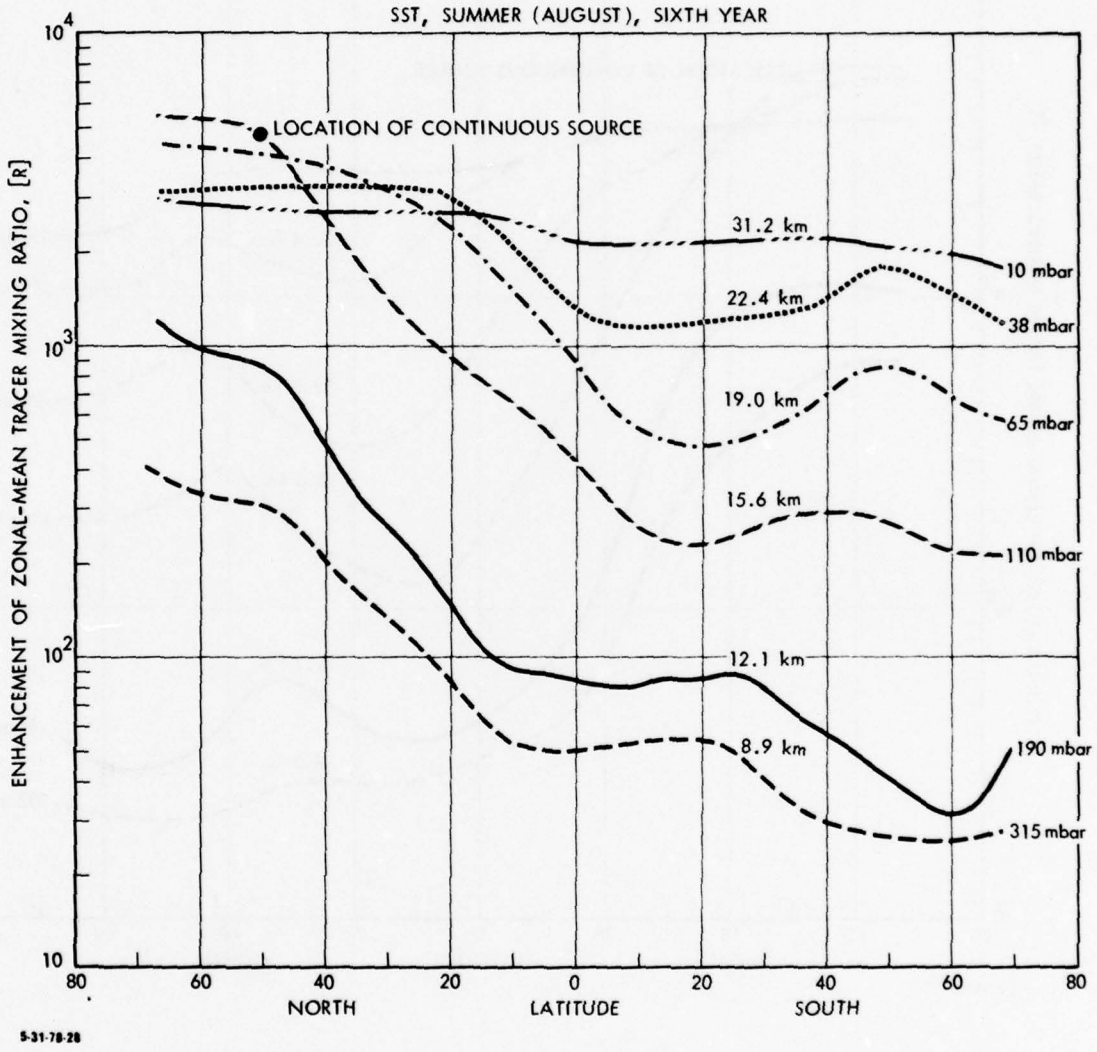

FIGURE 24. Enhancement of tracer mixing ratio as a function of latitude and altitude during summer (August) of the sixth year for a simulated SST-like continuous release of tracer material as per Eq. (20). (Source: Mahlman and Moxim, 1978)

stratospheres, for example, during winter in the Northern Hemisphere. Figure 21 for the reference stratosphere shows significant vertical gradients in the tracer mixing ratio at 40°N above 15.6 km, whereas Fig. 23 for the perturbed stratosphere indicates corresponding negligible vertical gradients and a nearly uniform mixing ratio at every northern latitude above 22.4 km. *The significance of these results is that the mixing length hypothesis would then predict negligible vertical eddy motions in a uniformly mixed perturbed stratosphere during winter [i.e., $\alpha = \beta = \nabla\chi = 0$ in Fig. 18 and $w^* = 0$ in Eq. (12)], if it were used with the perturbed transient tracer configuration derived from the primitive equations. Conversely, the eddy coefficients derived from the mixing length hypothesis from the tracer configuration in the reference stratosphere (i.e., $[\alpha] \neq 0$, $[\beta] \neq 0$, $[\alpha] >> [\beta]$) could not predict the transient, uniformly mixed conditions of the perturbed stratosphere obtained from the primitive equations.*

- Figures 23 and 24 for the perturbed winter and summer seasons indicate that the tracer emitted at the continuous source propagates to the ozone production region (M1, Table 1) at the higher altitudes and lower latitudes in the Northern Hemisphere. Hence, the upward vertical transports of tracer mixing ratio from the continuous source pressure level to the middle stratosphere ($20 < z < 30$ km) are also important in the assessment of aviation effects on the ozone column.

The significant difference in the tracer configurations of Figs. 21 and 23 can further be illustrated by examining the relative roles of the mass transports (Eq. 19) by the meridional circulation and eddy motions in the reference and perturbed stratospheres. *These interactions are shown in Figs. 25 and 26, which imply a rather drastic difference in the relative roles of the meridional circulation and eddy motions in the transports of*

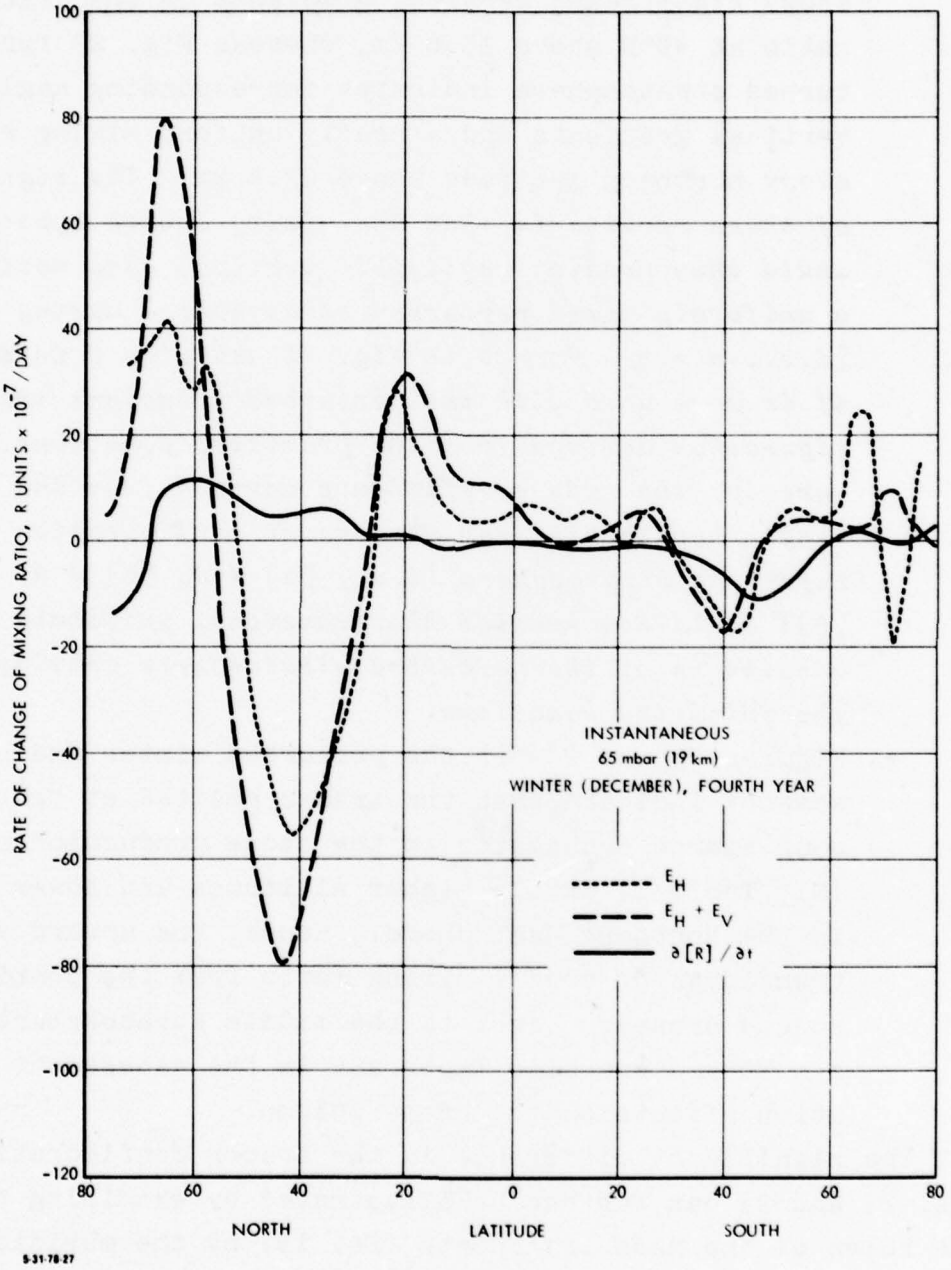

FIGURE 25. Eddy transports and the local rate of change of mixing ratio (Eq. 19) at 65 mbar during winter (December) of the fourth year after an instantaneous release of passive tracer material. (Source: Mahlman and Moxim, 1978)

mixing ratio at 65 mbar in the reference (Fig. 25) and perturbed (Fig. 26) stratospheres even though the continuous source itself is at a lower pressure level (~ 110 mbar). The significance of these results, utilizing the same dynamics (Tables 16, 17) for the reference and perturbed atmospheres, is, again, that extensions of empirical parameterizations of eddy mass transports in the reference stratosphere to describe the eddy transports of engine effluents in the perturbed stratosphere cannot be justified from the conservation equations for the stratospheric motions.

Returning to the basic considerations concerning the hypothesis of large-scale diffusion in the stratosphere (Section 4.1.2), *it now becomes important to emphasize that the Newell (1964) conceptual explanation of countergradient eddy fluxes of ozone or heat could not be based on actual observations.* The reasons for this situation are (a) the physical impossibility of observing the slope (α) of the mixing length path (Fig. 18) due to the fact that the eddy transports are not actually decoupled from the meridional circulation (Tables 16 and 17), and (b) the smallness of the slope [α] as indicated, for example, by the Crutzen and Widhopf models themselves (Tables 13 and 14). Furthermore, since the numerical solutions of the primitive equations for the instantaneous and continuous injections yield the vertical and horizontal eddy transports of tracer mixing ratio, it becomes possible to calculate α as stipulated in Fig. 18; i.e., $[\alpha] = [w^*R^*]/[v^*R^*]$. These results are illustrated in Table 18 for winter, corresponding to the conditions in Figs. 21 and 23, and it includes those for summer (June) for the SST case. A comparison of the winter [α] values for the instantaneous injection in Table 18 with the corresponding Crutzen and Widhopf values in Tables 13 and 14 indicates that the absolute magnitudes of [α] in the lower stratosphere at the middle northern latitudes, for example, would be larger for the solutions of the primitive equations. This discrepancy in the ratio of vertical to horizontal eddy transports leads, then, to drastic corresponding differences in the K_{zz} and K_{yy} coefficients, which can be determined from

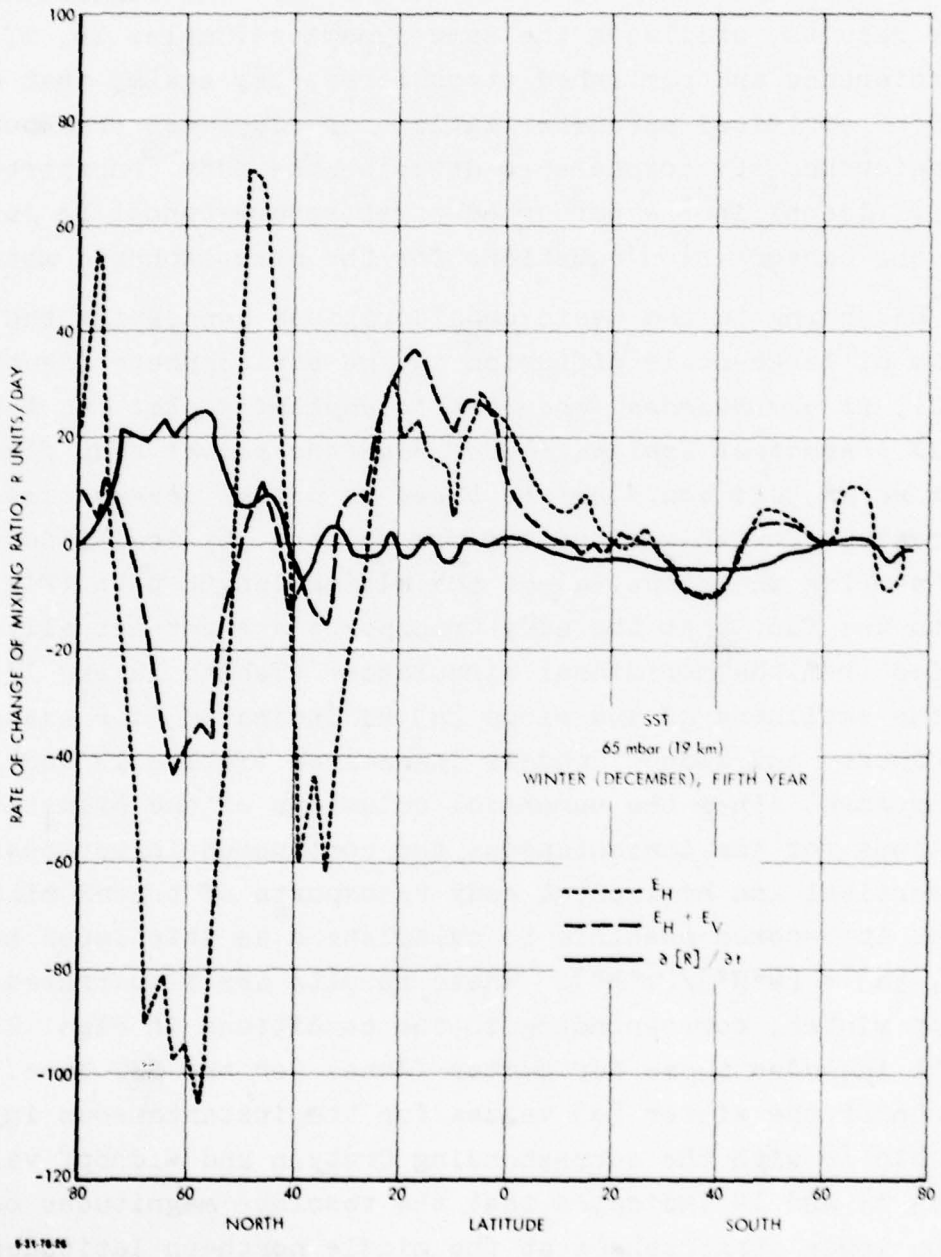

FIGURE 26. Eddy transports and local rate of change of mixing ratio (Eq. 19) at 65 mbar during winter (December) after 5 years of an SST-like continuous release of passive tracer material. (Source: Mahlman and Moxim, 1978)

TABLE 18. SLOPE OF MIXING LENGTH PATH AS GIVEN BY PRIMITIVE EQUATIONS, $[\alpha]$, (10^{-4})*

(Source: Mahlman, 1978)

Level, mbar	Standard Height, km	Latitude						
		72°N	48°N	24°N	0	24°S	48°S	72°S
		Instantaneous Injection, Winter (December), Fourth Year						
38	22.4	- 3.8	- 31.6	10.3	8.9	- 42.0	20.5	-132.0
65	19.0	- 6.4	- 31.2	7.2	- 1.4	- 39.4	23.5	-256.0
110	15.6	- 41.1	- 42.0	23.3	254.0	- 21.6	32.5	+231.0
190	12.1	- 20.1	- 26.5	84.2	18.0	+116.0	67.6	-525.0
315	8.9	-235.0	- 41.1	287.0	44.1	-281.0	-202.0	+844.0
		SST Injections, Winter (December), Fifth Year						
38	22.4	8.1	46.8	- 3.5	0.2	-102.0	- 5.9	- 56.1
65	19.0	46.4	13.2	- 1.7	1.9	-136.0	1.2	- 89.1
110	15.6	13.2	- 19.5	- 1.0	18.9	- 30.0	8.3	+188.0
190	12.1	- 10.2	- 25.3	19.4	76.1	27.7	70.7	-547.0
315	8.9	53.9	- 20.9	79.5	73.9	99.5	53.5	+640.0
		SST Injections, Summer (June), Fifth Year						
38	22.4	- 8.0	- 6.0	- 95.7	- 9.8	- 20.3	8.1	- 93.4
65	19.0	+ 13.2	+ 0.4	+ 3.5	3.2	+ 40.6	10.6	- 60.4
110	15.6	- 7.0	-2630.0	+ 15.1	23.1	- 98.4	8.7	30.7
190	12.1	- 89.6	- 7.9	- 43.2	84.6	32.3	1880.0	91.0
315	8.9	+ 3.4	48.1	+166.0	314.0	51.3	5.2	114.0

*For instantaneous injection at 38 mbar and 72°N, for example, $[\alpha] = -3.8 \times 10^{-4}$.

Eqs. (16) and either (17) or (18), using results from the numerical solutions of the primitive equations for the eddy fluxes and gradients of the mixing ratio. The results are as given in Tables 19 and 20, which indicate that K_{yy} and K_{zz} for the reference stratosphere would have to be either positive or negative. As indicated by Eq. (18), the change in the signs of K_{zz} and K_{yy} must take place simultaneously at a given location. Furthermore, Eqs. (16) and (17) show that this change of sign must come from the denominator. Hence, every time there is a change of sign in K_{yy} and K_{zz}, the denominator must go through zero; i.e., a condition that implies extremely large local values for K_{zz} and K_{yy} as both become infinity.

The results in Tables 18-20 include the eddy coefficients derived from the primitive equations for the perturbed winter and summer stratospheres. The results in Table 18 indicate that the slopes of the mixing length path for winter conditions in the reference and perturbed stratospheres are not identical, for example, in the lower stratosphere, at middle northern latitudes, which is an assumption in the Crutzen and Widhopf 2-D photochemical models. Similar considerations apply to the K_{zz} and K_{yy} eddy coefficients as exhibited in Tables 19 and 20.

Finally, it must be recognized that the Mahlman-Moxim numerical solutions of the primitive equations may not necessarily be an *exact* simulation of the dispersion of engine effluents in the actual perturbed stratosphere. However, it is also important to emphasize the following:

- The evaluation of the extension of the mixing length hypothesis to the perturbed stratosphere is based on a relative instead of absolute basis (e.g., Fig. 25 vs. Fig. 26).
- The primitive solutions do duplicate, first, the observed behavior of the slope [β] (Figs. 18 and 20) for the tracer mixing ratio at middle northern latitudes in the reference stratosphere; and second, the charac-

TABLE 19. VERTICAL EDDY COEFFICIENTS AS GIVEN BY PRIMITIVE EQUATIONS, K_{zz}, (10^4 cm^2/sec)*

(Source: Mahlman, 1978)

Level, mbar	Standard Height, km	Latitude						
		72°N	48°N	24°N	0	24°S	48°S	72°N
		Instantaneous Injections, Winter (December), Fourth Year						
38	22.4	6.4(-1)	-1.6(1)	1.5(0)	9.6(-2)	4.0(-1)	1.2(0)	-3.0(0)
65	19.0	1.9(-1)	-5.7(1)	4.6(-1)	8.8(-3)	9.2(-2)	4.7(-1)	-2.5(0)
110	15.6	7.5(-1)	+3.4(2)	1.3(0)	-4.9(-2)	9.0(-1)	6.6(-1)	-6.0(0)
190	12.1	8.0(-1)	+6.3(0)	4.4(0)	-1.2(-1)	2.1(0)	8.0(-1)	-7.8(0)
315	8.9	1.3(0)	+3.7(0)	2.6(1)	-1.9(0)	6.0(0)	2.9(0)	-2.4(1)
		SST Injections, Winter (December), Fifth Year						
38	22.4	3.4(-1)	-1.6(0)	1.8(-1)	1.0(-4)	1.1(0)	1.3(-1)	-2.0(0)
65	19.0	9.3(-1)	-3.3(1)	6.8(-2)	1.7(-2)	1.5(-1)	9.3(-3)	-1.7(0)
110	15.6	1.3(-1)	-1.3(1)	8.2(-3)	2.7(0)	9.0(-1)	1.5(-1)	-4.4(0)
190	12.1	3.6(-1)	+1.5(0)	4.7(-1)	3.4(0)	1.4(0)	3.9(-1)	-6.7(0)
315	8.9	1.5(0)	+6.6(0)	5.7(0)	7.3(0)	3.4(0)	2.2(0)	-2.2(1)
		SST Injections, Summer (June), Fifth Year						
38	22.4	1.4(-1)	2.4(-1)	3.1(0)	1.1(-1)	8.0(-1)	-1.0(0)	-1.2(0)
65	19.0	3.9(1)	-2.9(-3)	1.8(-1)	3.1(-2)	4.9(-1)	5.5(-1)	-2.1(-1)
110	15.6	-1.9(0)	8.8(-1)	9.6(-1)	2.6(0)	1.1(0)	1.5(0)	-3.1(-1)
190	12.1	+3.3(-1)	6.4(-1)	2.1(0)	4.7(0)	1.4(0)	4.5(-1)	-2.4(0)
315	8.9	-1.5(-3)	1.2(0)	9.9(0)	3.2(1)	2.0(0)	-7.1(-1)	-1.1(1)

*For instantaneous injection at 38 mbar and 72°N, for example, $K_{zz} = 6.4(10^{-1}) \cdot 10^4 = 6.4 \times 10^3$ cm^2/sec. Note that (0) denotes 10^0.

TABLE 20. HORIZONTAL EDDY COEFFICIENTS AS GIVEN BY PRIMITIVE EQUATIONS, K_{yy}, (10^{10} cm^2/sec)*

(Source: Mahlman, 1978)

Level, mbar	Standard Height, km	Latitude						
		72°N	48°N	24°N	0	24°S	48°S	72°S
		Instantaneous Injections, Winter (December), Fourth Year						
38	22.4	4.5(0)	-1.6(0)	1.4(0)	1.2(-1)	2.3(-2)	2.8(-1)	-1.7(-2)
65	19.0	4.6(-1)	-5.8(0)	9.0(-1)	4.4(-1)	5.9(-3)	8.6(-2)	-3.8(-3)
110	15.6	4.4(-2)	+1.9(1)	2.4(-1)	-7.6(-5)	1.9(-1)	6.2(-2)	-1.1(-2)
190	12.1	2.0(-1)	+8.9(-1)	6.2(-2)	-3.7(-2)	1.6(-2)	1.7(-2)	-2.8(-3)
315	8.9	2.3(-3)	+2.2(-1)	3.1(-2)	-9.8(-2)	7.6(-3)	7.2(-3)	-3.4(-3)
		SST Injections, Winter (December), Fifth Year						
38	22.4	5.2(-1)	-7.2(-2)	1.5(0)	2.2(-1)	1.0(-2)	3.7(-1)	-6.5(-2)
65	19.0	4.3(-2)	-1.9(1)	2.5(0)	4.5(-1)	8.1(-4)	6.3(-1)	-2.1(-2)
110	15.6	7.3(-2)	-3.5(0)	8.4(-1)	7.5(-1)	1.0(-1)	2.2(-1)	-1.2(-2)
190	12.1	3.5(-1)	+2.3(-1)	1.3(-1)	5.9(-2)	1.9(-1)	7.8(-3)	-2.3(-3)
315	8.9	5.3(-2)	+1.5(0)	9.0(-2)	1.3(-1)	3.5(-2)	7.6(-2)	-5.5(-3)
		SST Injections, Summer (June), Fifth Year						
38	22.4	2.2(-1)	6.7(-1)	3.4(-2)	1.2(-1)	1.9(-1)	-1.6(0)	-1.4(-2)
65	19.0	2.2(1)	1.5(0)	1.5(0)	3.1(-1)	3.0(-2)	4.9(-1)	-5.8(-3)
110	15.6	-3.8(0)	1.3(-5)	4.2(-1)	4.9(-1)	1.1(-2)	1.9(0)	-3.2(-2)
190	12.1	+4.1(-3)	1.0(0)	1.2(-1)	6.6(-2)	1.4(-1)	1.3(-5)	-2.9(-2)
315	8.9	-1.2(-2)	5.0(-2)	3.6(-2)	3.3(-2)	7.5(-2)	-2.6(0)	-8.8(-2)

*For instantaneous injection at 38 mbar and 72°N, for example, $K_{yy} = 4.5(10^0) \cdot 10^{10} = 4.5 \times 10^{10}$ cm^2/sec. Note that (0) denotes 10^0.

teristics of the other parameters (e.g., potential vorticity) which are strongly correlated with the ozone distributions in the stratosphere (Mahlman and Moxim, 1978).

- The configuration of tracer mixing ratio in the reference stratosphere is in qualitative agreement with the rather rough observations of the dispersion of nuclear debris in the lower stratosphere (Telegadas, 1974; Mahlman and Moxim, 1978).
- The empirical parameterization of eddy coefficients based on the Reed and German (1965) use of the Prandtl mixing length concept for the eddy mass transports in the reference atmosphere is not, by itself, a critical issue.* It should be noted that such parameterizations could be based on other hypotheses such as the G. I. Taylor (1932) formulation for microscale turbulent transports of vorticity and heat (instead of momentum, as in the mixing length hypothesis) or even the arbitrary modifications of Eq. (10) for R*. Since the empirical parameterizations of the (unknown) eddy coefficients in the lower stratosphere do not require a unique mathematical model, their validity must rest on the accuracy of the appropriate observations as well as on the internal consistency of their

*In fairness to the memory of a late scientist, and with permission of G. D. Robinson, it becomes appropriate to quote his review comment in regard to the application of the Prandtl mixing-length concept to the mass transports in the atmosphere: "Since I once met Prandtl, my sympathies go out to him, revolving, as he must be, in his grave. What he said was--if an entity is conserved in a fluctuating transport process, then the averaged flux in a given direction is proportional to the component in that direction of the gradient of the averaged concentration. Time averages are implied, over times long compared with the time scale of fluctuations. There are not many entities or locations in the atmosphere which meet these conditions."

calculations. The basic issue, then, is the extension of the same empirical parameterizations of eddy coefficients for the reference atmosphere to the dispersion of engine effluents in the perturbed atmosphere, an issue that comes about from the fact that the assessment of aviation effects on the ozone column involves an accurate calculation of the difference of two large numbers, as described in Section 1.

- The 2-D formulation of the dynamics for the *perturbed* upper troposphere and stratosphere must not be based on the Reed and German (1965) formulation that invokes the modified Prandtl mixing length hypothesis, *which must always assume a combination of countergradient and gradient components of the eddy transports whenever* $\alpha >> \beta$ *(Fig. 18).* It must be noted that more modern concepts for the formulations of the 2-D dynamics involve statistical considerations of the eddy parameters in Table 17 instead of using parameterizations based on K coefficients.

4.3 STATISTICAL-DYNAMICAL FORMULATION OF 2-D DYNAMICS

The splitting of the dependent variables (χ = u, v, w, T, R) into zonal averages ($[\chi]$) and eddy components (χ^*) introduces the classical, unsolved problem of closure of the equations for turbulent motion. This closure problem comes about because the splitting procedure cannot, of course, provide additional equations to calculate the eddy transports. For example, the derivation of Eq. (9) for $\partial[R_i]/\partial t$ brought about the double correlations $[\chi^* R^*]$ for the poleward and vertical eddy transports of mixing ratio. This first averaging procedure is also known, in this case, as the first moment of the continuity equation. To obtain additional equations for the double correlations, it is possible to take the second moment of the continuity equation by multiplying it by R_i. However,

this second moment now generates triple correlations, which would, in turn, require the third moment of the continuity equation. Since this procedure would continue in the same manner through the successive higher moments, it is seen that it is not possible to close the overall system of equations. Since the conservation equations are closed, it is a fundamental question to inquire how the averaging process has managed to convert them into an open set. Batchelor (1971) has provided two complementary concepts to answer this question: (a) the conservation equations may, indeed, be considered to be open in time, because any instantaneous configuration or "realization" must be integrated over the whole (future) time domain before they can give exact values for the various correlations; and (b) *the additional correlations from the higher moments provide less and less additional information, so that only a finite number of correlations is required to determine the properties of the turbulence field with some specified accuracy.* It is this second concept that is of interest in the statistical-dynamical formulations of turbulence; which attempts to close the equations of motion by parameterizations of the triple, instead of the double, correlations as in the Prandtl mixing length approach (i.e., Eqs. 11a, b). The main intent of such statistical approach is to improve the physics of turbulent models by taking into account additional energy transfer processes among the eddy and mean flow components.

The history of the application of the statistical approach to the troposphere includes efforts by Smagorinsky (1964), who calculated the eddy transports of momentum and heat by using phenomenological properties of the Rossby waves involved in such transports. This approach was able to calculate the maximum values of the transports of momentum and heat at the correct latitudes for the separation of the tropospheric Hadley and Ferrel cells near 30°, as well as the Ferrel and polar cells near 60° (Fig. 19). It is important to emphasize that these

results did not use the modified Prandtl mixing length hypothesis (Eqs. 11a, b) for the poleward eddy transports of momentum and heat, and that the triple correlations in this approach can be shown to be identically zero (Hidalgo, 1972). Other examples of the application of statistical-dynamical formulation to the tropospheric motions are those by Saltzman (1968), Kurihara (1970), and more recently by Vernekar and Chang (1978).

The 2-D statistical-dynamical formulation must be based on the respective equations for the meridional circulation (Table 16) and eddy motions (Table 17). However, the results in these tables must consider also the continuity equation for the tracers so as to derive the corresponding terms for [R] and R*. Such a formulation is being considered at GFDL by Yen-Huei Lee and Mahlman and it consists of five equations. The first equation is the conservation of the mean tracer mixing ratio (Eq. 9). The next three are second moments of the momentum equation for the poleward direction, the energy equation, and the continuity equation for R_i, respectively. These equations yield, respectively, the local rate of change of the northward eddy tracer flux [v*R*], the vertical eddy tracer flux [ω*R*], and the local rate of change of the eddy mixing ratio [R^{*2}]. The fifth one is a relationship for the term [T*R*] that appears in the energy equation. Important points in regard to this 2-D statistical-dynamics formulation are the following:

- It does not require the use of the modified Prandtl mixing length hypothesis (Eqs. 11a, b), but must utilize meteorological know-how and experience based on both observations and 3- model results.
- It will have to establish parameterizations for triple correlations involving eddy tracer terms such as [$v^{*2}R^*$], [v*ω*R*], etc.
- The solution of this system of equations would require inputs for the mean (i.e., [v], [ω], [T]) as well as

double correlations (i.e., $[v^{*2}]$, $[v^*\omega^*]$, $[v^*T^*]$, $[\omega^*T^*]$, $[T^{*2}]$ in the stratosphere.

- The potential payoff of such statistical-dynamical formulations for the reference atmosphere would be a greater confidence in the validity of its results when extended to the mass eddy transports $[\chi^*R^*]$ in the perturbed stratosphere. However, because of the difficulty of the endeavor, the advent of a valid statistical-dynamical formulation of the stratospheric dynamics may be a few years away, depending upon the priority placed on such effort by dynamic meteorologists.

REFERENCES

Andrews, D.G., and M.E. McIntyre, "Planetary Waves in Horizontal and Vertical Shear: The Generalized Eliassen-Palm Relation and the Mean Zonal Acceleration," *J. Atmos. Sci.*, Vol. *33*, No. 11, pp. 2031-2048, November 1976.

Arnold, I., F.J. Comes, and G.K. Moortgat, "Laser Flash Photolysis Quantum Yield of O('D)--Formation From Ozone," Max Planck Institute for Chemistry, Mainz, West Germany, Preprint, 1977.

Bannon, J.K., and L.P. Steele, "Average Water-Vapor Content of the Air," *Meteorol. Res. Papers*, Air Ministry, London, No. 1075, pp. 1-18, 1957.

Batchelor, G.K., *The Theory of Homogeneous Turbulence*, Cambridge University Press, 1971.

Broderick, A., "Stratospheric Effects from Aviation," presented at AIAA/SAE 13th Propulsion Conference, Orlando, Florida, July 11-13, 1977. U.S. Department of Transportation, Federal Aviation Administration. AIAA Preprint No. 77-799.

Burrows, J.D., G.W. Harris, B.A. Thrush, "Rates of Reaction of HO_2 with HO and O Studied by Laser Magnetic Resources," *Nature*, Vol. *267*, pp. 233-234, 1977.

Chan, W.H., W.M. Uselman, J.G. Calvert, and J.A. Shaw, "The Pressure Dependence of the Rate Constant for the Reaction HO + CO → H + CO_2," *Chem. Phys. Lett.*, Vol. *45*, pp. 240-243, 1977.

Chang, J., Chairman, *Meeting of Experts on Ozone Modeling and Stratospheric/Tropospheric Exchange Processes*, World Meteorological Organization, Geneva, August 25-29, 1977.

Chang, J.S., and F. Kaufman, "Determination of an Upper Limit to the Rate Constant of the Reaction OH + HO_2 → H_2O + O_2," Spring Meeting, American Geophysical Union, June 2-3, 1977, Washington, D.C. Also *J. Chem. Phys.*, Vol. *66*, p. 4989, 1977.

Chang, J., H. Hidalgo, and H. Johnston, CIAP Monograph 3, "The Stratosphere Perturbed by Propulsion Effluents," DOT-TST-75-53, U.S. Department of Transportation, September 1975.

Chapman, S., "A Theory of Upper-Atmosphere Ozone," *Mem. Roy. Meteorol. Soc.*, Vol. *3*, pp. 103-125, 1930.

Charney, J.G., and P.G. Drazin, "Propagation of Planetary Scale Disturbances From the Lower Into the Upper Atmosphere," *J. Geophys. Res.*, Vol. *66*, pp. 83-109, 1961.

CIAP, Monograph 1, *The Natural Atmosphere of 1974*, U.S. Department of Transportation, Climatic Impact Assessment Program DOT-TST-75-51, September 1, 1975.

Cox, R.A., R.G. Derwent, P.M. Holt, and J.A. Kerr, "Photooxidation of Methane in the Presence of NO and NO_2," *J. Chem. Soc.*, Faraday I, Vol. *72*, pp. 2044-2060, 1976.

Crutzen, P.J., private communication, National Center for Atmospheric Research, Boulder, Colorado, 1978.

Crutzen, P.J., "Upper Limits on Atmospheric Ozone Reductions Following Increased Application of Fixed Nitrogen to the Soil," *Geophys. Res. Lett.*, Vol. *3*, pp. 169-172, 1976.

Crutzen, P.J., "A Two-Dimensional Photochemical Model of the Atmosphere Below 55 km: Estimates of Natural and Man-Caused Ozone Perturbations due to NO_x," *Proceedings, Fourth Conference on CIAP*, DOT-TSC-OST-75-38, pp. 264-279, February 4-7, 1975.

Crutzen, P.J., I.S.A. Isaksen, J.R. McAfee, "The Impact of the Chlorocarbon Industry in the Ozone Layer," *J. Geophys. Res.*, Vol. *83*, No. C1, pp. 345-363, January 20, 1978.

Crutzen, P.J., and C.J. Howard, "The Effect of the HO_2 + NO Reaction Rate Constant on One-Dimensional Model Calculations of Stratospheric Ozone Perturbations," to appear in *PAGEOPH*, 1977/1978.

Crutzen, P.J., and J. Fishman, "Average Concentrations of OH in the Northern Hemisphere and the Budgets of CH_4, CO, H_2 and CH_3CCl_3," *Geophys. Res. Lett.*, Vol. *4*, No. 8, pp. 321-324, August 1977.

Cunnold, D.M., F. Alyea, and R. Prinn, "Relative Effects on Atmospheric Ozone of Latitude and Altitude of Supersonic Flight," *AIAA Journal*, Vol. *5*, No. 3, pp. 337-345, March 1977.

Cunnold, D., F. Alyea, N. Phillips, and R. Prinn, "A Three-Dimensional Dynamical-Chemical Model of Atmospheric Ozone," *J. Atmos. Sci.*, Vol. *32*, No. 1, pp. 170-194, 1975.

Danielsen, E.F., and V.A. Mohnen, "Project Dust Storm Report: Ozone Transport, In-Situ Measurements and Meteorological Analysis of Tropopause Folding," *J. Geophys. Res.*, Vol. *82*, No. 37, pp. 5867-5877, December 20, 1977.

Danielsen, E.F., and J.F. Louis, "Transport in the Stratosphere," from *The Upper Atmosphere and Magnetosphere (Studies in Geophysics)*, Geophysics Study Committee, National Research Council, National Academy of Sciences, Washington, D.C., 1975.

Davidson, B., J.P. Friend, and H. Seitz, "Numerical Models of Diffusion and Rainout of Stratospheric Radioactive Materials," *Tellus*, Vol. *18*, pp. 301-315, 1966.

Dopplick, T.G., "The Energetics of the Lower Stratosphere, Including Radiative Effects," *Quart. J. Roy. Meteorol. Soc.*, Vol. *97*, pp. 209-237, 1971.

Drummond, J., *Atmospheric Measurements of Nitric Oxide Using Chemiluminescence*, Ph.D. Dissertation, Department of Physics, University of Wyoming, Laramie, 1977.

Duewer, W.H., D.J. Wuebbles, H.W. Ellsaesser, and J.S. Chang, "NO_x Catalytic Ozone Destruction: Sensitivity to Rate Coefficients," *J. Geophys. Res.*, Vol. *82*, No. 6, pp. 935-942, February 20, 1977.

Dütsch, H.U., "Photochemistry of Atmospheric Ozone," *Adv. in Geophys.*, Vol. *15*, pp. 219-322, 1971.

Fabian, P., and P.G. Pruchniewicz, "Meridional Distribution of Ozone in the Troposphere and its Seasonal Variations," *J. Geophys. Res.*, Vol. *82*, pp. 2063-2073, 1977.

Fishman, J., and P.J. Crutzen, "The Distribution of the Hydroxyl Radical in the Troposphere," Atmospheric Science Paper No. 284, Colorado State University, Department of Atmospheric Science, Fort Collins, Colorado, 1978.

Friend, J.P., H.W. Feely, P.W. Krey, J. Spar, and W. Walton, *Discussion on HASP Results*, Defense Atomic Support Agency, DASA 1300, Vol. *3*, Washington, D.C., 1961.

Grobecker, A.J., S.C. Coroniti, and R.H. Cannon, Jr., *Report of Findings - The Effects of Stratospheric Pollution by Aircraft*, DOT-TST-75-50, prepared by Department of Transportation, CIAP, December 1974.

Harris, J.E., "The Distribution of Water Vapor in the Stratosphere," Rev. of Geophys. and Space Sciences, *14*, pp. 565-575, 1976.

Heath, D.F., A.J. Krueger, and P.J. Crutzen, "Solar Proton Event: Influence on Stratospheric Ozone," *Science*, Vol. *197*, No. 4306, pp. 886-888, August 26, 1977.

Hidalgo, H., "Assessment of Potential Impact of Stratospheric Flight on Earth's Ultraviolet Irradiance," *AIAA Journal*, Vol. *14*, No. 2, pp. 137-149, February 1976.

Hidalgo, H., "Understanding Anthropogenic Effects on Ultraviolet Radiation and Climate," *IEEE Trans. Geosci. Electron.*, Vol. *GE-16*, No. 1, pp. 4-22, January 1978.

Hidalgo, H., *Some Considerations on the Feasibility of Advertent Climate Modification*, P-856, Institute for Defense Analyses, Arlington, Virginia, October 1972.

Hidalgo, H., and P.J. Crutzen, "The Tropospheric and Stratospheric Composition Perturbed by NO_x Emission of High Altitude Aircraft," *J. Geophys. Res.*, Vol. *82*, No. 37, pp. 5833-5866, December 20, 1977.

Holton, J.R., private communication, July 1978.

Holton, J.R., "The Dynamic Meteorology of the Stratosphere and Mesosphere," *Meteorol. Monographs*, Vol. *15*, No. 37, August 1975.

Howard, C.J., "Recent Developments in Atmospheric HO_2 Chemistry - WMO Symposium on the Geophysical Aspects and Consequences of Changes in the Composition of the Stratosphere," Toronto, Canada, June 26-30, 1978.

Howard, C.J., participant at NASA Chlorofluoromethane Assessment Workshop, Goddard Space Flight Center, Maryland, 1977.

Howard, C.J., and K.M. Evenson, "Kinetics of the Reaction of HO_2 with NO," *Geophys. Res. Lett.*, Vol. *4*, No. 10, pp. 437-440, October 1977.

Hunten, D.M., "Estimates of Stratospheric Pollution by an Analytic Model," *Proc. Natl. Acad. Sci.*, Vol. *72*, pp. 4711-4715, 1975.

Johnston, H.S., "Global Ozone Balance in the Natural Stratosphere," *Rev. Geophys. Space Phys.*, Vol. *13*, pp. 637-649, 1975.

Junge, C.E., *Air Chemistry and Radioactivity*, Academic Press, New York and London, p. 10, 1963.

Kaufman, F., and B. Reimann, 13th Informal Conference on Photochemistry, Clearwater Beach, Florida, January 4-7, 1978.

Krueger, A.J., D.F. Heath, and C.L. Mateer, "Variations in Stratospheric Ozone Field Inferred From Nimbus Satellite Observations," *Pure Appl. Geophys.*, Vol. *106*, No. 108, pp. 1254-1263, 1973.

Kurihara, Y., "A Statistical-Dynamical Model of the General Circulation of the Atmosphere," *J. Atmos. Sci.*, September 1970.

Liu, S.C., *et al.*, "Sources and Sinks of Atmospheric N_2O and the Possible Ozone Reduction Due to Industrial Fixed Nitrogen Fertilizers," *Tellus*, Vol. *29*, pp. 251-263, 1977.

Lorenz, E.N., *The Nature and Theory of the General Circulation of the Atmosphere*, World Meteorological Organization, WMO No. 218, TP115, 1967.

Louis, J.F., in CIAP Monograph 3, *The Stratosphere Perturbed by Propulsion Effluents*, U.S. Department of Transportation, Climatic Impact Assessment Program, DOT-TST-75-53, pp. 4-112-4-113, September 1975.

Louis, J.F., *A Two-Dimensional Transport Model of the Atmosphere*, Ph.D. Dissertation, University of Colorado, Boulder, Colorado, 1974.

Louis, J.F., J. London, and E. Danielsen, "The Interaction of Radiation and the Meridional Circulation of the Stratosphere," *IAMAP First Special Assembly*, Melbourne, Australia, January 1974.

Luther, F.M., *Monthly Values of Eddy Diffusion Coefficients in the Lower Stratosphere*, UCRL Report 74616, also AIAA Paper No. 73-498, AIAA/AMS International Conference on the Environmental Impact of Aerospace Operations in the High Atmosphere, Denver, Colorado, June 1973.

Mahlman, J.D., private communication, Geophysical Fluid Dynamics Laboratory, NOAA, Princeton University, 1978.

Mahlman, J.D., "Some Fundamental Limitations of Simplified Transport Models as Implied by Results from a Three-Dimensional General Circulator/Tracer Model," *Proceedings, Fourth Conference on CIAP*, DOT-TSC-OST-75-38, pp. 132-146, February 1975.

Mahlman, J.D., "A Three-Dimensional Stratospheric Point-Source Experiment and Its Implications for Dispersion of Effluents From a Fleet of Supersonic Aircraft," presented at the AIAA/AMS International Conference on the Environmental Impact of Aerospace Operations in the High Atmosphere, Denver, Colorado, AIAA Paper 73-528, June 1973.

Mahlman, J.D., and W.J. Moxim, "Tracer Simulation Using a Global General Circulation Model: Results from a Mid-Latitude Instantaneous Source Experiment," Geophysical Fluid Dynamics Laboratory, NOAA, Princeton University, November 1977. To be published in *J. Atmos. Sci.*, 1978.

Margitan, J.J., and J.G. Anderson, 13th Informal Conference on Photochemistry, Clearwater Beach, Florida, January 4-7, 1978.

McElroy, M.B., *et al.*, "Sources and Sinks for Atmospheric N_2O," *Rev. Geophys. Space Phys.*, Vol. *14*, pp. 143-150, 1976.

McElroy, M.B., S.C. Wofsy, J.E. Penner, and J.C. McConnell, "Atmospheric Ozone: Possible Impact of Stratospheric Aviation," *J. Atmos. Sci.*, Vol. *31*, No. 287-303, 1974.

Ming-Taun Leu, "Rate Constant for the Reaction $HO_2 + NO \rightarrow OH + NO_2$," Jet Propulsion Laboratory, California Institute of Technology, Pasadena, California, 91103. Poster Session Programme - WMO Symposium on the Geophysical Aspects and Consequences of Changes in the Composition of the Stratosphere, Toronto, Canada, June 26-30, 1978.

Moortgat, G.K., E. Kudszus, and P. Warneck, "Temperature Dependence of O('D)--Formation in Near U.V. Photolysis," Max Planck Institute of Chemistry, Mainz, West Germany, In press, 1977.

Moortgat, G.K., and P. Warneck, "Relative O('D) Quantum Yields in the Near U.V. Photolysis of Ozone at 298°K," *Z. Naturforsch*, Vol. *30a*, pp. 835-844, 1975.

NASA, *Chlorofluoromethane Assessment Workshop Report*, Goddard Space Flight Center, Maryland, 1977.

National Academy of Sciences, *Environmental Effects of Chlorofluoromethane Release*, Committee on Impacts of Stratospheric Change, National Research Council, 1976.

National Academy of Sciences, *Halocarbons: Effects on Stratospheric Ozone*, Panel on Atmospheric Chemistry, National Research Council, 1976.

National Academy of Sciences, *Environmental Impact of Stratospheric Flight, Biological and Climatic Effects of Aircraft Emissions in the Stratosphere*, Climatic Impact Committee, 1975.

Newell, R.E., "The Circulation of the Upper Atmosphere," *Sci. Am.*, Vol. *210*, No. 3, pp. 62-74, March 1964.

Noxon, J.F., "Tropospheric NO_2," *J. Geophys. Res.*, Vol. *83*, No. C6, June 20, 1978.

Oliver, R.C., *et al.*, *Aircraft Emissions: Potential Effects on Ozone and Climate*, prepared for High Altitude Pollution Program, FAA-EQ-77-3, U.S. Department of Transportation, Federal Aviation Administration, March 1977.

Oört, A.H., and E.M. Rasmusson, *Atmospheric Circulation Statistics*, NOAA Professional Paper 5, Geophysical Fluid Dynamics Laboratory, Princeton University, 1971.

Prabhakara, C., "Effects of Non-Photochemical Processes on the Meridional Distribution and Total Amount of Ozone in the Atmosphere," *Mon. Weather Rev.*, Vol. *91*, No. 9, pp. 411-431, September 1963.

Prandtl, L., "Über die ausgebildete Turbulenz," *ZAMM*, Vol. *5*, No. 136, 1925, and *Proc. of II Int. Cong. Appl. Mech.*, Zürich, 1926.

Reed, R.J., and K.E. German, "A Contribution to the Problem of Stratospheric Diffusion by Large-Scale Mixing," *Mon. Weather Rev.*, Vol. *93*, No. 5, pp. 313-321, May 1965.

Saltzman, B., "Surface Boundary Effects on the General Circulation and Macroclimate: A Review of the Theory of the Quasi-Stationary Perturbations in the Atmosphere," *The Causes of Climate Change, Meteorol. Monographs*, No. 30, pp. 4-49, 1968.

Saltzman, B., and A.D. Vernekar, "An Equilibrium Solution for the Axially Symmetric Component of the Earth's Macroclimate," *J. Grophys. Res.*, Vol. *76*, pp. 1498-1524, 1963.

Seiler, W., "The Cycle of Atmospheric CO," *Tellus*, Vol. *26*, pp. 116-135, 1974.

Sie, B.K.T., R. Simonitis, and J. Heicklen, "The Reaction of OH with CO," *Int. J. Chem. Kinetics*, Vol. *8*, pp. 85-88, 1976.

Smagorinsky, J., "Some Aspects of the General Circulation," *Quart. Roy. Meteorol. Soc.*, Vol. *90*, No. 383, pp. 1-14, January 1964.

Taylor, G.I., "The Transport of Vorticity and Heat Through Fluids in Turbulent Motion," *Proc. Roy. Soc. A*, Vol. *135*, p. 685, 1932.

Telegadas, K., *Radioactivity Distribution in the Stratosphere From Chinese and French High-Yield Nuclear Tests (1967-1970)*, U.S. Atomic Energy Commission, Fallout Program Quarterly Summary Report, April 1, 1974, pp. 1-112. Also HASL Report 281, 1974.

Venkateswaran, S.V., *et al.*, CIAP Monograph 4, "The Natural and Radiatively Perturbed Troposphere," DOT-TST-75-54, U.S. Department of Transportation, Washington, D.C., September 1975.

Vernekar, A.D., and H.D. Chang, "A Statistical-Dynamical Model for Stationary Perturbations in the Atmosphere," *J. Atmos. Sci.*, Vol. *35*, pp. 433-444, March 1978.

Widhopf, G.F., private communication, The Aerospace Corporation, Los Angeles, California, 1978.

Widhopf, G.F., and L. Glatt, "Numerical Modeling of Atmospheric Pollution," presented at Sixth International Conference on Numerical Methods in Fluid Dynamics held in Tbilisi, USSR, June 20-25, 1978. To appear in Meeting Proceedings, Springer-Verlag.

Widhopf, G.F., L. Glatt, and R.F. Kramer, "Potential Ozone Column Increase Resulting from Subsonic and Supersonic Aircraft NO_x Emissions," *AIAAJ.*, Vol. *15*, No. 9, pp. 1322-1330, September 1977.

Zahniser, M.S., and C.J. Howard, "A Direct Measurement of the Temperature Dependence of the Rate Constant for the Reaction $HO_2 + O_3 \rightarrow OH + 2\ O_2$," Poster Session Programme - WMO Symposium on the Geophysical Aspects and Consequences of Changes in the Composition of the Stratosphere, Toronto, Canada, June 26-30, 1978.

*U.S. GOVERNMENT PRINTING OFFICE: 1979 623-897/884 1-3

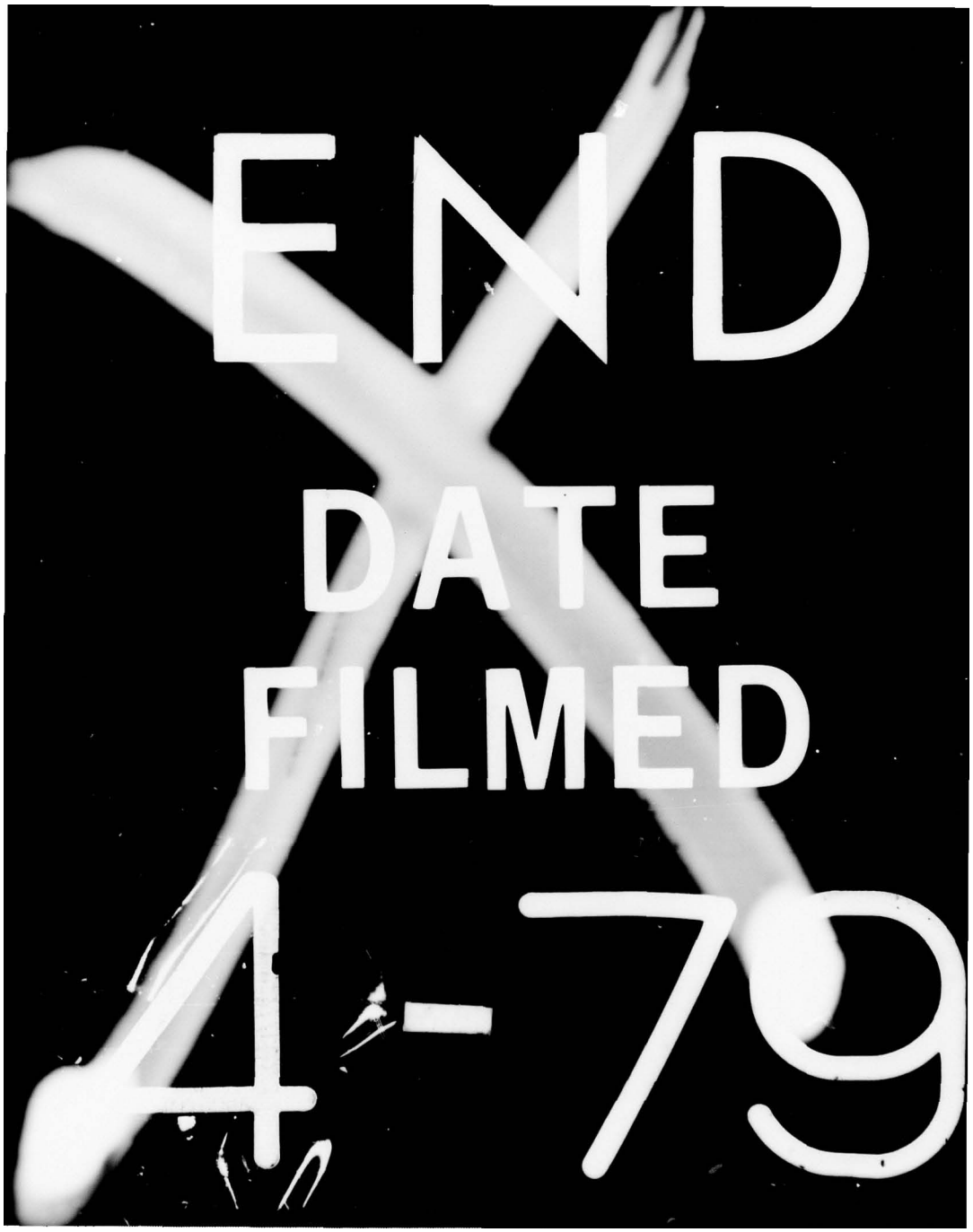
END
DATE
FILMED
4-79

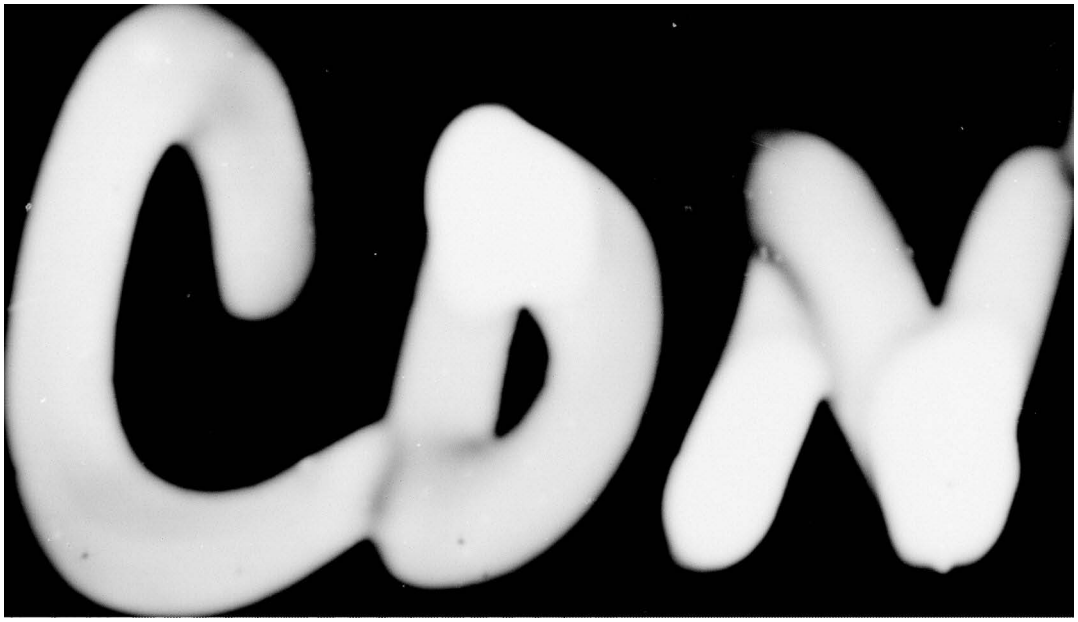
CDN

AD-A065 472 INSTITUTE FOR DEFENSE ANALYSES ARLINGTON VA F/G 4/1
STATUS OF REPRESENTATIVE TWO-DIMENSIONAL MODELS OF THE STRATOSP--ETC(U)
OCT 78 H HIDALGO DOT-FA-77WA-3965
UNCLASSIFIED P-1341 FAA-AEE-78-23 NL

3 OF 3
AD A065 472

END
DATE FILMED
9-79
DDC

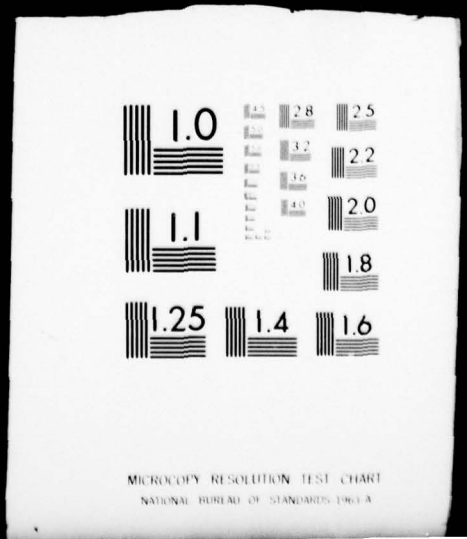

SUPPLEMENTARY

INFORMATION

Note added July 1979 to Report No. FAA-AEE-78-23,
Status of Representative Two-Dimensional Models of the Stratosphere and Troposphere as of Mid-1978,
by Henry Hidalgo (See pp. 102-105)

1. Eqs. 16-18 may be valid only at middle latitudes. Efforts are currently being made to calculate the relevant Reed and German $[\alpha^{*2}]/[\alpha]^2$ parameter from wind data of a general circulation model. Results are expected to be published in the near future.

2. Available results indicate that the three 2-D parameterizations of stratospheric dynamics (pages 104, 105) do not always yield valid values for $[\alpha^{*2}]/[\alpha]^2$.

3. In view of (1) above, and contrary to the statements on pages 104, 105, the three 2-D parameterizations of stratospheric dynamics may, in fact, be consistent within themselves. However, in view of (2), the three parameterizations remain inconsistent with each other and may also be inconsistent with the basic Reed and German formulation.